

# RADHE SHYAM SHARMA

WL-213, Department of Electrical Engineering, IIT Kanpur, Kanpur- 208016, UP, India

[Homepage](#) 

[Google Scholar](#) 

[LinkedIn](#) 

 [sharma.radhe@gmail.com](mailto:sharma.radhe@gmail.com)

 +91-8604220525

## ACADEMIC DETAILS

- **PhD** (Electrical Engineering)

**Institute:** Indian Institute of Technology (IIT) Kanpur, India, 2020

(*Date of Defense:* June 15, 2020)

**CPI:** 9 out of 10

[List of Courses](#) 

- **M.Tech.** (Modelling & Simulation)

**Institute:** Defence Institute of Advanced Technology (DIAT) Pune, India, 2013

**Percentage:** 75.25

[List of Courses](#) 

- **B.E.** (Biomedical Engineering)

**Institute:** Samrat Ashok Technological Institute (SATI) Vidisha, India, 2007

**Percentage:** 74.25

[List of Courses](#) 

## RESEARCH INTERESTS

- Visual Servoing
- Robot Learning
- Autonomous Navigation
- Multi-Robot Systems

## PUBLICATIONS

1. **Radhe Shyam Sharma**, Arindam Mondal, Laxmidhar Behera, “Tracking Control of Mobile Robots in Formation in the Presence of Disturbances,” *IEEE Transactions on Industrial Informatics*, 2020. [PDF](#)   
[Video of the Experiments](#) 
2. **Radhe Shyam Sharma**, Ranjith Ravindranathan Nair, Pooja Agrawal, Laxmidhar Behera, K. S. Venkatesh, “Robust Hybrid Visual Servoing using Reinforcement Learning and Finite Time Adaptive FOSMC,” *IEEE Systems Journal*, vol. 13, no. 3, pp. 3467–3478, 2018. [PDF](#)   
[Video of the Experiments](#) 
3. **Radhe Shyam Sharma**, Santosh Shukla, Laxmidhar Behera, Venkatesh K S, “Position Based Visual Servoing of a Mobile Robot With an Automatic Extrinsic Calibration Scheme,” *Robotica*, vol. 38, no. 5, pp. 831–844, 2020. [PDF](#)   
[Video of the Experiments](#) 
4. **Radhe Shyam Sharma**, Santosh Shukla, Hamad Karki, Amit Shukla, Laxmidhar Behera, Venkatesh K S, “DMP Based Trajectory Tracking for a Nonholonomic Mobile Robot With Automatic Goal Adaptation and Obstacle Avoidance,” *IEEE International Conference on Robotics and Automation (ICRA)*, pp. 8613-8619, 2019. [PDF](#)   
[Video of the Experiments](#) 
5. Atulya Shivam Shree, **Radhe Shyam Sharma**, Laxmidhar Behera, K. S. Venkatesh, “Position Based Visual Control of The Hovering Quadcopter,” *International Conference on Intelligent Human Computer Interaction*, pages 15–26. Springer, 2016. [PDF](#)   
[Video of the Experiments](#) 

6. **Radhe Shyam Sharma**, Laxmidhar Behera, Venkatesh K Subramanian, Rajesh Sinha, Jenssen Chang “An Approach for Transferring Human Skill to a Group: Trajectory Tracking by a Flexible Formation of Nonholonomic Mobile Robots,” under review. [Video of the Experiments](#) 

## AWARDS AND FELLOWSHIPS

- Visiting research scholar at Khalifa University, Abu Dhabi, UAE, Oct - Nov 2018.
- Received Institute fellowship for doctoral studies from Indian institute of Technology (IIT) Kanpur, India, Jan 2015 - Dec 2019.
- Received GATE scholarship for Master of Technology course from MHRD, Govt of India, Aug 2011- May 2013.

## PROJECTS

- A condition monitoring system with multi-agent mechanism for external non-contact smart inspection of buried oil and gas pipelines  
*The Petroleum Institute (PI), Khalifa University, Abu Dhabi, UAE*
- Study on personal drone benefits for driver assistance  
*Renault Nissan Technology and Business Center India (RNTBCI), Chennai, India*
- Robotics and Automation in Agriculture  
*Ministry of Electronics and Information Technology, India*

## EXPERIENCE

- Project Scientist  
*IIT Kanpur, India*  
*From 16-06-2020 to Till Date*
- Research Associate  
*IIT Kanpur, India*  
*From 01-01-2020 to 31-05-2020*
- Faculty  
*NIT Raipur, India*  
*From 15-07-2013 to 31-05-2014*
- Lecturer  
*SGSITS Indore, India*  
*From 15-07-2008 to 11-08-2011*
- Lecturer  
*SATI Vidisha, India*  
*From 11-09-2007 to 14-07-2008*

## TUTORSHIPS

- Lab Tutor for Introduction to Electronics (ESc201A), 2018-19-II Semester, IIT Kanpur
- Theory Tutor for Introduction to Electronics (ESc201A), 2019-20-I Semester, IIT Kanpur
- Theory Tutor for Introduction to Electronics (ESc201A), 2019-20-II Semester, IIT Kanpur

## TEACHING ASSISTANTSHIPS

- Signals, Systems and Networks, IIT Kanpur
- Probabilistic Mobile Robotics, IIT Kanpur
- Intelligent Systems and Control, IIT Kanpur
- Neural Networks, IIT Kanpur

## PROFESSIONAL ASSOCIATIONS

- Reviewer for IEEE Systems Journal
- Reviewer for IEEE Robotics and Automation Letters
- Reviewer for IEEE Transactions on Instrumentation and Measurement
- Reviewer for IEEE RO-MAN (Robot and Human Interactive Communication)
- Student member of IEEE
- Member of IEEE Robotics and Automation Society
- Visiting research scholar in the Department of Mechanical Engineering at Khalifa University, Abu Dhabi, UAE
- Speaker for GIAN (Global Initiative of Academic Networks) course on Selected Topics in Internet of Things, Jan 2018

## POSITIONS OF RESPONSIBILITY

- Academic Mentor, Counselling Service, IIT Kanpur, 2015
- Advisor of Light & Decoration Committee in *Techno Vision, 2008*
- Convener of SAC Committee In *SU-2007*
- Co-Convener of Audio-Visual Committee In *SU-2006*

## TRAININGS ATTENDED

- National workshop on “SVM in pattern recognition & its applications in biological sciences” at *NIT Raipur (Jan 2014)*
- Faculty training/orientation program at *SGSITS Indore (Dec 2008)*
- Major training on “Imaging systems” at *AFMC (Armed Forces Medical College) Pune (Jun-Jul 2006)*
- Minor training on “Biomedical Equipments” at *MH (Military Hospital) Gwalior (Jun-Jul 2005)*

## TECHNICAL SKILLS

- Languages: MatLab, C++, Python
- Operating Systems: Linux, ROS (**Robot Operating System**)
- Others: L<sup>A</sup>T<sub>E</sub>X, GNU Octave, R, Mathematica, ExtendSim
- Hands-on experience with **unmanned ground and aerial vehicles** – Pioneer P3-DX, Guardian mobile platform, Segway RMP, Nayan, and AscTec Hummingbird.



(a) Pioneer P3-DX



(b) Guardian robot



(c) Segway RMP



(d) Nayan



(e) AscTec Hummingbird

## TREKKING AND CAMPING EXPERIENCE

- Gaumukh Tapovan Trek
- Dodital Trek
- NSS CAMP

## INTEREST AND HOBBIES

- Adventure trekking
- Robotics
- Horse riding

## REFERENCES

Prof. Laxmidhar Behera  
Department of Electrical Engineering  
Indian Institute of Technology (IIT) Kanpur  
Kanpur, UP, India.  
✉ lbehera@iitk.ac.in  
☎ +91-512-259-7198, +91-8318968101

Prof. Venkatesh K. Subramanian  
Department of Electrical Engineering  
Indian Institute of Technology (IIT) Kanpur  
Kanpur, UP, India.  
✉ venkats@iitk.ac.in  
☎ +91-512-259-7486, +91-9451284966

## List of Publications

---

1. **Radhe Shyam Sharma**, Arindam Mondal, Laxmidhar Behera, "Tracking Control of Mobile Robots in Formation in the Presence of Disturbances," *IEEE Transactions on Industrial Informatics*, 2020. [PDF](#)  
**YouTube** video link: <https://youtu.be/EX2Hw-Bb7Gw>  
**DOI:** [10.1109/TII.2020.2983646](https://doi.org/10.1109/TII.2020.2983646)  
**ISSN:** [1551-3203](https://doi.org/10.1109/TII.2020.2983646)  
**Impact Factor:** [9.112](https://doi.org/10.1109/TII.2020.2983646)
2. **Radhe Shyam Sharma**, Ranjith Ravindranathan Nair, Pooja Agrawal, Laxmidhar Behera, K. S. Venkatesh, "Robust Hybrid Visual Servoing using Reinforcement Learning and Finite Time Adaptive FOSMC," *IEEE Systems Journal*, vol. 13, no. 3, pp. 3467–3478, 2018. [PDF](#)  
**YouTube** video link: <https://youtu.be/N0a4gvzheNw>  
**DOI:** [10.1109/JSYST.2018.2875789](https://doi.org/10.1109/JSYST.2018.2875789)  
**ISSN:** [1932-8184](https://doi.org/10.1109/JSYST.2018.2875789)  
**Impact Factor:** [4.463](https://doi.org/10.1109/JSYST.2018.2875789)
3. **Radhe Shyam Sharma**, Santosh Shukla, Laxmidhar Behera, Venkatesh K S, "Position Based Visual Servoing of a Mobile Robot With an Automatic Extrinsic Calibration Scheme," *Robotica*, vol. 38, no. 5, pp. 831–844, 2020. [PDF](#)  
**YouTube** video link: <https://youtu.be/I1IY5lynRgU>  
**DOI:** [10.1017/S0263574719001115](https://doi.org/10.1017/S0263574719001115)  
**ISSN:** [0263-5747](https://doi.org/10.1017/S0263574719001115)  
**Impact Factor:** [1.509](https://doi.org/10.1017/S0263574719001115)
4. **Radhe Shyam Sharma**, Santosh Shukla, Hamad Karki, Amit Shukla, Laxmidhar Behera, Venkatesh K S, "DMP Based Trajectory Tracking for a Nonholonomic Mobile Robot With Automatic Goal Adaptation and Obstacle Avoidance," *IEEE International Conference on Robotics and Automation (ICRA)*, pp. 8613–8619, 2019. [PDF](#)  
**YouTube** video link: <https://youtu.be/jOTLOEZZCk>  
**DOI:** [10.1109/ICRA.2019.8793911](https://doi.org/10.1109/ICRA.2019.8793911)
5. **Radhe Shyam Sharma**, Laxmidhar Behera, Venkatesh K Subramanian, Rajesh Sinha, Jenssen Chang "An Approach for Transferring Human Skill to a Group: Trajectory Tracking by a Flexible Formation of Nonholonomic Mobile Robots," under review. **YouTube** video link: <https://youtu.be/iFjuHBusE14>
6. Atulya Shivam Shree, **Radhe Shyam Sharma**, Laxmidhar Behera, K. S. Venkatesh, "Position Based Visual Control of The Hovering Quadcopter," Springer International Conference on Intelligent Human Computer Interaction (IHCI), pp. 15–26, 2016. [PDF](#)  
**YouTube** video link: <https://youtu.be/L7imtmpw8mU>  
**DOI:** [10.1007/978-3-319-52503-7\\_2](https://doi.org/10.1007/978-3-319-52503-7_2)  
*Part of the Lecture Notes in Computer Science book series (LNCS, volume 10127)*

# Robust Hybrid Visual Servoing Using Reinforcement Learning and Finite-Time Adaptive FOSMC

Radhe Shyam Sharma , Ranjith Ravindranathan Nair, Pooja Agrawal , Laxmidhar Behera , and Venkatesh K. Subramanian

**Abstract**—In this paper, we present and implement a hybrid approach to robust visual servoing for autonomous ground vehicles. A vision integrated model for nonholonomic mobile robots is derived that obviates the need for actual depth data for image-based visual servoing by assuming planar motion. A fractional order sliding-mode controller has been designed where the parameters of the sliding surface are adapted in real time. These adaptive laws are so derived that ensure finite-time convergence. An optical flow based heading restoration law is designed to handle the severe external perturbations, i.e., when the visual marker disappears from the field of view of the camera. The heading restoration law is combined with the reinforcement learning to solve this visibility problem. The proposed algorithm enables the robot to reach the home location even when the visual marker momentarily disappears from the camera field of view due to external disturbances. The proposed algorithm is validated in real time using Pioneer P3-DX robots through perturbation studies. Both simulation and experimental results prove the efficacy of the proposed scheme.

**Index Terms**—Fractional order sliding-mode controller (FOSMC), hybrid approach, nonholonomic robots, reinforcement learning, visual servoing (VS).

## I. INTRODUCTION

ROBOTIC systems integrated with vision can perform various tasks autonomously in structured and unstructured environments. The process of controlling a robot using visual information extracted from single or multiple cameras to achieve a desired task is known as visual servoing (VS). The concept has various applications, viz., surveillance [1], security, medical applications [2], etc. The basics of VS can be found in [3] and [4]. In [5], spherical image feature based error is used to generate the control signals. Fundamental matrix based visual servo regulation strategy has been designed for nonholonomic mobile robots in [6]; it requires the estimation of the camera's intrinsic parameters. This may increase the computational complexity. A VS strategy based on the homography matrix to obtain camera to robot parameters has been presented in [7]. In [7], backstepping-based control technique has been adopted. In both the works [6], [7], only asymptotic stability is guaranteed. Visual servo control approaches can mainly be categorized into position-based VS (PBVS) approaches and image-based VS (IBVS) approaches. A PBVS seeks to obtain position in Cartesian space

and, hence, requires sufficient information for this purpose from the camera. The PBVS output is positional error also in Cartesian space. On the other hand, an IBVS system completely sidesteps Cartesian space and deals entirely with visual information in the image plane. The output of an IBVS is, therefore, positional error in image plane. The work in [8] utilized a model that directly depends on image information. The image-based techniques do not require image interpretation. IBVS techniques avoid the errors due to camera modeling and calibration. The computational cost of IBVS techniques is much lighter than the PBVS.

Visibility of features, number and type of features, convergence, and robustness are key challenges in the VS. Any conventional visual servo controller totally depends on the visibility of the visual features. If the visual features being used move out from the field of view (FOV) due to motion of the robot or any other disturbances, then VS will completely fail. Hence, in the literature, many efforts have been made to solve this issue [9]–[12]. A potential field approach is utilized in [9] to repel the feature points from the image boundary to keep them within the FOV. Navigation function based approaches are given in [10] and [11] to keep the visual feature in the FOV. Potential field and navigation function based approaches [9]–[11] give static solutions and cannot improve their performance online. This problem is addressed in [13]. In [13], *Q*-learning (reinforcement learning) is developed to keep the feature in the FOV. However, none of these existing methods survive under severe disturbances because once a marker is totally lost from the FOV at any point of time, there is no provision for getting it back in. This is precisely one of the problems we address in this paper: how to restore a visual feature even after it has been lost from the FOV. Hence, we design a robust hybrid approach that handles severe disturbances.

A robust controller is extremely significant for smooth performance in target seeking operations. Considering its robustness features, sliding-mode control (SMC) [14] is highly preferred for such applications. Different types of SMC schemes are depicted in the literature [15]–[18]. An adaptive nonsingular terminal SMC has been depicted in [19] for the finite-time fault tolerant formation control of multi-robot systems. Similarly, a higher order SMC-based control scheme has been proposed in [20] for the tracking control of wheeled robots with sliding effects. Among the different variants of SMC available in the literature, fractional order SMC (FOSMC) is unique in terms of its control and sliding precision. FOSMC techniques are depicted in [17] and [21]–[24]. In [21], an adaptive fuzzy-based FOSMC technique has been designed for a three-phase active power filter, in which a fuzzy-inference mechanism is utilized to approximate the unknown dynamic model, and the fuzzy parameters are updated using an adaptive algorithm. In [22],

Manuscript received March 3, 2018; revised July 10, 2018; accepted October 6, 2018. Date of publication October 30, 2018; date of current version August 23, 2019. (Corresponding author: Laxmidhar Behera.)

The authors are with the Department of Electrical Engineering, Indian Institute of Technology Kanpur, Kanpur 208016, India (e-mail: sharmas@iitk.ac.in; ranjith@iitk.ac.in; pooja.iitd@gmail.com; lbehera@iitk.ac.in; venkats@iitk.ac.in).

Digital Object Identifier 10.1109/JSYST.2018.2875789

Delghavi *et al.* proposed an advanced FOSMC-based voltage control strategy for off-grid electrification systems. Similarly, in [17], a fractional order nonsingular terminal sliding surface has been proposed for designing a robust controller for robot manipulators. In both the cases, a sliding surface involving error derivatives has been considered. Moreover, the parameters of the sliding surface are precomputed offline. This may not be suitable for systems with varying operating conditions such as online operations. An adaptive fractional order nonsingular terminal SMC has been proposed in [23], where an adaptation scheme has been developed for tuning the reaching law gains. In addition to this, second-order dynamics is also required for implementing the same. Most of the adaptation schemes depicted in the literature are designed to guarantee only asymptotic convergence, where finite-time stability cannot be guaranteed. The robust and effective algorithms are needed in every field of research. An energy-efficient content delivery system is proposed in [25] to minimize energy consumption in smart cities. The work in [26] introduced an integrated solution for device-to-device communication over ultra-dense networks to maximize the video quality, spectrum efficiency, and energy efficiency. In contrast to [25] and [26], a hybrid VS scheme is proposed to enable the robot to reach the home location even when the visual marker momentarily disappears from the FOV due to severe external disturbances.

In this paper, a hybrid approach is developed to simultaneously solve the finite-time convergence and heading restoration problems. A novel adaptive algorithm to deal with system uncertainties is derived. The proposed controller ensures finite-time stability, which is analyzed mathematically. Most of the FOSMC-based designs are restricted to simulation-based validations. In contrast, in the present paper, we have performed real-time experiments to analyze implementation issues of the proposed scheme.

The key contributions of this paper are as follows.

- 1) A unique approach has been presented that integrates the image Jacobian with the robot Jacobian, from a control application point of view.
- 2) Since an IBVS demands knowledge of each feature depth, we have derived a vision integrated depth free model assuming planar motion for nonholonomic mobile robots.
- 3) To improve control precision, an adaptive FOSMC has been proposed. Novel adaptive algorithms are derived for tuning the sliding surface parameters in such a way that finite-time convergence is guaranteed.
- 4) A novel heading restoration law is designed using conditional optical flow to bring the marker back in the FOV.
- 5) Robust hybrid approach has been designed to acquire and then follow the target under severe disturbances.
- 6) The implementation issues of the proposed approach have been tested through rigorous perturbation studies conducted based on real-time experimentations.

The proposed approach works well in the presence of noise and different levels of disturbances. Different cases have been explored to validate the adaptive nature of the tuning parameters. Hybrid approach solves the problem of visibility and guarantees finite-time convergence. The proposed scheme is adaptive and robust enough to handle different operating conditions. To the best of our knowledge, this is the first work to integrate finite-time adaptive FOSMC, learning, and conditional optical flow based search mode with image-based VS in order to handle severe disturbances during the experiment.

The paper is organized as follows: Section II presents the VS followed by the control design and finite-time stability analysis in Section III. Hybrid approach is given in Section IV. Simulation and experimental results are provided in Section V. Conclusions are drawn in Section VI.

## II. IMAGE-BASED VS

### A. Image Interaction Matrix

Time variation of image features and camera velocities can be related using image interaction matrix  $L$

$$\dot{r} = LV$$

where  $\dot{r} \in \mathbb{R}^{2n}$ , and  $n$  is the number of features.  $V \in \mathbb{R}^6$ , representing three translational and three rotational components

$$\dot{r} = [x_1 \quad \dot{y}_1 \quad \dots \quad \dot{x}_n \quad \dot{y}_n]^T$$

$$V = [v_x \quad v_y \quad v_z \quad \omega_x \quad \omega_y \quad \omega_z]^T$$

$$L = \begin{bmatrix} -\frac{f}{Z_1} & 0 & \frac{x_1}{Z_1} & \frac{x_1 y_1}{f} & \frac{-(f^2 + x_1^2)}{f} & y_1 \\ 0 & -\frac{f}{Z_1} & \frac{y_1}{Z_1} & \frac{(f^2 + y_1^2)}{f} & \frac{-x_1 y_1}{f} & -x_1 \\ \vdots & \vdots & \vdots & \vdots & \vdots & \vdots \\ -\frac{f}{Z_n} & 0 & \frac{x_n}{Z_n} & \frac{x_n y_n}{f} & \frac{-(f^2 + x_n^2)}{f} & y_n \\ 0 & -\frac{f}{Z_n} & \frac{y_n}{Z_n} & \frac{(f^2 + y_n^2)}{f} & \frac{-x_n y_n}{f} & -x_n \end{bmatrix}.$$

Here,  $x_n$  and  $y_n$  are coordinates of the  $n$ th point of interest;  $Z_n$  represents the distance from the center of the camera to the  $n$ th feature point. The focal length is represented by  $f \in \mathbb{R}^+$ . In this paper, we used a monocular camera fixed rigidly to the follower autonomous ground vehicle (AGV), and placed a marker on the target AGV.  $L_{mr}$  and  $v_{mr}$  are obtained from  $L$  and  $V$  by setting one linear and two angular velocities to zero. Hence, the relation between camera motion and feature motion can be represented by (1)

$$\dot{r} = L_{mr} v_{mr} \quad (1)$$

where  $L_{mr}$  and  $v_{mr}$  are the particular cases for the mobile ground vehicle

$$L_{mr} = \begin{bmatrix} -\frac{f}{Z_1} & 0 & \dots & -\frac{f}{Z_n} & 0 \\ \frac{x_1}{Z_1} & \frac{y_1}{Z_1} & \dots & \frac{x_n}{Z_n} & \frac{y_n}{Z_n} \\ -\frac{(f^2 + x_1^2)}{f} & -\frac{x_1 y_1}{f} & \dots & -\frac{(f^2 + x_n^2)}{f} & -\frac{x_n y_n}{f} \end{bmatrix}^T$$

$$v_{mr} = [v_x \quad v_z \quad \omega_y]^T.$$

### B. Vision Augmented Model

Using Fig. 1, the nonlinear kinematic model of the nonholonomic robot is defined as follows:

$$\dot{x} = v_r \cos(\theta); \quad \dot{y} = v_r \sin(\theta); \quad \dot{\theta} = \omega_r$$

where  $X = (x, y, \theta)$  is the robot position and orientation in world reference frame, and the pair  $(v_r, \omega_r)$  is the control input encompassing the linear and angular velocities. This model can

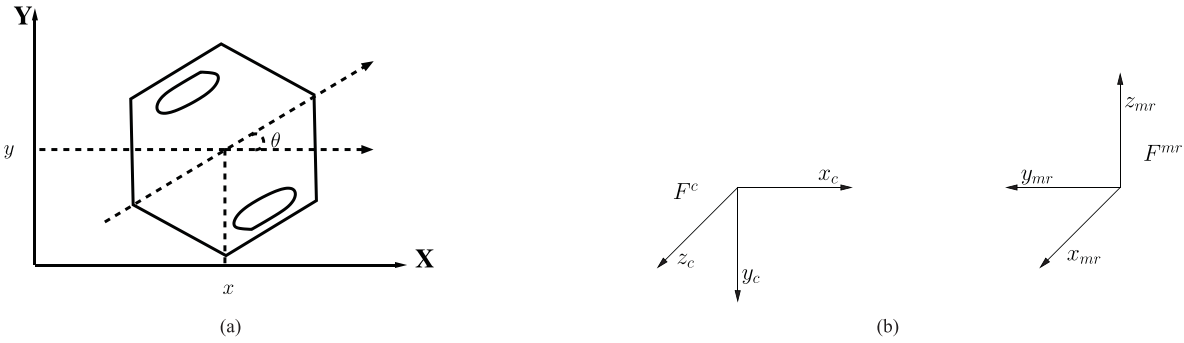


Fig. 1. Coordinate frames. (a) Unicycle model of the mobile robot. (b) Camera and mobile robot frames.

be represented in the following vector form:

$$\dot{X} = \mathbf{J}_{mr} u \quad (2)$$

where

$$\dot{X} = [\dot{x} \ \dot{y} \ \dot{\theta}]^T, \quad u = [v_r \ \omega_r]^T, \quad \mathbf{J}_{mr} = \begin{bmatrix} \cos(\theta) & 0 \\ \sin(\theta) & 0 \\ 0 & 1 \end{bmatrix}.$$

1) *Coordinate Systems*: Let \$F^{mr}\$ and \$F^c\$ denote the robot frame and the camera frame, respectively. The notation \$R\_{mr}^c\$ is used to denote a transformation matrix from coordinate frame \$F^{mr}\$ to coordinate frame \$F^c\$. The transformation matrix is given below

$$R_{mr}^c = \begin{bmatrix} 0 & -1 & 0 \\ 1 & 0 & 0 \\ 0 & 0 & -1 \end{bmatrix}$$

$$v_{mr} = R_{mr}^c \dot{X}. \quad (3)$$

With the help of (1), (2), and (3), the following vector form is obtained:

$$\dot{r} = \mathbf{J}u. \quad (4)$$

We define \$\mathbf{J}\$ to directly relate feature motion to the vehicle motion as the product of \$L\_{mr}\$, \$R\_{mr}^c\$, and \$\mathbf{J}\_{mr}

$$\mathbf{J} = \begin{bmatrix} (x_1 \cos(\theta) + f \sin(\theta))/Z_1 & (f^2 + x_1^2)/f \\ y_1 \cos(\theta)/Z_1 & x_1 y_1/f \\ \vdots & \vdots \\ (x_n \cos(\theta) + f \sin(\theta))/Z_n & (f^2 + x_n^2)/f \\ y_n \cos(\theta)/Z_n & x_n y_n/f \end{bmatrix}.$$

Let \$Y\_n\$ represents the height of the \$n\$th feature of interest. The above-mentioned model can be simplified using planar motion constraint, as follows:

$$\mathbf{J} = \begin{bmatrix} (x_1 y_1 \cos(\theta) + f y_1 \sin(\theta))/Y_1 & (f^2 + x_1^2)/f \\ y_1^2 \cos(\theta)/Y_1 & x_1 y_1/f \\ \vdots & \vdots \\ (x_n y_n \cos(\theta) + f y_n \sin(\theta))/Y_n & (f^2 + x_n^2)/f \\ y_n^2 \cos(\theta)/Y_n & x_n y_n/f \end{bmatrix}.$$

2) *Problem Statement*: Given (4), the VS problem is formulated to address the following questions.

- 1) How do we avoid the requirement of depth information?
- 2) How do we adapt the sliding surface parameters to ensure finite-time convergence?

- 3) How do we enable the robot to reach the home location when the visual marker momentarily goes out of the camera's FOV?

The problem is formally stated as follows.

Design and implement a hybrid scheme for robust VS to enable the follower AGV to reach the home location even when the visual marker momentarily goes out of camera FOV.

### III. CONTROL DESIGN

#### A. Finite-Time Fractional Order Adaptive Sliding Surface

Error vector is defined as \$e = r - r^d\$. Here, \$r^d\$ represents the vector of desired image features and is given by

$$r^d = [x_1^d \ y_1^d \ \dots \ x_n^d \ y_n^d]^T.$$

Consider a fractional order sliding surface defined as follows:

$$s = \lambda_1 e + \hat{\lambda}_2 \int e dt + \hat{\lambda}_3 D^{\alpha-1} e. \quad (5)$$

*Definition 1*: The fractional order derivative has been approximated using Grunwald–Letnikov method [27]. The Grunwald–Letnikov derivative of order \$\alpha > 0\$ of a function \$f(t)\$ is given below

$$D^\alpha f(t)|_{t=N\Delta t} = \lim_{\Delta t \rightarrow 0} \frac{1}{\Delta t^\alpha} \sum_{j=0}^N (-1)^j \binom{\alpha}{j} f(N\Delta t - j\Delta t) \quad (6)$$

where \$\binom{\alpha}{j}\$ is a binomial coefficient, \$\Delta t\$ is the sampling time, and \$N\$ indicates the \$N\$th instant. Control input can be designed as

$$u = -\frac{\mathbf{J}^+}{\lambda_1} (\hat{\lambda}_3 D^\alpha e + \hat{\lambda}_2 e - \lambda_1 \dot{r}^d + k \tanh(\gamma s)) \quad (7)$$

where \$\mathbf{J}^+\$ is the pseudo-inverse of \$\mathbf{J}

$$k = \text{diag}\{k_1, k_2, \dots, k_{2n}\}; s = [s_1, s_2, \dots, s_{2n}]^T$$

$$\tanh(\gamma s) = [\tanh(\gamma s_1), \tanh(\gamma s_2), \dots, \tanh(\gamma s_{2n})]^T.$$

To improve the sliding precision, we have proposed the adaptive tuning laws for updating the parameters of the proposed fractional order sliding surface, which requires only the image features error as shown in Fig. 2. The novel adaptation laws are derived to ensure the finite-time stability of the system.

*Lemma 1*: [28] For the given system, \$\dot{x} = f(x)\$, \$f(0) = 0\$, \$x(0) = x^0\$, \$x \in \mathbb{R}^n\$, suppose that there exists a positive definite continuous function \$V(x)\$ in the neighborhood of the origin,

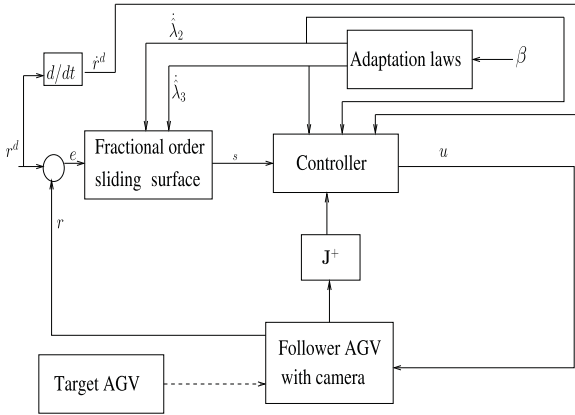


Fig. 2. Schematic diagram of our proposed scheme.

real number  $k > 0$ ,  $\alpha \in (0, 1)$ , so that  $\dot{V}(x) + cV^\alpha(x) \leq 0$ , thus, the system is finite-time stable and settling  $T$  is such that  $T \leq \frac{V^{1-\alpha}(x(0))}{c(1-\alpha)}$ .

**Theorem 1:** For the given system with the kinematics as defined in (4), with sliding surface defined in (5), the control law is given by

$$u = -\frac{\mathbf{J}^+}{\lambda_1}(\hat{\lambda}_3 D^\alpha e + \hat{\lambda}_2 e - \lambda_1 \dot{r}^d + k \tanh(\gamma s)) \quad (8)$$

that can make the system finite-time stable, i.e., the system error converges to the origin in finite time, if the parameters of the sliding surface are updated using the following update laws:

$$\dot{\hat{\lambda}}_2 = -\beta(D^{\alpha-1}e)^T \quad (9)$$

$$\dot{\hat{\lambda}}_3 = \beta \left( \int edt \right)^T \quad (10)$$

where  $\beta \in \Re^n$ .

*Proof:* Consider the Lyapunov function

$$V(s) = \frac{1}{2}s^T s \quad (11)$$

taking the derivative

$$\dot{V}(s) = s^T \dot{s}. \quad (12)$$

Let's evaluate  $\dot{s}$

$$\begin{aligned} \dot{s} &= \lambda_1 \dot{e} + \dot{\hat{\lambda}}_2 \int edt + \hat{\lambda}_2 e + \dot{\hat{\lambda}}_3 D^{\alpha-1} e + \hat{\lambda}_3 D^\alpha e \\ &= \lambda_1(\dot{r} - \dot{r}^d) + \dot{\hat{\lambda}}_2 \int edt + \hat{\lambda}_2 e + \dot{\hat{\lambda}}_3 D^{\alpha-1} e + \hat{\lambda}_3 D^\alpha e \\ &= \lambda_1(\mathbf{J}u - \dot{r}^d) + \dot{\hat{\lambda}}_2 \int edt + \hat{\lambda}_2 e + \dot{\hat{\lambda}}_3 D^{\alpha-1} e + \hat{\lambda}_3 D^\alpha e. \end{aligned}$$

Substituting for  $u$  using (7)

$$\dot{s} = -k \tanh(\gamma s) + \dot{\hat{\lambda}}_2 \int edt + \dot{\hat{\lambda}}_3 D^{\alpha-1} e. \quad (13)$$

Substituting for  $\dot{s}$  in (12) using (13)

$$\dot{V}(s) = s^T \left[ -k \tanh(\gamma s) + \dot{\hat{\lambda}}_2 \int edt + \dot{\hat{\lambda}}_3 D^{\alpha-1} e \right].$$

If the sliding surface parameters are updated using (9) and (10), then

$$\begin{aligned} \dot{V}(s) &= -s^T k \tanh(\gamma s) \\ &\leq -\lambda_{\min}(k) s^T \tanh(\gamma s) \\ &\leq -\lambda_{\min}(k) \|s\| \\ &\leq -\lambda_{\min}(k) \sqrt{(s^T s)} \\ &\leq -\lambda_{\min}(k) \sqrt{2(V(s))} \\ \dot{V}(s) + \lambda_{\min}(k) \sqrt{2(V(s))} &\leq 0. \end{aligned}$$

By the Lemma 1 for finite-time stability, the system is finite-time stable and the system error converges to the origin in finite time, which is given by  $T \leq \frac{\sqrt{2V(s(0))}}{\lambda_{\min}(k)}$ . ■

A conventional sliding mode controller is taken to compare the performance of the proposed strategy.

### B. Conventional Sliding Mode Controller

Sliding surface is chosen as  $s = r - r^d$ . Control input can be designed as

$$u = \mathbf{J}^+(\dot{r}^d - k \operatorname{sgn}(\gamma s)). \quad (14)$$

To reduce the chattering problem, the discontinuous signum function is replaced by a continuous smooth approximation, i.e., hyperbolic tangent function.

## IV. HYBRID SCHEME FOR THE ROBUST VS

### A. Search Mode

In an eye-in-hand system, the features move toward the right when we give a positive angular velocity to the mobile robot. Suppose that this positive velocity (as a disturbance) takes the marker away from the FOV. Evidently, VS can operate only when the marker lies in the FOV. We allow for the possibility of a sufficiently large and sudden disturbance that can disrupt the robot sufficiently to displace the marker entirely out of the FOV in the time between two consecutive frames. It is precisely such a situation that our approach comes into play. By maintaining a record of the current direction of marker's motion, the algorithm explores further, beyond the current FOV until the marker is found. Once the marker is seen again, the visual servo algorithm can proceed, so it is absolutely essential to bring the marker back in the FOV for the VS to resume. We, therefore, design a hybrid approach that includes an optical flow based control law as follows to bring the marker back in FOV. The blocks constituting the hybrid approach are seen in Fig. 4. Here, we present the conditional flow based search mode

$$u_N = \begin{bmatrix} 0 & -\rho \operatorname{sgn} \left( \frac{x_N + y_N - (x_{N-1} + y_{N-1})}{\Delta t} \right) \end{bmatrix}^T \quad (15)$$

where  $\rho(0 < \rho < 1)$  is a scaling factor. Subscript  $N$  indicates the  $N$ th instant;  $\operatorname{sgn}$  indicates the signum function, it is defined as

$$\operatorname{sgn}(b) = \begin{cases} 1; & b > 0 \\ 0; & b = 0 \\ -1; & b < 0. \end{cases} \quad (16)$$

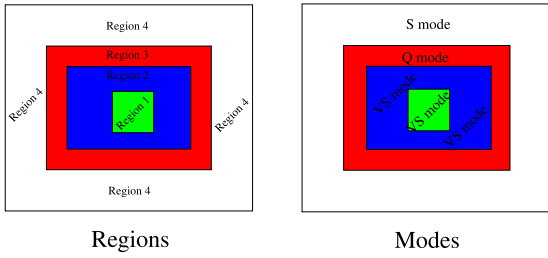


Fig. 3. Various regions and modes to implement hybrid approach.

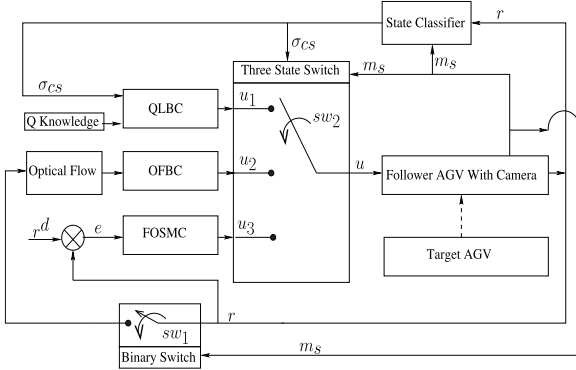


Fig. 4. Block diagram of a robust hybrid control scheme.

Since,  $-\rho \leq u_N \leq \rho$ , it also means that both the control inputs of the mobile robot designed here are bounded.

### B. Reinforcement Learning Mode

For this part, we proceed along the lines of [13] with appropriate modifications. An important simplification we make is to obviate the need for depth from a sensor. On the other hand, since we consider and accommodate the possibility of the marker entirely disappearing from the FOV during the experiment, we need to provide for a new binary variable called the marker (visibility) status  $m_s$ .

The entire image plane is divided into four different regions, as shown in Fig. 3. Each region is considered as a separate state to implement reinforcement learning. Let us define a set  $C = \{1, 2, 3, 4\}$ . Then, a set of states can be represented as  $\sigma = \{\sigma_i\}$ ,  $i \in C$ . An image point is converted into the grid point as  $(x_{gr}, y_{gr}) = INT((x/80, y/80))$  and then respective state is logically assigned as follows:

$$\sigma(x_{gr}, y_{gr}, m_s) = \begin{cases} \sigma_4; & m_s = 0 \\ \sigma_1; & (m_s = 1) \wedge ((x_{gr}, y_{gr}) \in \sigma_1) \\ \sigma_3; & (m_s = 1) \wedge ((x_{gr}, y_{gr}) \in \sigma_3) \\ \sigma_2; & \text{elsewhere} \end{cases} \quad (17)$$

where the marker status is denoted by  $m_s$ . In subscript  $gr$  indicates the grid point. A set of actions is defined as  $A = \{a_j\}$ ,  $j \in C$ . There are four possible actions. At each state, the follower AGV can take any one of the following actions:

$$a_i = \begin{cases} v = 0.1 \text{ m/s}, \omega = 0.0 \text{ rad/s}; & i = 1 \\ v = -0.1 \text{ m/s}, \omega = 0.0 \text{ rad/s}; & i = 2 \\ v = 0.0 \text{ m/s}, \omega = 0.1 \text{ rad/s}; & i = 3 \\ v = 0.0 \text{ m/s}, \omega = -0.1 \text{ rad/s}; & i = 4. \end{cases} \quad (18)$$

We update the state after each action. The reward ( $R$ ) is then assigned as

$$R(\sigma) = \begin{cases} 200; & \sigma \in \sigma_1 \\ 0; & \sigma \in \sigma_2 \\ -10; & \sigma \in \sigma_3 \\ -20; & \sigma \in \sigma_4. \end{cases} \quad (19)$$

The knowledge of  $Q$  is updated as

$$Q(\sigma_{cs}, a_k) = (1 - \eta)Q(\sigma_{cs}, a_k) + \eta(R + \gamma_q \max(Q(\sigma_{ns}, a_1), Q(\sigma_{ns}, a_2), Q(\sigma_{ns}, a_3), Q(\sigma_{ns}, a_4))) \quad (20)$$

where  $\gamma_q$  ( $0 < \gamma_q < 1$ ) is a discount factor;  $\eta$  ( $0 < \eta < 1$ ) indicates the learning rate. The current state and the next state are represented by  $\sigma_{cs}$  and  $\sigma_{ns}$ , respectively.

### C. Robust and Effective Solution for Visibility Problem

In Fig. 4,  $Q$ -learning-based controller (QLBC) and optical flow based controller (OFBC) are combined with FOSMC-based VS mode to obtain robust performance. QLBC is a knowledge-based controller, which is responsible for centering the feature point. Knowledge of this controller is a learned  $Q$  matrix during the training. OFBC captures the direction of the feature point's movement. It does not demand the entire history of the feature point; instead, it utilizes previous and current states only. The role of the OFBC is to bring the marker back in the FOV. Operation of the FOSMC is based on the target and current feature values. This controller is responsible for tuning the sliding surface parameters in such a way that finite-time convergence is guaranteed. The hybrid scheme is a tri-mode operation. Different modes of hybrid approach are shown in Fig. 3. The search mode (S mode) brings the marker back in the FOV. Further, the speed of the search can be varied by  $\rho$ . Reinforcement learning mode ( $Q$  mode) pushes the feature point toward the region 1. In Fig. 4, the control input  $u$  depends on the position of the switch  $sw_2$ . The logic for selection of the appropriate  $u$ , considerably changed from [13], is given below

$$u(x_{gr}, y_{gr}, m_s) = \begin{cases} u_2; & m_s = 0 \\ u_1; & (x_{gr}, y_{gr}) \in \sigma_3 \\ u_3; & \text{elsewhere.} \end{cases} \quad (21)$$

Binary switch  $sw_1$  plays an essential role to accomplish the task of search mode. Switch  $sw_1$  opens only when  $m_s = 0$ . Our hybrid scheme selects the appropriate controller based on marker status and the feature state. FOSMC-based action drives the robot until the feature point is in region 1 or region 2. When it is in region 3, then  $Q$  mode will activate to push the feature point toward region 1. When the disturbance is more powerful, and pushes the point in region 4, the marker status is reset and S mode activates to bring the marker back in the FOV. To summarize, each control mode serves a specific function: the S mode takes over to bring the marker back into the FOV, when the marker is reset. The  $Q$  mode activates for centering the feature point, when the marker is set, but the feature is not centered. Finally, the FOSMC operates to ensure finite-time convergence and to auto tune the surface parameters.

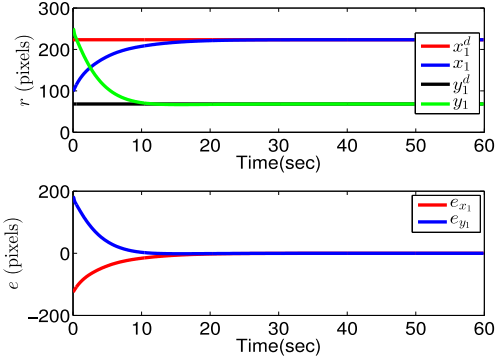


Fig. 5. Simulation: Feature tracking and error response.

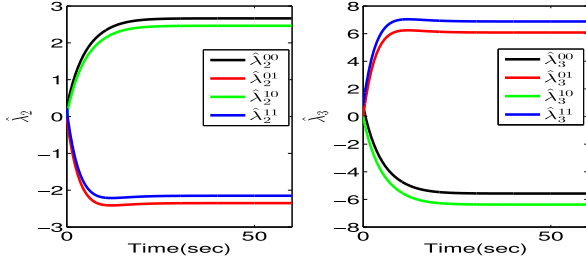
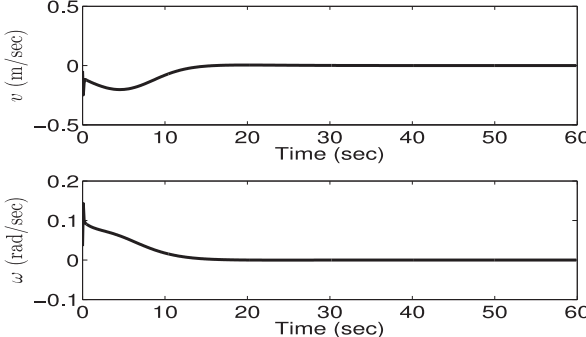
Fig. 6. Simulation: Tuning response of  $\hat{\lambda}_2$  and  $\hat{\lambda}_3$ .

Fig. 7. Simulation: Linear and angular velocities.

## V. RESULTS AND DISCUSSIONS

### A. Simulation Results

1) *IBVS Using the FOSMC*: We have analyzed the performance of the proposed approach in different situations to check the robustness and adaptive response of the parameters. In ordinary case, the target and current features are set at  $(223.491, 68.3107)^T$  and  $(100, 250)^T$ , respectively. Feature tracking and error response can be seen in Fig. 5. Fig. 6 shows the tuning response of  $\hat{\lambda}_2$  and  $\hat{\lambda}_3$ . Control inputs are given in Fig. 7. To test the performance of the proposed algorithm in the presence of noise, we added Gaussian noise with zero mean and a unit variance with current feature values in between the time interval  $(30 \leq t \leq 40)$ , where  $t$  is the time dimension. Feature tracking in the presence of noise is shown in the first subplot of Fig. 8. Profiles for linear and angular velocities are highlighted using red color in Fig. 9. Noise effect can be seen in Fig. 9. As a constant disturbance, we added 10 pixels in current feature values in two different time intervals ( $24 \leq t \leq 25$ ) and ( $39 \leq t \leq 40$ ). Feature tracking in the presence of constant

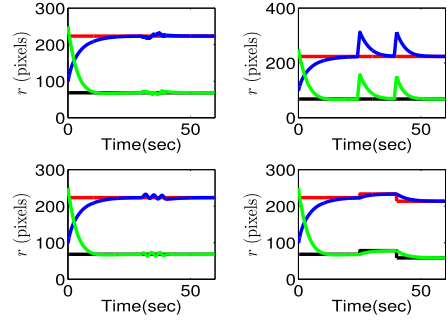
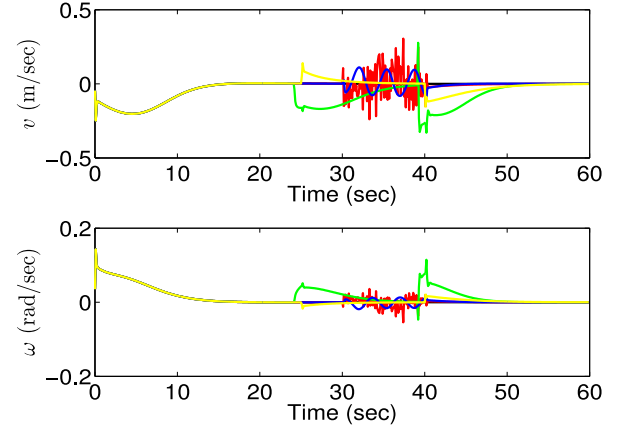
Fig. 8. Simulation: Feature tracking in various cases ( $x_1^d$  by red color;  $x_1$  by blue color;  $y_1^d$  by black color; and  $y_1$  by green color).

Fig. 9. Simulation: Linear and angular velocities in various cases (noisy case: by red color; constant disturbance case: by green color; sinusoidal disturbance case: by blue color; and target perturbation case: by yellow color).

disturbance is shown in the second subplot of Fig. 8. Obtained profiles in this case are plotted with green color in Fig. 9. The performance of the proposed algorithm has also been tested in the presence of sinusoidal disturbance. In the time interval from  $t = 30$  to  $t = 40$  s,  $\sin(0.6t)$  and  $\cos(0.6t)$  are added with  $x$  and  $y$ , respectively. Feature tracking in the presence of sinusoidal disturbance is shown in Fig. 8. With the help of blue color, the sinusoidal disturbance effect can be noticed in Fig. 9. We have changed the position of the target point twice in different directions at  $t = 25$  and  $t = 40$  s. Robustness with respect to the perturbed target location in feature plane can be seen using fourth subplot of Fig. 8. Control input profiles over the time are shown in Fig. 9 with yellow color. Adaptive nature of sliding surface parameters in various cases can be seen with the help of Figs. 10 and 11. In order to show the tuning drift of the adapted sliding surface parameters, the simulation is repeated with three different initial conditions, and the corresponding tuning responses of  $\hat{\lambda}_2$  and  $\hat{\lambda}_3$  are given in Figs. 12 and 13, respectively. From this, it can be seen that the gains are settling to different nominal values at different operating conditions.

2) *Hybrid Scheme*: Marker status and state of the feature point are shown in Fig. 14. In Fig. 15, VS mode is utilized till the feature is in the region of interest. The operation of this mode is shown using green color.  $Q$  mode activates when the feature point is in third region. The blue color indicates the operation of the reinforcement learning mode. When the marker goes out

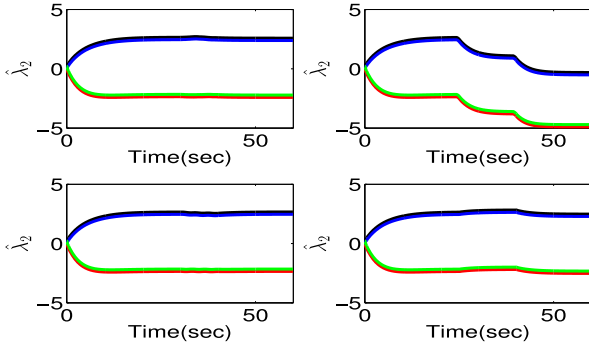
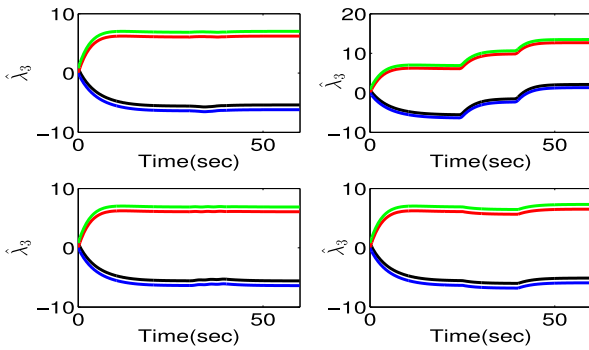
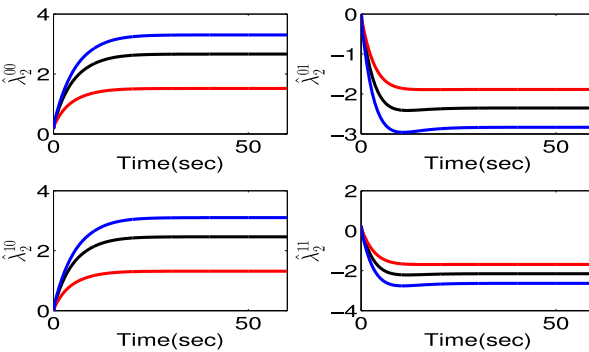
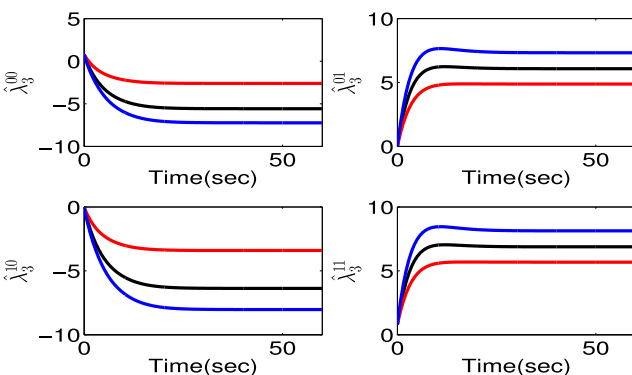
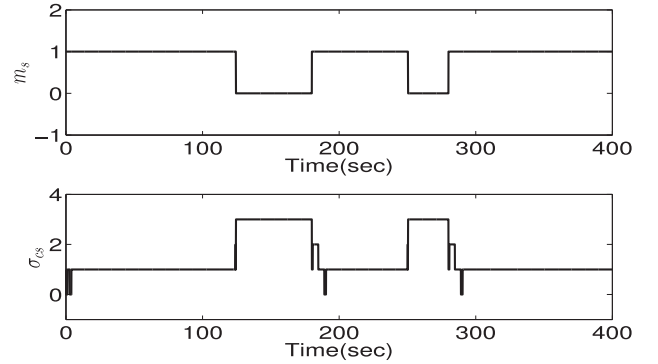
Fig. 10. Simulation: Tuning response of  $\hat{\lambda}_2$  in various cases.Fig. 11. Simulation: Tuning response of  $\hat{\lambda}_3$  in various cases.Fig. 12. Simulation: Tuning response of  $\hat{\lambda}_2$  at different operating conditions.Fig. 13. Simulation: Tuning response of  $\hat{\lambda}_3$  at different operating conditions.

Fig. 14. Simulation: Marker status and state of feature (first subplot: marker status over the time and second subplot: state of the feature point over the time).

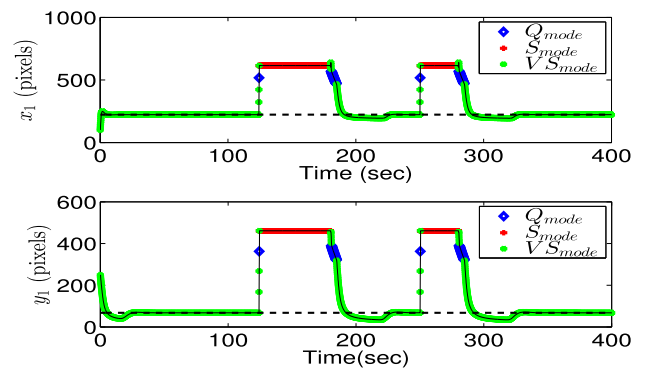
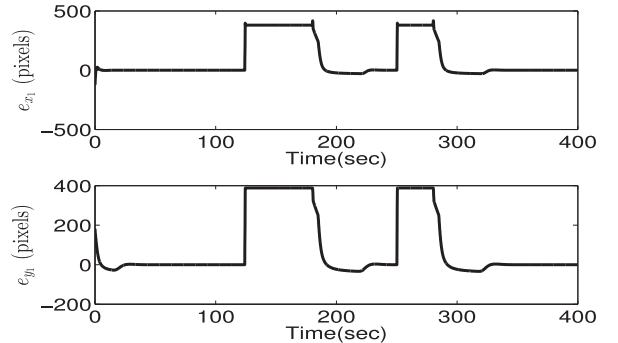
Fig. 15. Simulation: Feature tracking (green color: by IBVS using the FOSMC; blue diamond: by  $Q$  mode; red plus: by search mode; and dashed black line: desired value).

Fig. 16. Simulation: Error response using hybrid scheme.

of the FOV, search mode will activate. The operation of the search mode is highlighted using red color. With the help of Figs. 14–16, it can be inferred that based on the feature's state, the appropriate controller is activated to ensure the convergence even when marker is momentarily gone out of view due to external disturbances. Profiles of linear and angular velocities using the hybrid scheme are shown in Fig. 17.

### B. Hardware Description and Experimental Results

The real-time experimentations are performed using Pioneer P3-DX robots, as shown in Table I. They are differential driven nonholonomic robots equipped with onboard PC running on

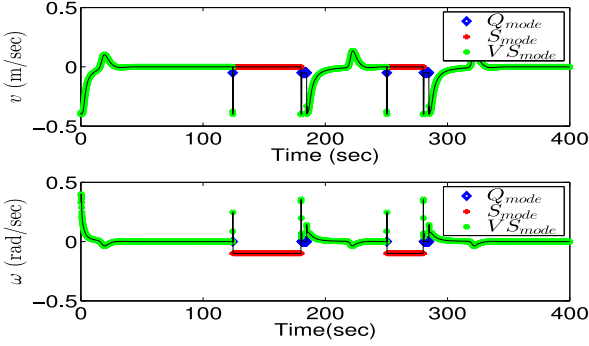


Fig. 17. Simulation: Control inputs (green color: by IBVS using the FOSMC; blue diamond: by  $Q$  mode; and red plus: by search mode).

TABLE I  
EXPERIMENTAL SETUP



Ubuntu platform, sonars, encoders, etc., weighing around 16 kg. Follower AGV is equipped with a webcam and laptop, whereas target AGV has an onboard XU3 system with WiFi module 3. Both the platforms are running on Linux environment, with robot operating system (ROS). In Pioneer mobile robots, the user writes the code at the higher level layer, which accepts  $v_r$  and  $\omega_r$  as control inputs. For such systems, user deals with outer loop, i.e.,  $v_r$  and  $\omega_r$  are the control inputs for the system, and  $x$ ,  $y$ , and  $\theta$  represent the state of the system. This is one of the reasons for incorporating the unicycle model in this paper. Camera specifications are as follow: FOV =  $60^\circ$ ,  $f = 4$  mm, resolution =  $640 \times 480$ . There are three main concerns in context to the camera, which are as follows.

- 1) Fixing the camera on the follower AGV: It should be adequately fixed using some adhesive material like double sideband, or it can also be attached using a mounting stand. There should be no relative motion between the follower AGV and its camera.
- 2) Lighting conditions: In indoor environments, lighting does not change continuously but in outdoor, it is good to use autofocus and auto gain camera to avoid inconvenience due to continuous change in lighting conditions.
- 3) Frame rate: More than ten fps (frames per second).

In short, it is good to have an auto gain and high frame rate camera that should be fixed properly on the follower AGV to achieve robust performance in both indoor and outdoor environments. For experiments, Aruco marker [29] is placed on the target AGV. The OpenCV library enables us to detect the top left corner of the marker in the image plane. The readings obtained for the feature of interest are noisy, hence, data from the camera are filtered using a low-pass filter. The entire

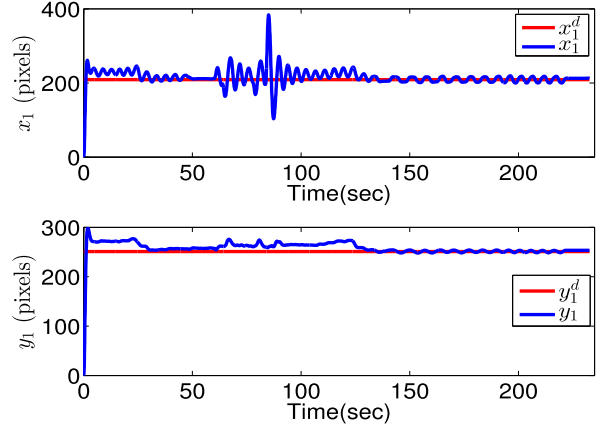


Fig. 18. Experiment: Feature tracking.

code for this experiment runs on laptop. RosAria is used to perform all required two-way communication between the onboard computer and the AGV. The RosAria node provides a ROS interface for mobile robot bases. The RosAria package uses the ARIA library from MobileRobots to communicate with robot and robot-specific integrated devices. More details can be found at <http://wiki.ros.org/ROSARIA>. Reliability of the communication protocol depends on the following.

- 1) DB9 serial connector: There should not be any loose connection.
- 2) Batteries backup of target AGV, follower AGV, on board computer (OBC), and laptop as well: All power batteries should be charged enough to perform experiments.
- 3) WiFi connection and ROS network: Its better to use local dedicated network to maintain the network strength throughout the experiments.

Prior check for bidirectional data communication among all subsystems has to be done. OBC and laptop should have Linux and ROS as well. These systems should be on the same network. In order to initiate the different ROS nodes running on the onboard computer, the user remotely logs into the system via a WiFi network. The different nodes are then executed by doing an secure shell (SSH) into the system.  $\theta$  is obtained using odometry of the follower AGV. The experimental parameters are chosen as follows:  $\Delta t = 0.1$  s,  $\lambda_1 = 0.8$ ,  $Y_1 = 0.59$  m,  $\eta = 0.8$ ,  $\gamma_q = 0.9$ ,  $\rho = 0.1$ ,  $\alpha = 0.5$ ,  $\gamma = 0.1$ , and  $k = \text{diag}\{0.5, 0.1\}$ .

1) *IBVS Using the FOSMC*: Two different cases are tested in a single experiment. Initially, we have fixed the position of the target AGV and the follower AGV has to simply reach the target. The response of the proposed scheme can be seen with the help of Figs. 18–21 in the range from  $t = 0$  to  $t = 48$  s. The results indicate that the follower is able to reach the target in a very short span of time ( $t < 50$  s). After that we have considered a moving target in which the follower AGV has to follow the target AGV. The response can be viewed with the help of Figs. 18–21 in the range from  $t = 60$  to  $t = 200$  s. Fig. 18, shows that the follower is able to reach and then follow the target satisfactorily. The error responses in the image plane, expressed in pixels, are shown in Fig. 19. The tuning responses of  $\hat{\lambda}_2$  and  $\hat{\lambda}_3$  are given in Figs. 22 and 23, respectively. From this, it is clear that the gains are settling to different nominal values in each case. The position of follower AGV with respect to the target AGV can be seen using the first and second subplot of Fig. 20. Last subplot of Fig. 20 shows the orientation of the

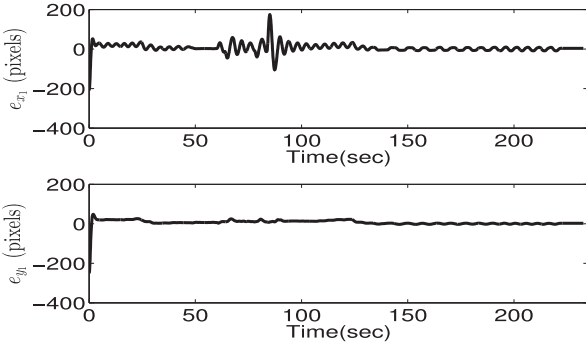


Fig. 19. Experiment: Error response in pixel units.

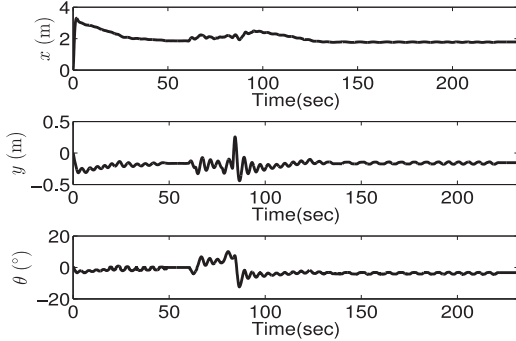


Fig. 20. Experiment: Relative position of the follower AGV with respect to the target AGV and orientation of the follower AGV.

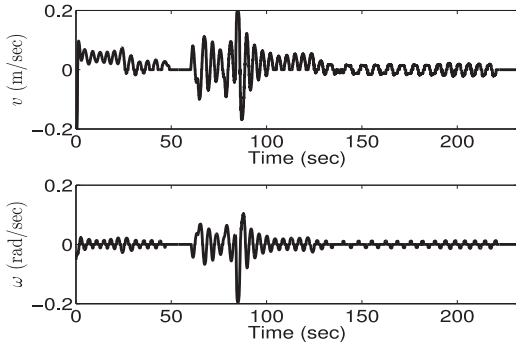
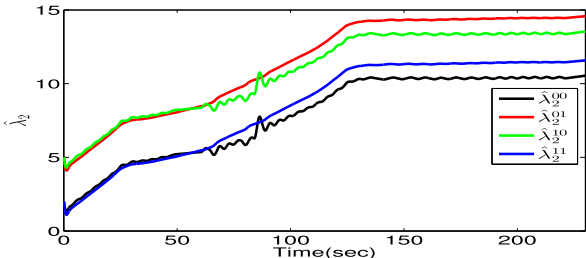
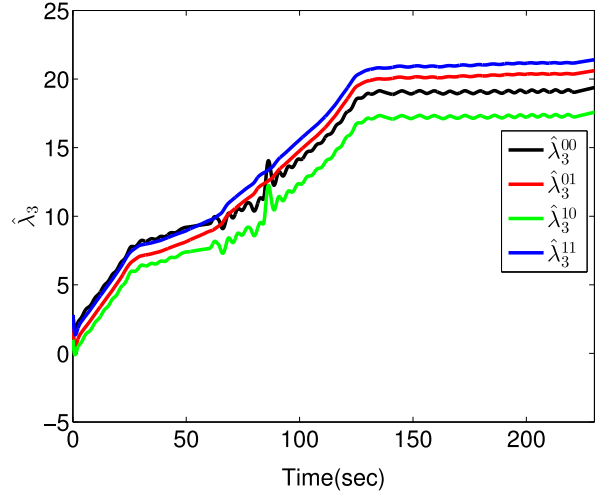
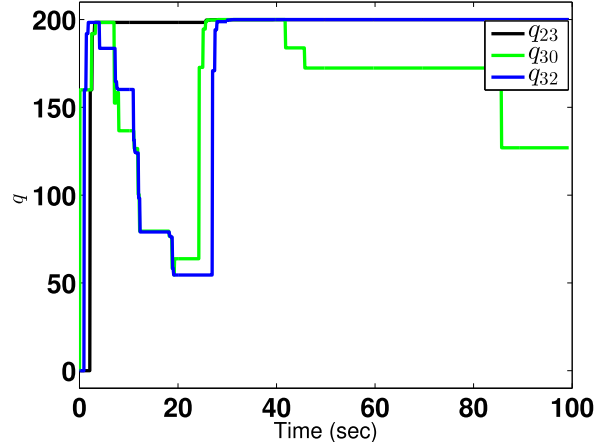


Fig. 21. Experiment: Linear and angular velocities.

Fig. 22. Experiment: Tuning response of  $\hat{\lambda}_2$ .

follower AGV over the time. Linear and angular velocities over the time are plotted in Fig. 21. Zero control efforts can be seen when the follower AGV has achieved the target ( $50 < t < 60$ ), after that the target AGV starts moving, and hence, there are non zero control inputs to follow the target. It can also be noticed that at the end of the experiment ( $t > 230.5$  s), there are zero

Fig. 23. Experiment: Tuning response of  $\hat{\lambda}_3$ .Fig. 24. Experiment: Convergence of some of the elements of the  $Q$  matrix.

control efforts that indicate that the target has been achieved. From the Figs. 18–21, it is evident that the proposed adaptive FOSMC scheme is able to deliver smooth performance. The finite-time stability property of the proposed control scheme is also evident from the results. It can be inferred that the precision in the control switching owing to the adaptive fractional order sliding surface accounts for the smooth performance in both the test cases. The computational cost can be reduced using the IBVS instead of PBVS. The simplicity is the main advantage of the proposed strategy in which we can directly control the motion of the vehicle using feature information on the image plane.

2) *Hybrid Scheme*: First, system goes through offline training to obtain a  $Q$  matrix. Fig. 24 shows the convergence of  $Q$  matrix. It means that the QLBC has learned how to select the correct action for each state [13]. After training, convergence can be judged in terms of task achieved. If VS mode always follows the  $Q$  mode, provided there is no severe disturbance during the  $Q$  mode operation. It also means that the QLBC adequately achieves the assigned task. Training results of  $Q$ -learning algorithm are shown in Fig. 24. The convergence is achieved, which can be seen using Fig. 24. This also means that the  $Q$  controller has learned that how to choose the correct action. After training, the response of

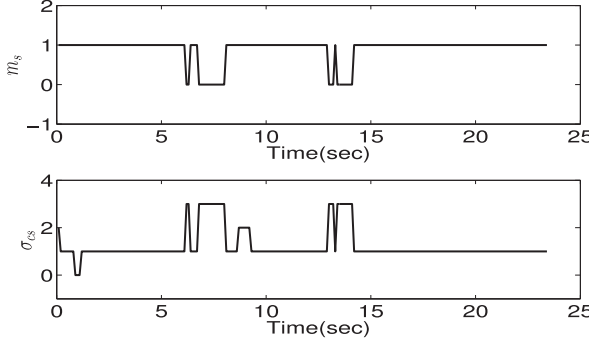


Fig. 25. Experiment: Marker status and state of feature (first subplot: marker status over the time and second subplot: state of the feature point over the time).

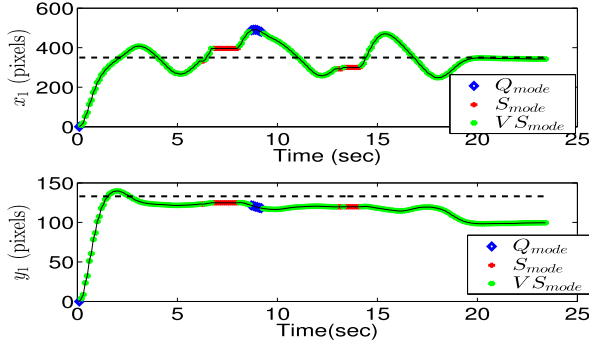


Fig. 26. Experiment: Feature tracking (green color: by IBVS using the FOSMC; blue diamond: by  $Q$  mode; red plus: by search mode; and dashed black line: desired value).

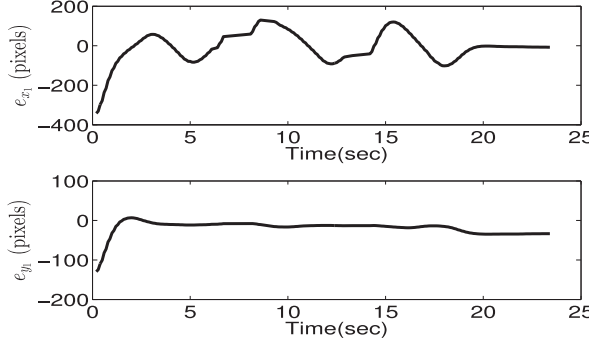


Fig. 27. Experiment: Error response using hybrid scheme.

$Q$ -learning is based on the obtained  $Q$  matrix. First subplot of Fig. 25 indicates the status of the marker. Initially,  $m_s = 1$ , which means that the marker is in the FOV. The mobile robot is driven using the FOSMC provided the feature point is either in region 1 or in region 2. In between the experiment, severe disturbances are applied to the follower AGV until marker is out to check its robustness, hence, the marker status will be reset. This response can be seen using Fig. 25. Search mode is activated to bring the marker back in the FOV. Search mode operation is highlighted using red color, as shown in Fig. 26. Whenever the feature point moves in region 3,  $Q$  mode will activate. In Fig. 26, blue color is used to highlight the operation of reinforcement learning mode. Error response and control input profiles are given in Figs. 27 and 28, respectively. Position and orientation of the follower AGV are shown in Fig. 29. The proposed approach works well in both indoor

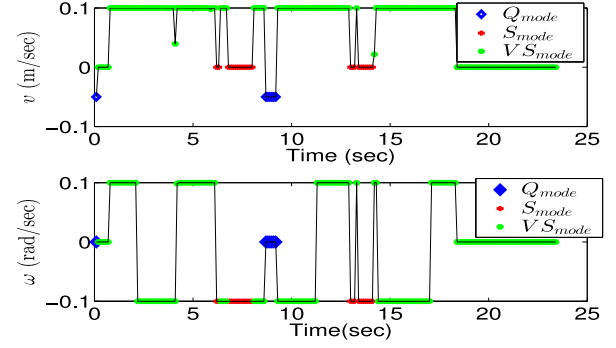


Fig. 28. Experiment: Control inputs (green color: by IBVS using the FOSMC; blue diamond: by  $Q$  mode; and red plus: by search mode).

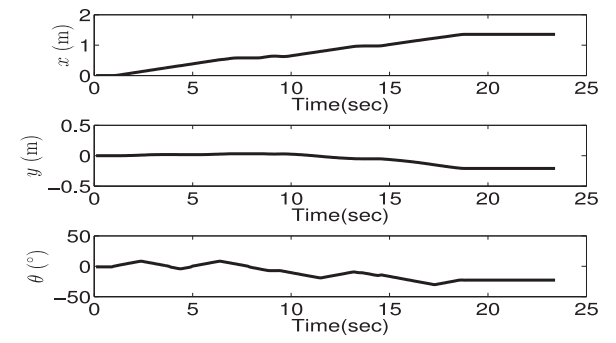
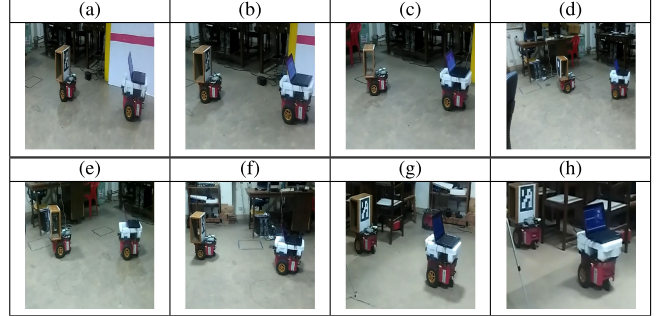


Fig. 29. Experiment: Position and orientation of the follower AGV.

TABLE II  
TAPED VIDEO IMAGE SEQUENCE (INDOOR ENVIRONMENT)



and outdoor environments. The taped video images for indoor and outdoor are shown in Tables II and III, respectively. The YouTube link for the videos recorded during the experiments is given in [30].

Comparison of the proposed FOSMC in relation to the conventional SMC is given in Figs. [30–32]. These results show that the proposed scheme gives smooth performance. Exponential convergence is ensured in [13]. In contrast, the proposed scheme guarantees the finite-time convergence. Scheme in [13] demands the depth of feature. In contrast to this, a depth-free approach is presented in this paper. To check the importance of the search mode along with  $Q$  mode in relation to  $Q$  mode alone [13], we performed two separate experiments. Results of these experiments are shown in Figs. 33 and 34. In Fig. 33, the experiment starts with  $m_s = 1$ , then a known disturbance ( $\omega = -0.2 \text{ rad/s}$ ) is applied to perturb the state of the feature point that causes the switching between  $Q$  and known

TABLE III  
TAPED VIDEO IMAGE SEQUENCE (OUTDOOR ENVIRONMENT)

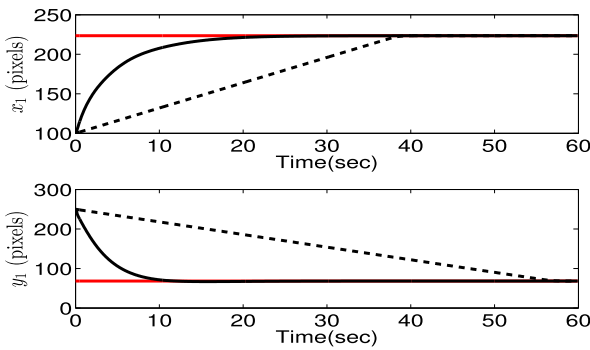
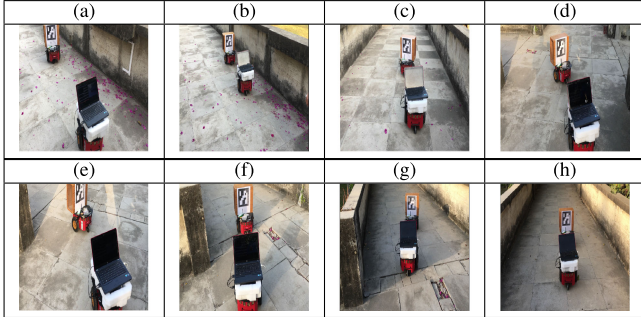


Fig. 30. Comparison: Feature tracking (solid black line: by the proposed method; dashed black line: by the conventional SMC; and red line: desired value).

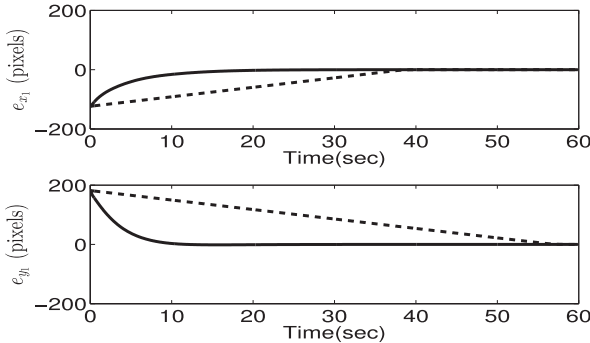


Fig. 31. Comparison: Error response (solid line: by the proposed method and dashed line: by the conventional SMC).

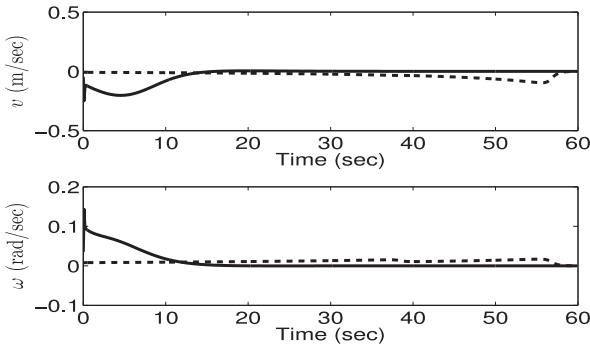


Fig. 32. Comparison: Linear and angular velocities (solid line: by the proposed method and dashed line: by the conventional SMC).

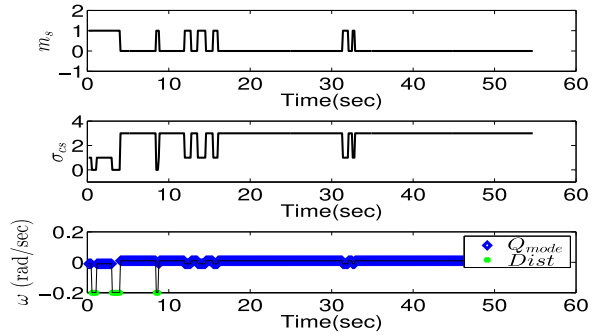


Fig. 33. Experiment: Performance of  $Q$  mode alone.

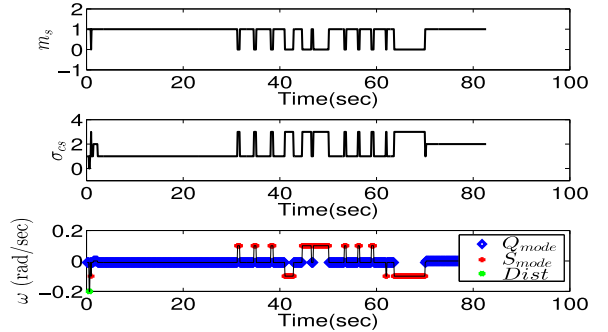


Fig. 34. Experiment: Performance of search mode along with  $Q$  mode.

disturbances. It can be noticed that the small disturbances are adequately handled by  $Q$  mode alone. However, it fails to recover the marker back in the FOV due to severe external disturbances. In Fig. 33,  $m_s$  is reset at  $t = 32.8$  s due to external disturbances and it cannot be recovered till  $t = 54.6$  s. However, in Fig. 34, it can be observed that dual mode ( $Q$  plus search) handles the similar scenario. In Fig. 34,  $m_s$  is reset at  $t = 63.6$  s due to external disturbances and then S mode activates. S mode successfully recovers the marker at  $t = 70$  s. It means that dual mode operation is superior to  $Q$  mode alone. The hybrid scheme is equipped with a heading restoration mechanism to handle the severe disturbances. This mechanism enables the robot to reach the home location even when the marker momentarily goes out from the FOV. It means that the proposed approach also works in a situation when (the region where) the existing VS-based methods fail. Hence, the proposed hybrid scheme increases the stability margins as compared to the existing work [13]. However, there is indeed the underlying assumption that the large disturbances that take the follower into search mode are sporadic and positionally bounded with sufficient time for a return to  $Q$  or VS modes between episodes.

## VI. CONCLUSION

A fractional order SMC approach has been proposed to control the vehicle motion using visual information in the image plane. The lower computational cost, simplicity, robustness, and finite-time convergence are major hall-marks of the proposed strategy. To cope up with the uncertainties in practical applications, novel adaptation rules are designed for tuning the sliding surface parameters, in such a way that the finite-time stability of the system is ensured. This technique performs well for both fixed and moving targets. We have tested this framework in both

indoor and outdoor environments, using vision-based feedback to acquire and then follow the target. For this purpose, a hybrid scheme is designed to solve the visibility problem. The hybrid approach enables the mobile robot to reach the home location even when the marker goes entirely out of view due to severe external disturbances. Both simulation and experimental results confirm the potential of the proposed scheme. This paper is concerned with the kinematic control and trajectory planning. It is assumed that the internal dynamic controller is able to follow the desired trajectory. Incorporation of vehicle dynamics will be done in the next work. The following are some suggested directions to take our work forward: incorporation of on-policy learning instead of off-policy learning in the proposed hybrid scheme; theoretical analysis in the presence of noise; stability analysis of the resultant switched system; multi-sensor and multi-controller output management along with obstacle avoidance.

## REFERENCES

- [1] C.-L. Hwang, C.-W. Lan, and Y.-J. Chou, "Search, track, and kick to virtual target point of humanoid robots by a neural-network-based active embedded vision system," *IEEE Syst. J.*, vol. 9, no. 1, pp. 107–118, Mar. 2015.
- [2] A. Krupa, D. Folio, C. Novales, P. Vieyres, and T. Li, "Robotized tele-echography: An assisting visibility tool to support expert diagnostic," *IEEE Syst. J.*, vol. 10, no. 3, pp. 974–983, Sep. 2016.
- [3] S. Hutchinson, G. D. Hager, and P. I. Corke, "A tutorial on visual servo control," *IEEE Trans. Robot. Automat.*, vol. 12, no. 5, pp. 651–670, Oct. 1996.
- [4] F. Chaumette and S. Hutchinson, "Visual servo control. I. Basic approaches," *IEEE Robot. Automat. Mag.*, vol. 13, no. 4, pp. 82–90, Dec. 2006.
- [5] T. Hamel and R. Mahony, "Visual servoing of an under-actuated dynamic rigid-body system: An image-based approach," *IEEE Trans. Robot. Automat.*, vol. 18, no. 2, pp. 187–198, Apr. 2002.
- [6] B. Li, Y. Fang, and X. Zhang, "Visual servo regulation of wheeled mobile robots with an uncalibrated onboard camera," *IEEE/ASME Trans. Mechatronics*, vol. 21, no. 5, pp. 2330–2342, Oct. 2016.
- [7] X. Zhang, Y. Fang, B. Li, and J. Wang, "Visual servoing of nonholonomic mobile robots with uncalibrated camera-to-robot parameters," *IEEE Trans. Ind. Electron.*, vol. 64, no. 1, pp. 390–400, Jan. 2017.
- [8] M. Gupta, L. Behera, V. K. Subramanian, and M. M. Jamshidi, "A robust visual human detection approach with UKF-based motion tracking for a mobile robot," *IEEE Syst. J.*, vol. 9, no. 4, pp. 1363–1375, Dec. 2015.
- [9] P. I. Corke and S. A. Hutchinson, "A new partitioned approach to image-based visual servo control," *IEEE Trans. Robot. Automat.*, vol. 17, no. 4, pp. 507–515, Aug. 2001.
- [10] N. J. Cowan, J. D. Weingarten, and D. E. Koditschek, "Visual servoing via navigation functions," *IEEE Trans. Robot. Automat.*, vol. 18, no. 4, pp. 521–533, Aug. 2002.
- [11] J. Chen, D. M. Dawson, W. E. Dixon, and V. K. Chitrakaran, "Navigation function-based visual servo control," *Automatica*, vol. 43, no. 7, pp. 1165–1177, 2007.
- [12] N. J. Cowan and D. E. Chang, "Geometric visual servoing," *IEEE Trans. Robot.*, vol. 21, no. 6, pp. 1128–1138, Dec. 2005.
- [13] Y. Wang, H. Lang, and C. W. De Silva, "A hybrid visual servo controller for robust grasping by wheeled mobile robots," *IEEE/ASME Trans. Mechatronics*, vol. 15, no. 5, pp. 757–769, Oct. 2010.
- [14] R. R. Nair, L. Behera, V. Kumar, and M. Jamshidi, "Multisatellite formation control for remote sensing applications using artificial potential field and adaptive fuzzy sliding mode control," *IEEE Syst. J.*, vol. 9, no. 2, pp. 508–518, Jun. 2015.
- [15] Q. Wu and M. Saif, "Robust fault diagnosis of a satellite system using a learning strategy and second order sliding mode observer," *IEEE Syst. J.*, vol. 4, no. 1, pp. 112–121, Mar. 2010.
- [16] S. S.-D. Xu, C.-C. Chen, and Z.-L. Wu, "Study of nonsingular fast terminal sliding-mode fault-tolerant control," *IEEE Trans. Ind. Electron.*, vol. 62, no. 6, pp. 3906–3913, Jun. 2015.
- [17] Y. Wang, L. Gu, Y. Xu, and X. Cao, "Practical tracking control of robot manipulators with continuous fractional-order nonsingular terminal sliding mode," *IEEE Trans. Ind. Electron.*, vol. 63, no. 10, pp. 6194–6204, Oct. 2016.
- [18] S. I. Han, "Prescribed consensus and formation error constrained finite-time sliding mode control for multi-agent mobile robot systems," *IET Control Theory Appl.*, vol. 12, no. 2, pp. 282–290, 2017.
- [19] R. Ravindranathan Nair, H. Karki, A. Shukla, L. Behera, and M. Jamshidi, "Fault-tolerant formation control of nonholonomic robots using fast adaptive gain nonsingular terminal sliding mode control," *IEEE Syst. J.*, vol. 13, no. 1, pp. 1006–1017, Mar. 2019.
- [20] F. Hamerlain, K. Achour, T. Floquet, and W. Perruquetti, "Higher order sliding mode control of wheeled mobile robots in the presence of sliding effects," in *Proc. 44th IEEE Conf. Dec. Control, Eur. Control Conf.*, 2005, pp. 1959–1963.
- [21] D. Cao and J. FEI, "Adaptive fractional fuzzy sliding mode control for three-phase active power filter," *IEEE Access*, vol. 4, pp. 6645–6651, 2016.
- [22] M. B. Delghavi, S. Shoja-Majidabad, and A. Yazdani, "Fractional-order sliding-mode control of islanded distributed energy resource systems," *IEEE Trans. Sustain. Energy*, vol. 7, no. 4, pp. 1482–1491, Oct. 2016.
- [23] D. Nojavan-Zadeh and M. Badamchizadeh, "Adaptive fractional-order non-singular fast terminal sliding mode control for robot manipulators," *IET Control Theory Appl.*, vol. 10, no. 13, pp. 1565–1572, 2016.
- [24] C. Izaguirre-Espinosa, A. J. Munoz-Vazquez, A. Sanchez-Orta, V. Parra-Vega, and P. Castillo, "Attitude control of quadrotors based on fractional sliding modes: Theory and experiments," *IET Control Theory Appl.*, vol. 10, no. 7, pp. 825–832, 2016.
- [25] L. Zhou, D. Wu, J. Chen, and Z. Dong, "Greening the smart cities: Energy-efficient massive content delivery via D2D communications," *IEEE Trans. Ind. Inform.*, vol. 14, no. 4, pp. 1626–1634, Apr. 2018.
- [26] L. Zhou, D. Wu, Z. Dong, and X. Li, "When collaboration hugs intelligence: Content delivery over ultra-dense networks," *IEEE Commun. Mag.*, vol. 55, no. 12, pp. 91–95, Dec. 2017.
- [27] C.-M. Chi and F. Gao, "Simulating fractional derivatives using matlab," *JSW*, vol. 8, no. 3, pp. 572–578, 2013.
- [28] S. Yu, X. Yu, B. Shirinzadeh, and Z. Man, "Continuous finite time control for robotic manipulators with terminal sliding mode," *Automatica*, vol. 41, no. 11, pp. 1957–1964, Nov. 2005.
- [29] S. Garrido-Jurado, R. Muñoz-Salinas, F. J. Madrid-Cuevas, and M. J. Marín-Jiménez, "Automatic generation and detection of highly reliable fiducial markers under occlusion," *Pattern Recognit.*, vol. 47, no. 6, pp. 2280–2292, 2014.
- [30] "Robust hybrid VS using reinforcement learning and finite time adaptive FOSMC," Feb. 2018. [Online]. Available: <https://youtu.be/N0a4gvzheNw>

# DMP Based Trajectory Tracking for a Nonholonomic Mobile Robot With Automatic Goal Adaptation and Obstacle Avoidance

Radhe Shyam Sharma, Santosh Shukla, Hamad Karki, Amit Shukla, Laxmidhar Behera, Venkatesh K S

**Abstract**— Dynamic Movement Primitive (DMP) which is popular for motion planning of a robot manipulator, has been adapted for a nonholonomic mobile robot to track the desired trajectory. DMP is a simple damped spring model with a forcing function, which learns the trajectory. The damped spring model attracts the robot towards the goal position, and the forcing function forces the robot to follow the given trajectory. Two Radial Basis Function Networks (RBFNs) have been used to learn the forcing function associated with the DMP model. Weight update laws are derived using the gradient descent approach to train the RBFNs. Fuzzy logic based steering angle dynamics is proposed to handle the asymmetric nature of an obstacle. The proposed scheme is capable enough to generate a smooth trajectory in the presence of an obstacle even when start and goal positions are altered, without losing the spatial information embedded while training. The convergence of the robot goal position has been shown using Lyapunov stability theory-based analysis. The approach has been extended to multiple static and dynamic obstacles for the successful convergence of the robot at the goal position. Both simulation and experimental results are provided to confirm the efficacy of the proposed scheme.

## I. INTRODUCTION

Autonomous navigation of mobile robots in complex situations like warehouse floor is still very challenging due to the dynamic environment and hundreds of mobile agents in the same space. This complex problem can be easily understood from the following story. Please refer to the sketch of Kanpur city in Fig. 1a where only two landmarks are shown – Indian Institute of Technology Kanpur (IITK) campus and Green Park Stadium (GPS). It is desired that an Autonomous Vehicle (AV) has to navigate to GPS from the IITK campus. A human demonstration is given to this vehicle such that AV moves from IITK Main Gate to Gate 1 of GPS as shown in Path 1. After the demonstration, the AV should reach the goal from the initial position – still it has to encounter dynamic obstacles on the demonstrated path. Obviously, AV will follow the Path 1 with smooth tracking while avoiding obstacles. Next, AV is asked to travel from the IITK Stadium to Gate 4 of the GPS. In this case, AV should follow the Path 1 primarily with smooth tracking while the initial path to this trajectory and final path from this trajectory to the new goal point should look like  $p_i$  and  $p_f$  but it should never follow the Path 2. This problem has been addressed in this paper

Radhe Shyam Sharma, Santosh Shukla, Laxmidhar Behera, Venkatesh K S are with Department of Electrical Engineering, Indian Institute of Technology Kanpur, Kanpur-208 016, UP, India (email: {sharmars, stark, lbehera, venkats}@iitk.ac.in).

Hamad Karki, Amit Shukla are with the Department of Mechanical Engineering, The Petroleum Institute, Abu Dhabi 2533, UAE (email: {hkarki, ashukla}@pi.ac.ae).

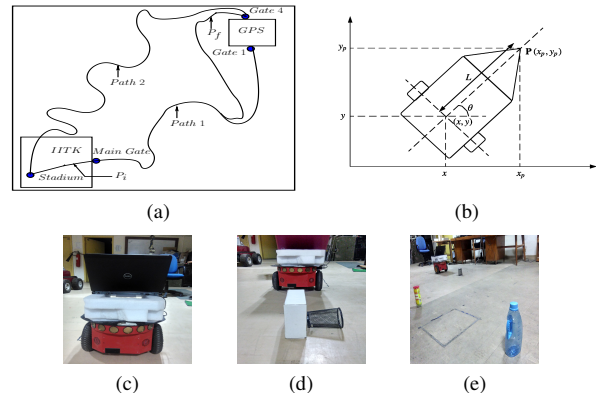


Fig. 1: (a) Map, (b) Mobile Robot in Cartesian Space, (c)-(e) experimental setup along with different type of obstacle scenarios.

as a proof of concept in a laboratory setting using DMP based learning from demonstration. There are many feasible paths between the start point to the goal point. The human demonstration tells the robot the best feasible path. The robot learns to track this path even if start points and goal points have variations.

Many motion planning algorithms suggested in literature are generally proposed for static environments [1]–[4]. Existing path planners for dynamic environment require replanning the entire trajectory, which is computationally expensive and requires the exploration of the entire environment again. A continuous-curvature path planning methodology is presented in [5]. The general approach for motion planning of nonholonomic robots is a two level process, where a path finding algorithm like A\* [6] searches for a collision free path in the configuration space. This collision free path is then approximated by a motion planner for a nonholonomic robot.

This paper is inspired from the works of Schaal [7] for robotic manipulators. The framework is known as DMP and it is used to generate complex trajectories by learning many simple trajectories. The framework, which will now be referred as DMP model, is a point attractor based dynamics. The system is attracted towards the target position. While getting attracted, a forcing function, as the name suggests, forces the system to move along a trajectory while approaching the goal. This is a key feature that motivates the use of DMP for path following of mobile robots. The DMP model was later developed by Ijspeert *et al.* [8]. It was then modified

by Kober *et al.* [9] for safe accelerations, with online changing path specifications. Modeling goal-directed behavior with nonlinear systems is presented in [10]. A further modification was proposed by Samant *et al.* [11], where they used a Piecewise Linear Canonical System (PLCS) for learning the DMP model parameters instead of the standard Exponential Canonical Systems (ECS), which showed that the learning of DMP parameters improved as compared to the then state of the art systems. Authors in [12], show that the DMP can be defined for non-minimal, and singularity free representations of orientation. DMP is used to model and learn the joint trajectories, and then reinforcement learning is employed to learn the trajectories with uncertainties [13]. However, the DMP model with all its properties is developed for robotic manipulators as a method of imitation learning [14]–[16].

When a mobile robot navigates toward the goal, it is more likely to encounter an obstacle in the environment. It is essential to design the mechanism to avoid the obstacle. Kinematic control based approaches to avoid the obstacles with the end-effector are discussed in [17]. The work by Hoffmann *et al.* [18] on DMP based obstacle avoidance, proposed, using the formulation suggested by Fajen and Warren [19], which models the dynamics of steering angle (defined as the angle between robots heading direction and robot to obstacle vector) of the obstacle as a potential function that repels the robot. However, the formulation was proposed for point obstacles. Thus, the formulation provided same steering angle change, when the robot passed through both sides of the obstacle. But in the real-world, obstacles may not be symmetric. The trajectory has to be different when the mobile robot is passed through both sides of an asymmetric obstacle. This is *precisely one of the challenges* we address in this paper. We incorporate a fuzzy logic based steering angle dynamics to solve this challenge.

This paper proposes a novel approach which develops a DMP framework for mobile robot and especially, nonholonomic mobile robots, where the robot's movement is restricted. This provides an additional challenge for applying the DMP model. The *presented framework offers* the online goal adaptation, adaptation to different initial points, conservation of shape, multiple static and dynamic obstacle avoidance, without the need of reusing the trajectory planner for a new path, thus reducing the computational cost and providing much flexibility.

The *key contributions* of this paper are listed below. (1) DMP based strategy for nonholonomic mobile robot has been designed to track the desired trajectory with automatic goal adaptation and obstacle avoidance in dynamic environment. (2) Weight update laws are derived using the gradient descent approach to train two RBFNs (RBFN<sub>1</sub> and RBFN<sub>2</sub>) to learn the forcing functions to shape the trajectory. (3) The dynamics of the steering angle is modified using fuzzy rules to consider an asymmetric obstacle. (4) The proposed strategy is extended to deal with multiple static and dynamic obstacles. (5) Convergence is proved mathematically in the sense of Lyapunov. (6) The implementation of the proposed scheme has been tested through rigorous perturbation studies

conducted based on real-time experimentations.

The remainder of this article is organized as follows. Section II describes the original DMP framework along with solution to nonholonomic constraint. Section III presents the DMP based framework for mobile robot. Extension of proposed framework for obstacle avoidance is shown in Section IV. Simulation and experimental results are incorporated in Section V. Section VI concludes this paper.

## II. PROBLEM FORMULATION

### A. Dynamic Movement Primitives

The DMP model is a simple damped-spring model, with addition of a forcing function  $f_x(z)$  and is given by the following equation [10],

$$\tau_1 \ddot{x} = \alpha_1 (\beta_1 (x_g - x) - \dot{x}) + (x_g - x_0) f_x(z) \quad (1)$$

Equation (1) can be rewritten as,

$$\tau_1 \ddot{x} = \gamma_1 (x_g - x) - \alpha_1 \dot{x} + (x_g - x_0) f_x(z) \quad (2)$$

where  $x$ ,  $\dot{x}$  and  $\ddot{x}$  are position, velocity and acceleration of the system.  $\tau_1$  is a time constant.  $\gamma_1 = \alpha_1 \beta_1$ , acts as a spring constant.  $\alpha_1$  represents the damping term.  $x_g$  and  $x_0$  are the final and initial values of the position. As seen in (1), if  $f_x(z) = 0$ , the system reduces to a simple Proportional Derivative (PD) controller. This is also considered as point attractor dynamics. The damping of the system can be varied by adjusting the values of  $\alpha_1$  and  $\beta_1$ . The system is made critically damped, when  $\alpha_1/\beta_1 = 4$ . The dynamics of the variable  $z$  is selected as PLCS [11], which is given below,

$$\tau_1 \dot{z} = \begin{cases} -k_1 & z \geq 0 \\ 0 & z < 0 \end{cases} \quad (3)$$

The equation describing the dynamics of the variable  $z$  is called as canonical dynamical system.  $k_1$  is the decay rate of  $z$ . The forcing function  $f_x(z)$  depends only on  $z$ , where  $z$  acts as a global clock for the entire system. There are some problems with equation (2): (a) If  $x_g = x_0$ , then system will remain in at  $x_0$ . (b) A small change in  $x_g$ , may lead to huge acceleration if  $x_g - x_0$  is close to zero. (c) Generalization is mirrored. Authors [18], suggested a modified version to overcome these issues as,

$$\tau_1 \ddot{x} = \gamma_1 (x_g - x) - \alpha_1 \dot{x} - \gamma_1 (x_g - x_0) z + \gamma_1 f_x(z) \quad (4)$$

Similarly, the equation (4) can be written for the movement in  $y$  dimension as,

$$\tau_2 \ddot{y} = \gamma_2 (y_g - y) - \alpha_2 \dot{y} - \gamma_2 (y_g - y_0) z + \gamma_2 f_y(z) \quad (5)$$

### B. Solution to nonholonomic constraint

The kinematic model of the nonholonomic mobile robot, as shown in Fig. 1b, is given as,

$$\dot{x} = v \cos \theta, \quad \dot{y} = v \sin \theta, \quad \dot{\theta} = \omega \quad (6)$$

where,  $v$  and  $\omega$  are the linear and angular input velocities, respectively.  $\theta$  is the robot's orientation in the world frame.  $x$  and  $y$  are the robot's position in world frame. It can be seen that the nonholonomic constraint arises from the fact that the

robot cannot, instantaneously, move side-ways. For example, consider the robot with an orientation of zero degrees, which means, the robot is facing  $x$  axis of the world frame. Thus, the state  $y$  is given as,  $\dot{y} = 0$ . It can be easily seen that control on  $y$  axis is lost. In order to control the  $y$  co-ordinate,  $\theta$  needs to be varied. Due to such constraints, system design is usually complex. Thus, the primary control from one position variable and orientation of the robot is shifted to both position variables, by transforming the system. Consider a point  $\mathbf{P}$ , on the  $x$  axis of the robot frame at an offset of, say,  $L$  units from the axis of rotation of the robot. Since, the point is considered to be associated with the rigid body of the robot, thus, the point dynamics upon the motion of the mobile robot can be found out as,

$$x_P = x + L \cos \theta, \quad y_P = y + L \sin \theta, \quad \theta_P = \theta \quad (7)$$

Equation (7), is differentiated with respect to time to obtain the dynamics of the point  $\mathbf{P}$ ,

$$\dot{x}_P = v \cos \theta - \omega L \sin \theta, \quad \dot{y}_P = v \sin \theta + \omega L \cos \theta, \quad \dot{\theta} = \omega \quad (8)$$

Since,  $\theta$  and  $\theta_P$  are same,  $\theta$  is used everywhere. Thus, it can be seen that both the inputs are directly controlling the  $x$  and  $y$  coordinates of the point  $\mathbf{P}$ . As the point  $\mathbf{P}$  is connected rigidly to the mobile robot, that means if point  $\mathbf{P}$  reaches a desired goal point, we can conclude that the mobile robot has reached its desired goal position. We let go of the control on  $\theta$  and focus on controlling  $x, y$  of the mobile robot. This modified kinematic equation provides us with the knowledge of  $x$  and  $y$  component of velocity on the offset point. Thus, we have,

$$v_x = v \cos \theta - \omega L \sin \theta, \quad v_y = v \sin \theta + \omega L \cos \theta, \quad \dot{\theta} = \omega \quad (9)$$

as the relation which is useful in training the DMPs and the derived inverse kinematic equations,

$$v = v_x \cos \theta + v_y \sin \theta, \quad \omega = \frac{v_y \cos \theta - v_x \sin \theta}{L} \quad (10)$$

To provide the mobile robot with the  $v_x$  and  $v_y$  obtained from the DMPs to drive the robot towards its goal position. So, in short, we are considering that the mobile robot is not controlled at the axis of robots rotation, but instead it is being controlled at an offset distance.

### C. Problem Statement

DMP as defined in equations (3), (4) and (5), has been developed for a nonholonomic mobile robot to address some of the key challenges. *Challenge 1* is to preserve the shape of the desired trajectory even when goal or start position is changed. *Challenge 2* is to obviate the requirement to recall the trajectory planner in case of any change in the environment. *Challenge 3* is to generate different trajectories for both sides of an asymmetric obstacle. *Challenge 4* is to eliminate the requirement of prior information about the trajectory of a moving obstacle.

The problem is formally stated as follows: *Design and implement a robust adaptive strategy which can preserve the shape while tracking the desired trajectory in the presence of obstacles even when either the initial or goal point is altered.*

### III. DMP BASED FRAMEWORK FOR MOBILE ROBOT

The capabilities of DMPs in manipulator systems motivate us to develop such a framework for mobile robots. We begin by using the transformed system (9) as derived in the previous section. Since the goal is to follow a path to reach the desired location in space, the orientation is not considered of much importance.

Two DMPs are required to learn the demonstrated trajectory. The forcing function associated with each DMP is parameterized using RBFN. Two RBF networks are used; one network learns the  $x$  behaviour, and the other learns  $y$  behaviour as given by the demonstration. After DMP has learned the demonstration, due to the dynamic environment, there are three possible constraints: (i) the goal position has changed; (ii) the initial position from where robot starts has changed; (iii) the obstacle has appeared on the demonstrated path. It is possible that all three may become true simultaneously. In this section, we will design a proper DMP based planner that will work in spite of the above three constraints.

The forcing functions can be written in terms of RBFN as,

$$f_x(z) = \sum_i w_x^i \phi^i(z) \quad (11)$$

$$f_y(z) = \sum_j w_y^j \phi^j(z) \quad (12)$$

where  $w_x^i$  and  $w_y^j$  are the weights of the neurons to learn;  $\phi^i(z)$  and  $\phi^j(z)$  are the Gaussian activation functions, defined as,

$$\phi^i(z) = \exp(-h^i(z - c^i)^2) \quad (13)$$

$$\phi^j(z) = \exp(-h^j(z - c^j)^2) \quad (14)$$

where  $c^i$  and  $h^i$  are the centers and variances of  $i^{th}$  neuron in RBFN<sub>1</sub>;  $c^j$  and  $h^j$  represent the centers and variances of  $j^{th}$  neuron in RBFN<sub>2</sub>.

To learn DMP parameters, we obtain the desired trajectory in terms of desired positions, velocities, and accelerations from the desired actuation inputs ( $v_d, \omega_d$ ). These desired actuations are obtained from the demonstration process. Fig. 2a shows the complete process to obtain the training data set. The learning of forcing function can be seen as a function approximation problem. Thus, the desired forcing functions are written as,

$$f_x^d(z) = (\dot{v}_x^d \tau_1 + \alpha_1 v_x^d) / \gamma_1 - (x_g - x^d) + (x_g - x_0)z \quad (15)$$

$$f_y^d(z) = (\dot{v}_y^d \tau_2 + \alpha_2 v_y^d) / \gamma_2 - (y_g - y^d) + (y_g - y_0)z \quad (16)$$

The following error function is minimized, to learn the DMP parameters,  $E = \frac{1}{2} \left( (f_x^d(z') - f_x(z'))^2 + (f_y^d(z') - f_y(z'))^2 \right)$   $z'$  is the value of  $z$  at  $t^{th}$  time instant. A gradient descent approach is used to derive the weight update laws [20] as,

$$w_x^i(t+1) = w_x^i(t) - \eta_1 \frac{\partial E}{\partial w_x^i} \quad (17)$$

$$w_y^j(t+1) = w_y^j(t) - \eta_2 \frac{\partial E}{\partial w_y^j} \quad (18)$$

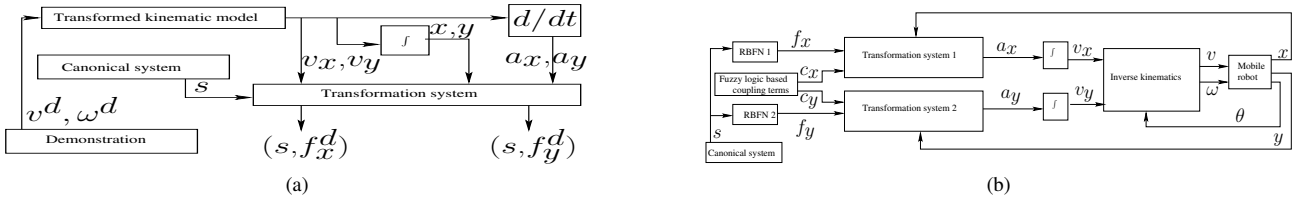


Fig. 2: (a) Process of gathering the training data, (b) Block diagram of the proposed scheme

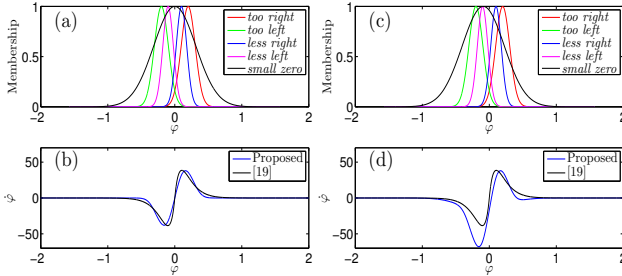


Fig. 3: Fuzzy logic design of steering dynamics: (a) Fuzzy input membership sets, (b) Change in  $\varphi$ , (c) Shift of *small zero*, (d) Shift of *small zero* influencing rate of steering.

where  $\eta_1$  and  $\eta_2$  are the learning rates; superscript  $i$ ,  $j$  indicate the  $i^{th}$  and  $j^{th}$  neuron in RBFN 1 and RBFN 2, respectively.

$$\begin{aligned}\frac{\partial E}{\partial w_x^i} &= \frac{1}{2} \frac{\partial}{\partial w_x^i} \left( (f_x^d(z^t) - f_x(z^t))^2 + (f_y^d(z^t) - f_y(z^t))^2 \right) \\ \frac{\partial E}{\partial w_x^i} &= (f_x^d(z^t) - f_x(z^t)) \frac{\partial}{\partial w_x^i} (-f_x(z^t))\end{aligned}$$

from (11), we have,

$$\begin{aligned}\frac{\partial E}{\partial w_x^i} &= (f_x^d(z^t) - f_x(z^t)) \frac{\partial}{\partial w_x^i} \left( -\sum_i w_x^i \phi^i(z) \right) \\ \frac{\partial E}{\partial w_x^i} &= (f_x^d(z^t) - f_x(z^t))(-\phi^i(z^t)).\end{aligned}$$

Using (17), the weight update law for  $w_x^i$  is given as,

$$w_x^i(t+1) = w_x^i(t) + \eta_1(f_x^d(z^t) - f_x(z^t))\phi^i(z^t) \quad (19)$$

$$\frac{\partial E}{\partial w_y^j} = (f_y^d(z^t) - f_y(z^t)) \frac{\partial}{\partial w_y^j} (-f_y(z^t))$$

from (12), we get,

$$\begin{aligned}\frac{\partial E}{\partial w_y^j} &= (f_y^d(z^t) - f_y(z^t)) \frac{\partial}{\partial w_y^j} \left( -\sum_j w_y^j \phi^j(z) \right) \\ \frac{\partial E}{\partial w_y^j} &= (f_y^d(z^t) - f_y(z^t))(-\phi^j(z^t)).\end{aligned}$$

Hence, the weight update law for  $w_y^j$  is given as,

$$w_y^j(t+1) = w_y^j(t) + \eta_2(f_y^d(z^t) - f_y(z^t))\phi^j(z^t) \quad (20)$$

Fig. 2b shows the complete work flow of the proposed framework. In this figure, equations (3), (4) and (5) are

referred as canonical system, transformation system 1 and transformation system 2, respectively.

#### IV. EXTENSION OF THE PROPOSED FRAMEWORK FOR OBSTACLE AVOIDANCE

Steering angle  $\varphi$ , is defined as the angle between the mobile robots heading direction vector and the robot to obstacle vector i.e.,  $\varphi = \arccos \left( \frac{(O-X)^T V}{\|(O-X)\| \|V\|} \right)$ . Let  $\dot{\varphi}$  be the rate of change in steering angle. Human obstacle avoidance is modeled [19] as,  $\dot{\varphi} = k_2 \varphi \exp(-k_3 |\varphi|)$ . A coupling term is designed [18] using the above mentioned model as,  $C_t = RV\dot{\varphi}$ . where  $R$  is a rotation matrix with axis  $(O-X) \times V$  and angle of rotation of  $90^\circ$ ;  $O = [o_x, o_y]^T$ ,  $X = [x, y]^T$ ,  $V = [v_x, v_y]^T$ ; vector  $O$  indicates the position of the obstacle. We modify the nature of steering angle dynamics using fuzzy logic to consider asymmetrical obstacles. The input  $\varphi$  is defined by five Gaussian fuzzy membership functions. These membership functions can be seen in Fig. 3a. We define five fuzzy rules: *too left*, *less left*, *small zero*, *less right*, *too right*. The dynamics of the rate of change in steering is proposed as,

$$\dot{\varphi} = k_1 \frac{\sum_{q=1}^5 g_q(\varphi) \mu_q}{\max(\sum_{q=1}^5 g_q \mu_q)} \quad (21)$$

where,  $g_q(\cdot)$  is the Gaussian fuzzy membership functions with centers at  $\mu_q$ ,  $q$  representing the  $q^{th}$  fuzzy rule,  $k_1$  is the scaling term. Depending on the need of shape of the obstacle,  $\dot{\varphi}$  can be changed by changing the location of the fuzzy rule *small zero*, as seen in Fig. 3c and 3d. The fuzzy rule *small zero* is shifted on the left, this leads to more steering in the left direction as shown in Fig. 3c, and 3d. The dynamics of  $\varphi$  is compared with [19]; comparative results can be seen in Fig. 3b, and 3d. Thus the term  $C_t$  is written as,

$$C_t = k_1 f_{mag} RV \frac{\sum_{q=1}^5 g_q(\varphi) \mu_q}{\max(\sum_{q=1}^5 g_q \mu_q)} \quad (22)$$

where  $C_t = [c_x, c_y]^T$  and  $f_{mag}$  is a magnitude flag which is defined below,

$$f_{mag} = \begin{cases} 0; & \|O-G\| > \|X-G\| \\ 1; & \text{elsewhere} \end{cases} \quad (23)$$

Equation (4) and Equation (5) can be written in vector form:

$$\dot{V} = \gamma(G-X) - \alpha V - \gamma(G-X_0)z + \gamma F \quad (24)$$

where  $\gamma = \text{diag}\{\gamma_1/\tau_1, \gamma_2/\tau_2\}$ ,  $\alpha = \text{diag}\{\alpha_1/\tau_1, \alpha_2/\tau_2\}$ ,  $G = [x_g, y_g]^T$ ,  $X_0 = [x_0, y_0]^T$ , and  $F = [f_x(z), f_y(z)]^T$ . The above equation with spatial coupling can be written as,

$$\dot{V} = \gamma(G - X) - \alpha V - \gamma(G - X_0)z + \gamma F + C_t \quad (25)$$

**Theorem 1:** Given the equations (3) and (25), if  $\alpha$  is a positive definite matrix then  $x \rightarrow x_g$  and  $y \rightarrow y_g$  as  $t \rightarrow \infty$ .

*Proof:* A Lyapunov candidate [21] is chosen as,

$$\begin{aligned} \rho &= \frac{1}{2}(G - X)^T \gamma(G - X) + \frac{1}{2}V^T V \\ \dot{\rho} &= -(G - X)^T \gamma \dot{X} + V^T \dot{V} = -V^T \gamma(G - X) + V^T \dot{V} \\ &= -V^T \gamma(G - X) + V^T (\gamma(G - X) - \alpha V - \gamma(G - X_0)z \\ &\quad + \gamma F + C_t) \\ &= -\underbrace{V^T \alpha V}_{1^{st}} - \underbrace{\gamma V^T (G - X_0)z}_{2^{nd}} + \underbrace{\gamma V^T F}_{3^{rd}} \\ &\quad + \underbrace{k_1 f_{mag} V^T RV \frac{\sum_{q=1}^5 g_q(\varphi) \mu_q}{\max(\sum_{q=1}^5 g_q \mu_q)}}_{4^{th}} \end{aligned}$$

Since  $z \rightarrow 0$  as  $t \rightarrow \infty \implies 2^{nd} \text{ term} \rightarrow 0$  and  $3^{rd} \text{ term} \rightarrow 0$ .  $\because R$  is a rotation by  $90^\circ \implies V^T RV = 0 \therefore 4^{th} \text{ term} \rightarrow 0$ . Further,  $\alpha$  is a positive definite matrix  $\implies \dot{\rho} \leq 0$ . If  $X \neq G$  and  $V \neq 0 \implies \dot{\rho} \neq 0$ . According to LaSalle's invariance theorem [21],  $X$  converges to  $G$ . ■

*Extension in the presence of multiple static obstacles:*

Let  $n$  represents the  $n^{th}$  obstacle in the environment. A special coupling is further modified as,

$$C_t = k_1 f_{mag} \sum_{p=1}^n R_p V \frac{\sum_{q=1}^5 g_q(\varphi_p) \mu_q}{\max(\sum_{q=1}^5 g_q(\varphi_p) \mu_q)} \quad (26)$$

*Extension in the presence of multiple dynamic obstacles:*

Let  $\dot{O}_n$  indicates the velocity of  $n^{th}$  dynamic obstacle. The coupling term  $C_t$  is given as,

$$C_t = k_1 f_{mag} \sum_{p=1}^n R_p (V - \dot{O}_n) \frac{\sum_{q=1}^5 g_q(\varphi_p) \mu_q}{\max(\sum_{q=1}^5 g_q(\varphi_p) \mu_q)} \quad (27)$$

In case of multiple obstacles,  $V^T R_n V = 0$ . In a dynamic obstacle scenario, at least one of the following conditions becomes true, as  $t \rightarrow \infty$ : (a)  $\|O - G\| > \|X - G\|$ ; (b)  $\dot{\varphi} \rightarrow 0$  for large  $\varphi$ , as shown in Fig. 3; (c)  $\dot{O}_n = 0$  (when it comes to an virtual standstill). Since in each case,  $V^T C_t \rightarrow 0$ , hence  $X$  converges to  $G$ .

## V. RESULTS AND DISCUSSIONS

### A. Simulation

The system is first trained from the trajectory generated by demonstration. The training was done through Gradient Descent, with one input, one output and 100 hidden layer neurons for each RBFN. Thus, for mobile robot two RBFNs are trained. It is seen in Fig. 4a that how the robot follows the path with the exact scenario it was trained with.

Different scenarios are constructed to test the re-planning capabilities of the presented framework. The **first scenario** is selected in which the initial position of the robot is moved

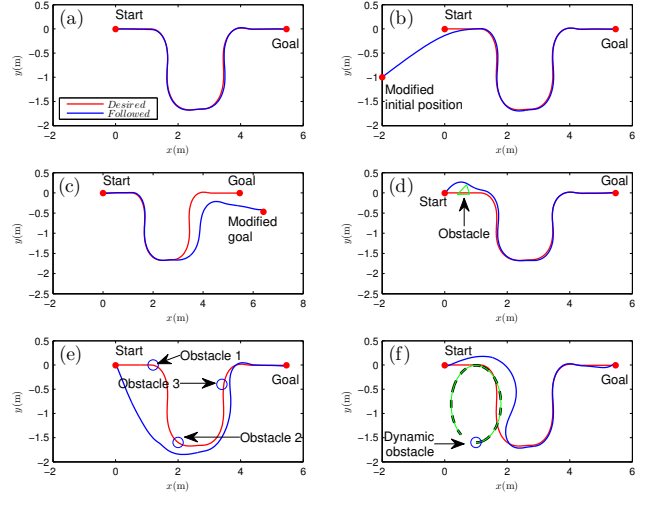


Fig. 4: Simulation: (a) Tracking performance (b) Trajectory with different initial position (c) Trajectory with modified goal position (d) Trajectory with obstacle avoidance (e) Performance in the presence of multiple obstacles (f) Performance in the presence of a dynamic obstacle

from  $(0m, 0m)$  to  $(-2m, -1m)$ . Fig. 4b shows how well the robot adjusts to the changes. The **second scenario** is comprised of changing the goal location at middle of the trajectory. At around 20s, the goal position is changed from  $(5.46m, 0m)$  to  $(6.5m, -0.5m)$ , and as seen from Fig. 4c the trajectory modifies in real time, while preserving the shape of trajectory learnt. This particular *conservation of shape is an important characteristic*, for scenarios where, the robot has to operate in an environment consisting of corridors. The **third scenario** is in the presence of an asymmetric obstacle at  $(0.7m, 0m)$ , which lies directly on the demonstrated trajectory. The DMP drives the mobile robot through the modified path as seen in Fig. 4d. The **fourth scenario** is to check the multi-obstacle avoidance capability of the proposed framework. Three obstacles (obstacle 1, obstacle 2, obstacle 3) are placed at  $(1.2m, 0m)$ ,  $(2m, -1.6m)$  and  $(3.4m, -0.4m)$ , respectively. The performance of the proposed method in the presence of multiple obstacles is given in Fig. 4e. All three obstacles are avoided while preserving the shape of the desired trajectory, as shown in the Fig. 4e. The **fifth scenario** is to test the performance of the proposed method in the presence of a dynamic obstacle. The tracking response along with a trajectory of a moving obstacle can be seen in Fig. 4f.

### B. Experiment

Experiments are performed using a Pioneer P3DX mobile robot as shown in Fig. 1c. The mobile robot is 16kg two wheel two motor differential drive robot. It is equipped with onboard PC running Robot Operating System (ROS) on Ubuntu 16.04, SONAR sensors, WiFi module, and encoders. The DMP parameters were learnt by demonstrating the trajectory that the mobile robot has to follow. Once the parameters are learnt, the robot is placed at the initial position

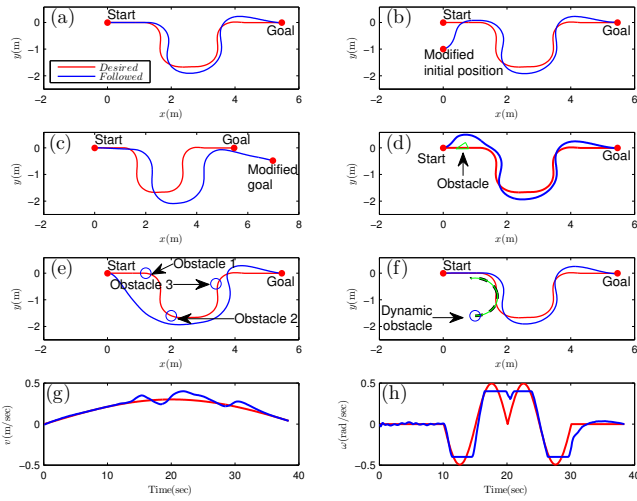


Fig. 5: Experiment: (a) Tracking performance, (b) Trajectory with different initial position, (c) Trajectory with modified goal position, (d) Trajectory with obstacle avoidance, (e) Performance in the presence of multiple obstacles, (f) Response in the presence of a dynamic obstacle, (g) Linear velocity, (h) Angular velocity



Fig. 6: Experiment : Robot following the trajectory learnt

as it can be seen from the top left image in Fig. 6. The blue box on the left in each image of Fig. 6 is an intermediate position that the robot should pass through and the blue box in the bottom right corner is the goal position. The DMP model drives the robot as seen in Fig. 6, whose trajectory is seen in Fig. 5a. The variation in path followed by mobile robot is not too much, with maximum deviation of around  $0.25m$ . That is caused by the saturation of input command velocities (hardware physical limits). As the robot is trained for higher velocities than it can operate, which can be seen in the velocity profile of the mobile robot in Fig. 5g, and 5h. Hence, the saturation is what is limiting the performance of the mobile robot.

The scenarios constructed for simulations are also tested experimentally. In the **first scenario**, the mobile robot's initial position is shifted to  $(0m, -1m)$ . Once the algorithm starts, the mobile robot rushes to approach the point, where it is supposed to be present at that time instant. The path traced by the mobile robot is seen in Fig. 5b. The **second scenario** illustrates the change in goal position. The mobile robot is seen modify its learnt trajectory, while preserving the path pattern, in Fig. 5c. The **third scenario** is to test obstacle avoidance. The trajectory while avoiding obstacle can be seen in Fig. 5d. Obstacle avoidance capability is verified by placing a  $0.21m \times 0.17m \times 0.07m$  box along with a mesh glass at approximately  $(0.7m, 0m)$ , as shown in Fig. 1d. The position of an obstacle is priorly known to the mobile robot.

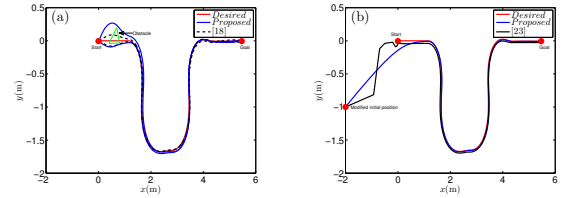


Fig. 7: Comparative results: (a) In the presence of an asymmetric obstacle, (b) When start position is modified

However, detection and location of obstacle can be found using stereo cameras or kinect. The **forth scenario** is to check the performance of the proposed framework in the presence of multiple obstacles. Three obstacles are placed at  $(1.2m, 0m)$ ,  $(2m, -1.6m)$  and  $(3.4m, -0.4m)$ , respectively as shown in Fig. 1e. The performance in the presence of three obstacles is shown in Fig. 5e. In the **fifth scenario**, one more Pioneer P3DX mobile robot is considered as a dynamic obstacle. Both robots are connected to the ROS environment; and Odomery call back is utilized to know the position and velocity of a dynamic obstacle in real-time. The tracking response in the presence of a dynamic obstacle is shown in Fig. 5f. The **YouTube** link for the videos recorded during the experiments is given in [22].

**Comparison:** The comparative performance of the proposed strategy is analyzed in relation to [18], [19], and [23]. Comparative results in relation to [19], are shown in Fig. 3 while considering both symmetric and asymmetric nature of an obstacle. Comparative results of the steering angle dynamics in both the cases are plotted in Fig. 3b and Fig. 3d, respectively. It can be inferred from Fig. 3d, that the proposed method can appropriately handle the case of an asymmetric obstacle as compared to [19]. Fig. 7a shows that the proposed scheme enables the robot to avoid an asymmetric configuration from both sides effectively, in contrast to [18]. It is observed from Fig. 7b that the proposed method gives smooth trajectory as compared to the existing method [23].

## VI. CONCLUSIONS

DMP based trajectory tracking strategy for a nonholonomic mobile robot has been designed and implemented. A new obstacle avoidance scheme is proposed to handle the asymmetric nature of an obstacle. The proposed scheme is further extended to avoid multiple static and dynamic obstacles. Various other dynamic environment scenarios are evaluated to verify the capability of the system. The comparison with [19] shows that the asymmetric heading angle can be generated in the presence of the asymmetric obstacle with the proposed scheme only. The comparison with [18] indicates that the proposed scheme can also avoid an asymmetric obstacle from both sides effectively. The comparison with [23] shows that the proposed scheme generates smooth trajectory even when the initial position is altered. The proposed approach addresses issues that are found in warehouse automation and elderly health care. In this sense, the contributions of the paper are very significant and relevant.

## REFERENCES

- [1] A. Ismail, A. Sheta, and M. Al-Weshah, "A mobile robot path planning using genetic algorithm in static environment," *Journal of Computer Science*, vol. 4, no. 4, pp. 341–344, 2008.
- [2] Q. Li, C. Zhang, C. Han, Y. Xu, Y. Yin, and W. Zhang, "Path planning based on fuzzy logic algorithm for mobile robots in static environment," in *Control and Decision Conference (CCDC), 2013 25th Chinese*. IEEE, 2013, pp. 2866–2871.
- [3] T.-K. Dao, T.-S. Pan, and J.-S. Pan, "A multi-objective optimal mobile robot path planning based on whale optimization algorithm," in *Signal Processing (ICSP), 2016 IEEE 13th International Conference on*. IEEE, 2016, pp. 337–342.
- [4] P. Švestka and M. H. Overmars, "Motion planning for carlike robots using a probabilistic learning approach," *The International Journal of Robotics Research*, vol. 16, no. 2, pp. 119–143, 1997.
- [5] S. Upadhyay and A. Ratnoo, "Continuous-curvature path planning with obstacle avoidance using four parameter logistic curves," *IEEE Robotics and Automation Letters*, vol. 1, no. 2, pp. 609–616, 2016.
- [6] N. J. Nilsson, *Principles of artificial intelligence*. Morgan Kaufmann, 2014.
- [7] S. Schaal, "Dynamic movement primitives-a framework for motor control in humans and humanoid robotics," in *Adaptive motion of animals and machines*. Springer, 2006, pp. 261–280.
- [8] A. J. Ijspeert, J. Nakanishi, and S. Schaal, "Movement imitation with nonlinear dynamical systems in humanoid robots," in *Robotics and Automation, 2002. Proceedings. ICRA'02. IEEE International Conference on*, vol. 2. IEEE, 2002, pp. 1398–1403.
- [9] J. Kober, K. Mülling, O. Krömer, C. H. Lampert, B. Schölkopf, and J. Peters, "Movement templates for learning of hitting and batting," in *Robotics and Automation (ICRA), 2010 IEEE International Conference on*. IEEE, 2010, pp. 853–858.
- [10] A. J. Ijspeert, J. Nakanishi, H. Hoffmann, P. Pastor, and S. Schaal, "Dynamical movement primitives: learning attractor models for motor behaviors," *Neural computation*, vol. 25, no. 2, pp. 328–373, 2013.
- [11] R. Samant, L. Behera, and G. Pandey, "Adaptive learning of dynamic movement primitives through demonstration," in *Neural Networks (IJCNN), 2016 International Joint Conference on*. IEEE, 2016, pp. 1068–1075.
- [12] A. Ude, B. Nemec, T. Petrić, and J. Morimoto, "Orientation in cartesian space dynamic movement primitives," in *Robotics and Automation (ICRA), 2014 IEEE International Conference on*. IEEE, 2014, pp. 2997–3004.
- [13] Z. Li, T. Zhao, F. Chen, Y. Hu, C.-Y. Su, and T. Fukuda, "Reinforcement learning of manipulation and grasping using dynamical movement primitives for a humanoidlike mobile manipulator," *IEEE/ASME Transactions on Mechatronics*, vol. 23, no. 1, pp. 121–131, 2018.
- [14] L. Armesto, J. Moura, V. Ivan, M. S. Erden, A. Sala, and S. Vijayakumar, "Constraint-aware learning of policies by demonstration," *The International Journal of Robotics Research*, p. 0278364918784354, 2018.
- [15] L. Armesto, V. Ivan, J. Moura, A. Sala, and S. Vijayakumar, "Learning constrained generalizable policies by demonstration," in *Robotics: Science and Systems*, 2017.
- [16] A. Rai, G. Sutanto, S. Schaal, and F. Meier, "Learning feedback terms for reactive planning and control," in *Robotics and Automation (ICRA), 2017 IEEE International Conference on*. IEEE, 2017, pp. 2184–2191.
- [17] T. Petrić, A. Gams, N. Likar, and L. Žlajpah, "Obstacle avoidance with industrial robots," in *Motion and Operation Planning of Robotic Systems*. Springer, 2015, pp. 113–145.
- [18] H. Hoffmann, P. Pastor, D.-H. Park, and S. Schaal, "Biologically-inspired dynamical systems for movement generation: automatic real-time goal adaptation and obstacle avoidance," in *Robotics and Automation, 2009. ICRA'09. IEEE International Conference on*. IEEE, 2009, pp. 2587–2592.
- [19] B. R. Fajen and W. H. Warren, "Behavioral dynamics of steering, obstacle avoidance, and route selection," *Journal of Experimental Psychology: Human Perception and Performance*, vol. 29, no. 2, p. 343, 2003.
- [20] L. Behera and I. Kar, *Intelligent Systems and control principles and applications*. Oxford University Press, Inc., 2010.
- [21] H. K. Khalil, "Nonlinear systems," *Prentice-Hall, New Jersey*, vol. 2, no. 5, pp. 5–1, 1996.
- [22] "Trajectory tracking for a nonholonomic mobile robot with automatic goal adaptation and obstacle avoidance." [Online]. Available: <https://youtu.be/jOTL0EUZZCk>
- [23] Y. Wang, Z. Miao, H. Zhong, and Q. Pan, "Simultaneous stabilization and tracking of nonholonomic mobile robots: A lyapunov-based approach," *IEEE Transactions on Control Systems Technology*, vol. 23, no. 4, pp. 1440–1450, 2015.

# Tracking Control of Mobile Robots in Formation in the Presence of Disturbances

Radhe Shyam Sharma , *Student Member, IEEE*, Arindam Mondal ,  
and Laxmidhar Behera , *Senior Member, IEEE*

**Abstract**—The displacement-based formation control for perturbed multirobot systems, with practical issues like collision avoidance and connectivity assurance, is a challenging problem. This article presents and implements a two-step design process consisting of both holonomic and nonholonomic frameworks along with a process of demonstration to solve this problem. We use the process of demonstration to obtain the parameters of the desired trajectory. In a holonomic framework, each virtual robot is described as double integrator system. This framework generates a set of reference trajectories. The idea is to feed these generated reference points for the mobile robots to track under nonholonomic framework. This article formulates control laws under which multiple mobile robots simply connected are stable while ensuring collision avoidance and connectivity. Both holonomic and nonholonomic models are subjected to external disturbances. In the holonomic framework, the proposed controller ensures collision avoidance and connectivity while maintaining the desired formation. The proposed controller in the nonholonomic framework tracks the reference trajectories while guaranteeing Lyapunov stability. The proposed approach is scalable to any  $n$ -robot systems which are simply connected. Both simulation and experimental results prove the efficacy of the proposed approach.

**Index Terms**—Collision avoidance, connectivity assurance, formation control, multirobot systems, trajectory tracking.

## NOMENCLATURE

Symbol	Representation
$\mathcal{G}$	Graph of $N$ mobile robots.
$\mathcal{A}$	Adjacency matrix.
$L$	Laplacian matrix.
$\ \cdot\ $	Euclidean norm.
$R$	Communication radius.
$r_{in}$	Inner boundary.
$r_{out}$	Outer boundary.
$Z^*$	Desired formation shape.
$p_i^h$	Position vector of $i$ th Virtual Robot ( $i$ -VR).

Manuscript received August 12, 2019; revised December 5, 2019, February 8, 2020, and March 24, 2020; accepted March 24, 2020. Date of publication March 30, 2020; date of current version October 23, 2020. Paper no. TII-19-3709. (Corresponding author: Laxmidhar Behera.)

The authors are with the Department of Electrical Engineering, Indian Institute of Technology Kanpur, Kanpur 208016, India (e-mail: sharmars@iitk.ac.in; arindaminstru@gmail.com; lbehera@iitk.ac.in).

Color versions of one or more of the figures in this article are available online at <https://ieeexplore.ieee.org>.

Digital Object Identifier 10.1109/TII.2020.2983646

$v_i^h$	Velocity vector of $i$ -VR.
$p_i^{nh}$	Position vector of $i$ th Actual Robot ( $i$ -AR).
$u_i^h$	Control law vector for $i$ -VR.
$u_i^{nh}$	Control law vector for $i$ -AR.
$e_i$	Position error (consensus variable) vector.
$\delta_i$	Tracking error vector.
$\rho_i^h$	Disturbance (within a bound $\alpha$ ) for $i$ -VR.
$f_i$	Disturbance (within a bound $M$ ) for $i$ -AR.
$dist u_i^h$	Disturbance compensation term for $i$ -VR.
$dist u_i^{nh}$	Disturbance compensation term for $i$ -AR.
$\psi_{col}$	Repulsive potential function.
$\psi_{conn}$	Attractive Potential function.
$\otimes$	Kronecker product.

## I. INTRODUCTION

MULTIAGENT cooperative control has applications in exploration of unknown environments, surveillance, and intelligent transportation [1]. In such applications, each agent may refer to a mobile robot, unmanned aerial vehicle, or underwater vehicle.

Let us consider the problem of coordinating multirobot systems to transfer a payload from a point  $p_a$  to the point  $p_b$  through a specific path of interest.

We would call this problem as payload transport problem (PTP) in this article. In order to solve this problem as shown in Fig. 1, the multirobot systems must satisfy the following requirements.

- 1) The parameters of the desired path of interest should be known for an autonomous navigation.
- 2) A group of mobile robots should not collide during the navigation.
- 3) These robots should follow a desired path of interest.
- 4) The connectivity among the robots has to be maintained throughout the process.
- 5) These mobile robots should move in a required (desired) formation while performing the task.

Since the proposed method enables a group of mobile robots to meet all these above-mentioned requirements, hence, our method solves this problem effortlessly.

Furthermore, if the initial formation is different from the desired formation then it is essential to acquire the desired formation, and after that it has to be maintained as shown in Fig. 1. In such applications, coordinative movements [2] of robots are crucial. Formation control is one of the approaches to achieve

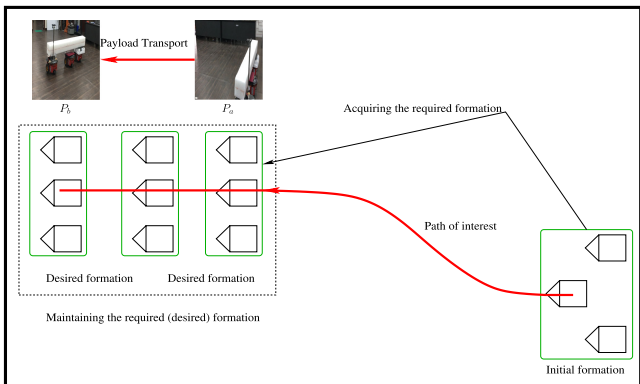


Fig. 1. Payload transport by a group of mobile robots.

coordinated movements. The formation control can be classified into three categories: position, displacement, and distance-based frameworks. In position-based formation control, agents require more sophisticated sensors, while interactions among the agents are not required. Position-based approaches are studied in [3]–[5]. In distance-based approach, the sensors are economical but interactions among agents become manifold. Some recent works on distance-based formation control can be found in [1], [6], [7]. In displacement-based approach, required sensors are not that sophisticated as in position control and the interactions are not that huge as in the distance-based formation control. Hence, the displacement-based formation control has advantages in terms of sensing and interaction [1] over other two approaches. The proposed work in this article is concerned with the displacement-based formation control.

Displacement-based formation control strategies are explained in [8]–[10]. A work on formation control integrated with orientation control has been presented in [11], where formation control is distance based, and orientation of the agents is controlled using the displacement-based approach. In these formation control algorithms, agents share their information states with each other to converge to a common value called the consensus [12]. The consensus problem for a group of dynamic agents has been discussed in [13], where directed and undirected graphs along with fixed and switching topology have been considered. Convergence analysis has been performed for all these cases in the presence and absence of time delays. An adaptive consensus control has been designed in [14] with parameter uncertainties and nonuniform communication delays. A formation control algorithm has been proposed in [15], which relies on intermittent communication in the presence of nonuniform delays and loss of information.

In many real world applications, it is more practical to enable a control law to ensure the connectivity of the graph instead of assuming the connectivity of the graph. This problem is called connectivity preservation problem. A cooperative target centric formation control strategy is proposed in [16], where authors have ensured the graph connectivity of nonholonomic agents. In multirobot formation control problems, the robots coordinate with each other to form the desired formation pattern. Collision avoidance is one of the important objectives in multirobot formation control. The artificial potential function (APF) [17] is the

most commonly adopted approach in controller design to avoid the collision. The concept of APF is used for collision-free robot navigation and path planning [18], [19]. The potential function based collision avoidance term generates a force by which robots repel one another to avoid the collision. Repulsive force due to the collision avoidance term within the coordination control law increases the chance of losing connectivity. Therefore, one of the main challenges is to maintain the connectivity in the presence of collision avoidance term in formation control law.

Formation control for nonholonomic agents has been studied in [20]. In [21], Montijano *et al.* have proposed the control law for the orientation of nonholonomic kinematics, and a distance-based controller has been considered for the holonomic control to reach the formation in position. Trajectory tracking in formation by a set of mobile robots, with practical issues like collision avoidance and connectivity assurance, is a challenging problem. In [10], this problem is discussed elaborately for the holonomic framework using double integrator model. This problem becomes more challenging when multirobot systems are perturbed, and especially, in the case of nonholonomic mobile robots, where the robots movement is restricted. Hence, an integrated two-step design has been presented in this article, where the mobile robot is described in terms of both holonomic (virtual mobile robot) and nonholonomic (actual mobile robot) models to solve this problem.

The main contributions of this article are as follows.

- 1) *High-level controller (HLC) design:* The control law for the holonomic model has been proposed in the presence of input disturbances ensuring both connectivity and collision avoidance.
- 2) *Low-level controller (LLC) design:* The control law for nonholonomic model in the presence of disturbance has been designed guaranteeing the nonholonomic mobile robots to follow the reference trajectories given by the holonomic model.
- 3) *Convergence analysis:* Convergence is proved mathematically in the sense of Lyapunov.
- 4) *Validation:* The proposed approach is validated from simulation and experimental point of view.

*Advantages of the proposed approach are listed below.*

- 1) *Applicability:* Most of schemes depicted in the literature are demonstrated in simulation only like in [22] and [10]. In contrast, the proposed approach is validated in real time. Further, the proposed approach is capable to solve some of the real world problems, such as surveillance of vast area, and transporting big objects. One of the real world problems has been demonstrated to transfer a payload.
- 2) *Simplicity:* One of the practical ways to obtain the parameters of desired trajectory by demonstration for a group of mobile robots is presented. In relation to [10], the presented scheme simplifies the task to obtain the parameters of the desired path of interest.
- 3) *Multiobjective navigation:* In many practical applications, it is essential to solve multiple problems during an autonomous navigation. Recently in [23], an adaptive trajectory tracking with an asymmetric obstacle avoidance is solved. In relation to [23], a multiobjective navigation

problem (trajectory tracking, formation control, collision avoidance, and connectivity assurance) for perturbed multirobot systems are addressed in this article.

- 4) *Robustness*: It is difficult to have noise free environment in real time. Therefore, the proposed scheme is analyzed in the presence of the disturbances; this in contrast to [10] and [24].

In short, an integrated two-step design, a novel aspect of demonstration for the formation control, the experimental validation, the analysis in the presence of perturbations with communication and collision constraints, are highlights of this article. Applicability, simplicity, scalability, and robustness are some of the interesting features of the proposed scheme.

The rest of this article is organized as follows. Section II provides the preliminaries for the remainder. Section III describes the formation control problem along with the constraints. Section IV presents an integrated framework along with its mathematical proofs of convergence. Section V illustrates the effectiveness of the design through both simulation and experimental results. This section also incorporates the comparison of the proposed scheme in relation to the other existing works. Finally, Section VI concludes this article.

## II. PRELIMINARIES

To depict the interaction among the mobile robots, a system is represented as a graph. The positions of mobile robots are represented as the vertices of the graph and their interaction defines the concept of edges. We consider a connected undirected graph of  $N$  mobile robots and it can mathematically be described as  $\mathcal{G} = (\mathcal{V}, \mathcal{E})$ , where  $\mathcal{V} = [V_1, V_2, \dots, V_n]$  is the set of vertices and  $\mathcal{E}$  is the edge set.  $\mathcal{A}$  is the adjacency matrix consisting of elements  $a_{ij}$ . In case of an undirected graph,  $a_{ij} = a_{ji}$  and  $\mathcal{E} = \{(i, j) | a_{ij} > 0\}$ . A graph has no self-loops when  $(i, j) \in \mathcal{E}$  implies that  $i \neq j$ . A graph is connected [25] (simply connected) if for any pair of vertices  $(i, j)$  there is a path from  $i$  to  $j$  consisting of edges in  $\mathcal{E}$ , and it is complete if for any pair of vertices  $(i, j)$  there is an edge in  $\mathcal{E}$  connecting them. The neighborhood of a mobile robot  $i$  is defined as  $\mathcal{N}_i = \{j : (i, j) \in \mathcal{E}\}$ . The degree of a vertex  $i$  is denoted as  $d_i$ , and is defined as the cardinality of the set  $\mathcal{N}_i$ . The degree matrix of graph  $\mathcal{G}$  is expressed as  $\Delta = \text{diag}(d_i)$ . The Laplacian matrix of  $\mathcal{G}$  is then defined as  $L = \Delta - \mathcal{A}$ . The concept of Laplacian is important in connectivity preservation analysis. For a connected graph, it is a symmetric and positive semidefinite matrix. Minimum eigenvalue of a Laplacian matrix is 0 with corresponding eigenvector  $\mathbf{1} = [1, 1, \dots, 1]^T$ , or  $L\mathbf{1} = \mathbf{0}$ , as the row-sum of  $L$  is zero. If  $\mathcal{G}$  is connected, the null space of the Laplacian is one-dimensional (1-D) and spanned by the vector  $\mathbf{1}$ . So the second smallest eigenvalue will always be greater than zero, i.e.,  $\lambda_2 > 0$  in a connected graph.

## III. PROBLEM DEFINITION AND FORMATION CONSTRAINTS

The proposed approach consists of  $N$  actual mobile robots and  $N$  virtual mobile robots as well. Each virtual robot is described in terms of holonomic representation (HR). However, the actual mobile robots are described in terms of nonholonomic representations (NHR). In HR, the robot is governed by a double integrator model while the robot is governed by the so-called

unicycle model in NHR. In this article, the double integrator model used for virtual robots is associated with massless points. Each actual robot has its local frame. Thus, one inertial frame and  $N$  local frames are involved in the problem. The control at the level of HR generates the desired reference trajectories for the mobile robots to track at the NHR level.

### A. Mathematical Representation for Virtual Robots

The dynamics in the presence of disturbances at the HR level for an  $i$ th virtual robot is defined as

$$\begin{aligned}\dot{p}_i^h &= v_i^h \\ \dot{v}_i^h &= u_i^h + \rho_i^h\end{aligned}\quad (1)$$

where superscript  $h$  is used to indicate the parameters of holonomic mobile robots.  $p_i^h \in \mathbb{R}^2$ ,  $v_i^h \in \mathbb{R}^2$ ,  $u_i^h \in \mathbb{R}^2$  are position, velocity, and control input vectors of the  $i$ th virtual robot in 2-D space.  $\rho_i^h \in \mathbb{R}^2$  is a bounded random disturbance, i.e.,  $\|\rho_i^h\| \leq \alpha$  with  $\alpha \geq 0$ .

### B. Mathematical Representation for Actual Robots

In Fig. 2(a), the pair  $(x_i^{nh}, y_i^{nh})$  identifies the position of the robot center of mass and the point  $q_i(x_i^{nh}, y_i^{nh})$  is placed along the heading direction of the  $i$ th robot at distance  $l$  from its center of mass. Since the point  $q_i \in \mathbb{R}^2$  is considered to be associated with the rigid body of an  $i$ th nonholonomic mobile robot, hence point dynamics can be expressed as

$$\begin{aligned}{}^q\dot{x}_i^{nh} &= v_i^{nh} \cos \theta_i^{nh} - l \omega_i^{nh} \sin \theta_i^{nh} \\ {}^qy_i^{nh} &= v_i^{nh} \sin \theta_i^{nh} + l \omega_i^{nh} \cos \theta_i^{nh} \\ \dot{\theta}_i^{nh} &= \omega_i^{nh}\end{aligned}\quad (2)$$

where superscript  $nh$  represents the parameters of nonholonomic mobile robots.  $v_i^{nh}$  and  $\omega_i^{nh}$  are the linear and angular input velocities, respectively.  $\theta_i^{nh}$  is the orientation of the robot in the world frame. The standard control variables of a nonholonomic mobile robot modeled as a unicycle system include the angle  $\theta_i^{nh}$ , so that the design of a position controller may result to be complicated. For this reason, the point  $q_i$  is taken into account, implying the regulation of two position control variables instead of a position and orientation control variable. Therefore, we are considering that the mobile robot is not controlled at the axis of robots rotation, but instead it is controlled at an offset distance.

We present the above-mentioned model in the presence of disturbances at the level of NHR as

$$p_i^{nh} = Q_i u_i^{nh} + f_i \quad (3)$$

$$\dot{\theta}_i^{nh} = \omega_i^{nh} \quad (4)$$

$$\text{where } p_i^{nh} = \begin{bmatrix} {}^q\dot{x}_i^{nh} \\ {}^q\dot{y}_i^{nh} \end{bmatrix} \in \mathbb{R}^2$$

$$Q_i = \begin{bmatrix} \cos \theta_i^{nh} & -l \sin \theta_i^{nh} \\ \sin \theta_i^{nh} & l \cos \theta_i^{nh} \end{bmatrix} \in \mathbb{R}^{2 \times 2}$$

$$u_i^{nh} = \begin{bmatrix} v_i^{nh} \\ \omega_i^{nh} \end{bmatrix} \in \mathbb{R}^2$$

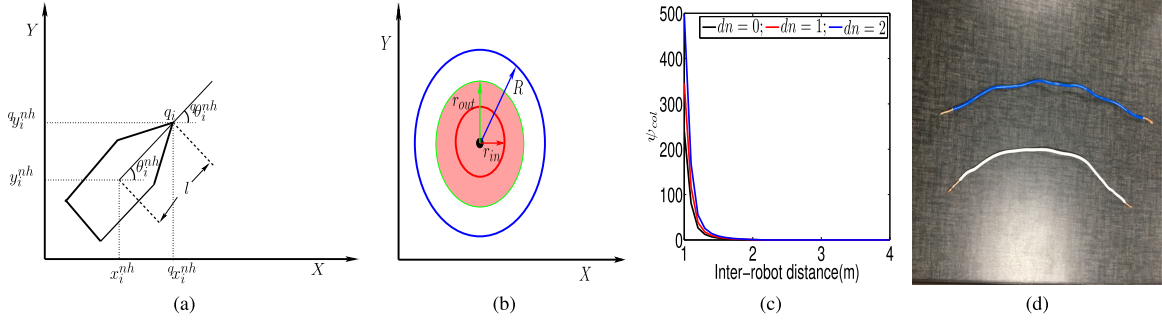


**Fig. 2.** (a)  $i$ th nonholonomic mobile robot in Cartesian frame. (b) Collision avoidance region. (c) Response at different value of  $dn$ . (d) Pair of wires for perturbation.

where  $f_i \in \mathbb{R}^2$  is a bounded random disturbance, i.e.,  $\|f_i\| \leq M$  with  $M \geq 0$ . The vector  $\delta_i$  is the position error between (1), and (3), i.e.,  $\delta_i = p_i^{nh} - p_i^h; p_i^{nh} \in \mathbb{R}^2$ .

### C. Problem Statement

A circular range of communication of radius  $R$  is assumed for all mobile robots. As discussed in Section II, the neighborhood of an  $i$ th mobile robot is the set of mobile robots that lie in this communication circle. Let  $\|p_{ij}^h\|$  be the Euclidean distance between an  $i$ th and  $j$ th virtual mobile robots. The connectivity among mobile robots is defined by the adjacency matrix,  $\mathcal{A}(t) \in \mathbb{R}^{N \times N}$ , having dynamic nature. The initial communication graph is connected and is defined as follows:

$$a_{ij}(0) = \begin{cases} 1, & \|p_{ij}^h(0)\| \leq R \\ 0, & \text{otherwise} \end{cases}.$$

The communication graph at time  $t > 0$  is defined as follows:

$$a_{ij}(t) = \begin{cases} 1, & \|p_{ij}^h(t)\| \leq R \& a_{ij}(t^-) = 1 \\ 0, & \text{otherwise} \end{cases} \quad (5)$$

where  $t^-$  denotes the previous time step for time instant  $t$  [10], i.e.,  $t^- = \lim_{\epsilon \rightarrow 0} (t - \epsilon)$ . The condition  $a_{ij}(t^-) = 1$  indicates that there is no chance to create a new connection over time. However, it is only possible to reduce the number of connections. The desired formation shape is given as  $Z^* = [(z_1^*)^T \dots (z_N^*)^T]^T \in (\mathbb{R}^2)^N$  in the inertial frame. The inertial frame is taken as East, North, Up frame. As shown in Fig. 2(b), to ensure collision avoidance, two different radii  $r_{in}$  and  $r_{out}$  are defined which represent inner and outer boundaries centered around the mobile robot and have fixed values ( $0 < r_{in} < r_{out} < R$ ). The mobile robots are made to achieve the desired formation and to track a predefined trajectory while maintaining the desired formation. The problem is formally stated as follows.

Derive a control law based on NHR to track a set of reference trajectories as computed by the controller for HR while maintaining the desired formation pattern  $Z^*$ . This control law must simultaneously ensure collision avoidance and connectivity preservation.

### D. Constraints on Formation Control

There are some constraints in formation control problem as presented in this article. These constraints are as follows.

- 1) To achieve and maintain the desired formation pattern

$$p_i^h - z_i^* = p_j^h - z_j^* \Rightarrow \|p_i^h - p_j^h\| = \|z_i^* - z_j^*\| \quad (6)$$

where  $i \in \{1 \dots N\}$  and  $j \in \mathcal{N}_i$ .

- 2) To avoid collision

$$\|p_i^h - p_j^h\| > r_{in} > 0 \quad (7)$$

where  $i \in \{1 \dots N\}$ ,  $j \in \mathcal{N}_i^c$

and  $\mathcal{N}_i^c = \{j : \|p_i^h - p_j^h\| \leq r_{out}\}$ .

- 3) To maintain the connectivity

$$0 < \|p_i^h - p_j^h\| \leq R \quad (8)$$

where  $i \in \{1 \dots N\}$ ,  $j \in \mathcal{N}_i / \mathcal{N}_i^c$   
and  $\mathcal{N}_i / \mathcal{N}_i^c = \{j : j \in \mathcal{N}_i \& j \notin \mathcal{N}_i^c\}$ .

In this article, we use position error as the consensus variable  $e_i = p_i^h - z_i^*$ . Thus, the constraint as given in (8) is transformed in terms of error variable. The upper and the lower bound of  $\|e_i - e_j\|$  are found using forward and reverse triangular inequality

$$\|e_i - e_j\| \leq \|p_i^h - p_j^h\| + \|z_j^* - z_i^*\| \quad (9)$$

$$\|e_i - e_j\| \geq \text{abs}(\|p_i^h - p_j^h\| - \|z_i^* - z_j^*\|). \quad (10)$$

Using (9) and (10), we get

$$\begin{aligned} \text{abs}(\|p_i^h - p_j^h\| - \|z_i^* - z_j^*\|) &\leq \|e_i - e_j\| \leq \|p_i^h - p_j^h\| \\ &+ \|z_j^* - z_i^*\|. \end{aligned} \quad (11)$$

### IV. INTEGRATED FRAMEWORK

The proposed approach includes a process of demonstration and a two-step design process, as shown in Figs. 3 and 4, respectively. These processes are described in the following sections, respectively.

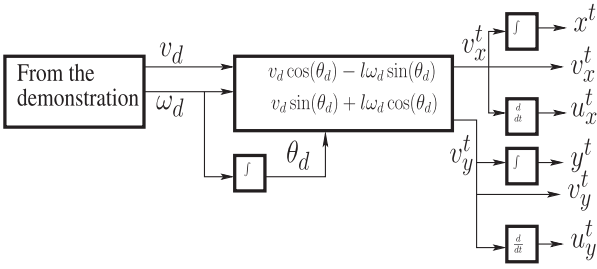


Fig. 3. Block diagram of the process of demonstration.

### A. Demonstration Process

In this process, a human demonstration is given to one of the nonholonomic mobile robots such that a mobile robot moves from some initial point to the goal point over the specific path of interest. The aim of this process is to obtain the parameters of the desired trajectory.

Demonstration process requires only one mobile robot from a group of  $N$  mobile robots. Hence, we choose one nonholonomic mobile robot from the group of robots. The selected nonholonomic mobile robot is manually controlled over the desired path of interest. Linear and angular velocities are recorded during the demonstration, i.e.,  $v_d$  and  $\omega_d$ . After that all required path parameters are calculated with help of transformed kinematic model [see (2)]. A complete work flow of this process is shown in Fig. 3. This process simplifies the task to obtain the parameters of any path of interest as a desired trajectory.

Robot learning from demonstration, which is famous for motion planning of a robot manipulator, has been adapted for a nonholonomic mobile robot in [23] to track the desired trajectory. In [23], the dynamic movement primitive parameters were learnt by demonstration. In relation to [23], the demonstration process is used to obtain the parameters of the desired trajectory for a group of mobile robots.

### B. Two-Step Design Process

There are two steps in this design process, i.e., HLC design and LLC design. A complete workflow of the two-step design process for an  $i$ th mobile robot is depicted in Fig. 4. HLC enables the virtual robots to generate a collision free reference trajectories while maintaining the desired formation. HLC also ensures the connectivity among the virtual robots throughout the process. State of an  $i$ th virtual robot acts as a reference for an  $i$ th nonholonomic mobile robot. The role of LLC is to track the reference trajectories.

**1) HLC design:** The control law for the holonomic model (1) is designed as

$$\begin{aligned} u_i^h &= \bar{u}_i^h + {}^{\text{dist}}u_i^h \\ &= \left\{ - \sum_{j \in \mathcal{N}_i} (e_i - e_j) - \sum_{j \in \mathcal{N}_i} (v_i^h - v_j^h) \right. \\ &\quad \left. - \sum_{j \in \mathcal{N}_i^c} \nabla_{p_i^h} \psi_{\text{col}}(\|p_{ij}^h\|) - \sum_{j \in \mathcal{N}_i / \mathcal{N}_i^c} \nabla_{e_i} \psi_{\text{conn}}(\|e_{ij}\|) \right\} \end{aligned}$$

$$- (v_i^h - v^t) - (e_i - p^t) + \dot{v}^t \} + {}^{\text{dist}}u_i^h \quad (12)$$

where  $e_{ij} = e_i - e_j$  and  $p_{ij}^h = p_i^h - p_j^h$ .  $p^t = [x^t, y^t]^T \in \mathbb{R}^2$ ,  $v^t = [v_x^t, v_y^t]^T \in \mathbb{R}^2$ , and  $\dot{v}^t = [u_x^t, u_y^t]^T \in \mathbb{R}^2$  are the position, velocity, and acceleration of the demonstrated trajectory.  $\nabla_{p_i^h}$  and  $\nabla_{e_i}$  represent the gradients along  $p_i^h$  and  $e_i$ , respectively.  ${}^{\text{dist}}u_i^h = P^h K^h$  is the disturbance compensation term for  $i$ th virtual mobile robot.  $P^h \in \mathbb{R}^{2 \times 2}$  is symmetric matrix and  $K^h \in \mathbb{R}^2$ . Collision avoidance and connectivity assurance terms are designed using APF [26]. For collision avoidance and connectivity assurance terms, we proceed along the lines of [10] with appropriate modification. An important modification we make is to adjust the range of the potential function in collision avoidance term.

**a) Potential function for collision avoidance:** The controller has to be designed so that no mobile robot enters the inner boundary of another mobile robot. This term functions for a pair of mobile robots  $i$  and  $j$  when

$$r_{\text{in}} \leq \|p_i^h - p_j^h\| < r_{\text{out}} < \min\{\|z_{ij}^*\|\} \quad \forall i, j.$$

The potential function has to be so chosen that the collision avoidance term becomes zero when  $\|p_i^h - p_j^h\| \geq r_{\text{out}}$ . A modified potential function is presented with finite cutoff at  $r_{\text{out}}$  as

$$\psi_{\text{col}}(\zeta) = \begin{cases} \int_{r_{\text{out}}}^{\zeta} \phi_{\text{col}}(s) ds; & \text{for } \zeta \in [r_{\text{in}}, r_{\text{out}}] \\ 0; & \text{otherwise} \end{cases}$$

where  $\zeta = \|p_i^h - p_j^h\|$ .  $\phi_{\text{col}}$  is such that a repulsive potential function ( $\psi_{\text{col}}(\zeta)$ ) is strictly decreasing, and attains its maximum value at  $r_{\text{in}}$ , as shown Fig. 2(c). The  $\phi_{\text{col}}$  is chosen as

$$\phi_{\text{col}} = - \frac{\|p_{ij}^h\| (r_{\text{out}} - r_{\text{in}})^{dn}}{(\|p_{ij}^h\| - r_{\text{in}})^2 + \frac{1}{Q_{\text{col}}}}.$$

The potential function above is novel as compared to [10]. It holds that  $dn \geq 0$  and  $Q_{\text{col}} > 0$ . The response of potential function for various value of  $dn$  can be seen in Fig. 2(c). In Fig. 2(c), the values of parameters are chosen as follows:  $r_{\text{in}} = 1$  m,  $r_{\text{out}} = 2.2$  m, and  $Q_{\text{col}} = 200$ . Fig. 2(c) suggests that the range of  $\psi_{\text{col}}$  can be increased by increasing the value of  $dn$ . The collision avoidance term for an  $i$ th robot ( $T_i^{\text{ca}}$ ) is defined as

$$T_i^{\text{ca}} = - \sum_{j \in \mathcal{N}_i^c} \nabla_{p_i^h} \psi_{\text{col}}(\|p_i^h - p_j^h\|).$$

Using the fundamental theorem of calculus with chain rule, the term  $T_i^{\text{ca}}$  can be expressed as

$$T_i^{\text{ca}} = - \sum_{j \in \mathcal{N}_i^c} \phi_{\text{col}}(\|p_i^h - p_j^h\|) \frac{p_i^h - p_j^h}{\|p_i^h - p_j^h\|}.$$

Whenever mobile robots are outside the outer boundary, the collision avoidance term remains inactive. This term becomes active when this condition is violated and the neighborhood concept changes during the avoidance of collision. The collision avoidance term generates a force inducing a robot to move away from its neighbor.

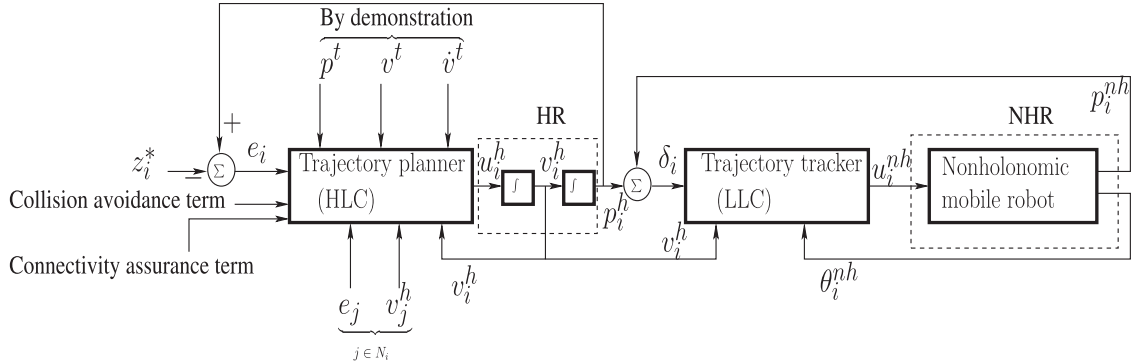


**Fig. 4.** Block diagram of a two-step design process.

*b) Potential function to maintain connectivity:* The potential function for connectivity preservation with finite cutoff  $R^e = (\text{abs}(R - \|z_{ij}^*\|))$  is chosen as [10]

$$\psi_{\text{conn}}(\eta) = \begin{cases} \int_{r_{\text{out}}^e}^{\eta} \phi_{\text{conn}}(s) ds, & \text{for } \eta \in [r_{\text{out}}^e, R^e] \\ 0, & \text{otherwise} \end{cases}$$

where  $\eta = \|e_i - e_j\|$ ,  $r_{\text{out}}^e = \text{abs}(r_{\text{out}} - \|z_{ij}^*\|)$ .  $\phi_{\text{conn}}(\eta)$  is to be so chosen that an attractive potential function ( $\psi_{\text{conn}}(\eta)$ ) is strictly increasing, and attains its minimum value at  $r_{\text{out}}^e$ . The  $\phi_{\text{conn}}$  is chosen as

$$\phi_{\text{conn}} = -\frac{\|e_{ij}\|}{(\|e_{ij}\| - R^e)^2 + \frac{1}{Q_{\text{conn}}}}$$

where  $Q_{\text{conn}} > 0$ . The connectivity assurance term ( $T_i^{\text{cass}}$ ) is defined in [10] as

$$T_i^{\text{cass}} = -\sum_{j \in \mathcal{N}_i / \mathcal{N}_i^c} \nabla_{e_i} \psi_{\text{conn}}(\|e_i - e_j\|).$$

The term  $T_i^{\text{cass}}$  can be written as

$$T_i^{\text{cass}} = -\sum_{j \in \mathcal{N}_i / \mathcal{N}_i^c} \phi_{\text{conn}}(\|e_i - e_j\|) \frac{e_i - e_j}{\|e_i - e_j\|}.$$

The connectivity assurance term produces a force attracting a robot toward its neighbors.

*Theorem 1:* The designed control law in (12) enables a set of virtual robots with the dynamics as defined in (1) to track the demonstrated trajectory in formation in the presence of disturbances, if the following conditions are satisfied:

- 1)  $P^h \in \mathbb{R}^{2 \times 2}$  is real symmetric negative definite matrix.
- 2)  $\|K^h\| = 1$ , where  $K^h \in \mathbb{R}^2$ .
- 3)  $(\lambda_{\max}(P^h) + \alpha) < 0$ .
- 4)  $(\lambda_{\max}(P^h) + \alpha) \leq -C\|\bar{v}_i\|$ , where  $C$  is a positive constant.

*Proof:* We consider the following positive semidefinite function [10] as follows:

$$V = \frac{1}{2} \sum_{i=1}^N \left[ \sum_{j \in \mathcal{N}_i^c} \psi_{\text{col}}(\|p_{ij}^h\|) + \sum_{j \in \mathcal{N}_i / \mathcal{N}_i^c} \psi_{\text{conn}}(\|e_{ij}\|) + \bar{e}_i^T \bar{e}_i + \bar{v}_i^T \bar{v}_i \right] + \frac{1}{2} e^T (L \otimes I_2) e \quad (13)$$

where  $L \in \mathbb{R}^{N \times N}$  is the Laplacian matrix of the graph of mobile robots.  $I_2 \in \mathbb{R}^{2 \times 2}$  is an identity matrix.  $L \otimes I_2$  denotes a Kronecker product of  $L$  and  $I_2$ .  $\bar{e}_i = e_i - p^t$ ,  $\bar{v}_i = v_i^h - v^t$ ,  $e = [e_1^T \cdots e_N^T]^T \in (\mathbb{R}^2)^N$ , and  $v = [(v_1^h)^T \cdots (v_N^h)^T]^T \in (\mathbb{R}^2)^N$ . It has been assumed that  $V(0) < V_{\text{up}}$ , where  $V_{\text{up}}$  is some upper bound

$$\begin{aligned} \dot{V} &= \sum_{i=1}^N \left[ (v_i^h)^T \sum_{j \in \mathcal{N}_i^c} \nabla_{p_i^h} \psi_{\text{col}}(\|p_{ij}^h\|) + \bar{e}_i^T \bar{v}_i + \bar{v}_i^T \dot{v}_i^h - \bar{v}_i^T v^t \right. \\ &\quad \left. + (v_i^h)^T \sum_{j \in \mathcal{N}_i / \mathcal{N}_i^c} \nabla_{e_i} \psi_{\text{conn}}(\|e_{ij}\|) \right] + e^T (L \otimes I_2) v \\ \dot{V} &= \sum_{i=1}^N \left[ (v_i^h)^T \sum_{j \in \mathcal{N}_i^c} \nabla_{p_i^h} \psi_{\text{col}}(\|p_{ij}^h\|) + \bar{e}_i^T \bar{v}_i \right. \\ &\quad \left. + (v_i^h)^T \sum_{j \in \mathcal{N}_i / \mathcal{N}_i^c} \nabla_{e_i} \psi_{\text{conn}}(\|e_{ij}\|) \right] + e^T (L \otimes I_2) v \\ &\quad + \sum_{i=1}^N \bar{v}_i^T u_i^h - \sum_{i=1}^N \bar{v}_i^T \dot{v}^t + \sum_{i=1}^N \bar{v}_i^T \rho_i^h \quad (14) \end{aligned}$$

$$\begin{aligned} \dot{V} &= \sum_{i=1}^N (v_i^h)^T \sum_{j \in \mathcal{N}_i^c} \nabla_{p_i^h} \psi_{\text{col}}(\|p_{ij}^h\|) + \sum_{i=1}^N \bar{e}_i^T \bar{v}_i \\ &\quad + \sum_{i=1}^N (v_i^h)^T \sum_{j \in \mathcal{N}_i / \mathcal{N}_i^c} \nabla_{e_i} \psi_{\text{conn}}(\|e_{ij}\|) + e^T (L \otimes I_2) v \\ &\quad + \sum_{i=1}^N \bar{v}_i^T \bar{u}_i^h - \sum_{i=1}^N \bar{v}_i^T \dot{v}^t + \sum_{i=1}^N \bar{v}_i^T \text{dist} u_i^h + \sum_{i=1}^N \bar{v}_i^T \rho_i^h. \quad (15) \end{aligned}$$

$$\begin{aligned} \dot{V} &= \sum_{i=1}^N (v_i^h)^T \sum_{j \in \mathcal{N}_i^c} \nabla_{p_i^h} \psi_{\text{col}}(\|p_{ij}^h\|) + \sum_{i=1}^N \bar{e}_i^T \bar{v}_i + \sum_{i=1}^N \bar{v}_i^T \rho_i^h \\ &\quad + \sum_{i=1}^N (v_i^h)^T \sum_{j \in \mathcal{N}_i / \mathcal{N}_i^c} \nabla_{e_i} \psi_{\text{conn}}(\|e_{ij}\|) + e^T (L \otimes I_2) v \end{aligned}$$

$$\begin{aligned}
& + \sum_{i=1}^N \bar{v}_i^T \left\{ - \sum_{j \in \mathcal{N}_i} (e_i - e_j) - \sum_{j \in \mathcal{N}_i} (v_i^h - v_j^h) \right. \\
& - \sum_{j \in \mathcal{N}_i^c} \nabla_{p_i^h} \psi_{\text{col}}(\|p_{ij}^h\|) - \sum_{j \in \mathcal{N}_i / \mathcal{N}_i^c} \nabla_{e_i} \psi_{\text{conn}}(\|e_{ij}\|) \\
& \left. - (v_i^h - v^t) - (e_i - p^t) + v^t \right\} - \sum_{i=1}^N \bar{v}_i^T \dot{v}^t + \sum_{i=1}^N \bar{v}_i^T \text{dist} u_i^h \\
& = \sum_{i=1}^N (v_i^h)^T \sum_{j \in \mathcal{N}_i^c} \nabla_{p_i^h} \psi_{\text{col}}(\|p_{ij}^h\|) + \sum_{i=1}^N \bar{e}_i^T \bar{v}_i \\
& + \sum_{i=1}^N (v_i^h)^T \sum_{j \in \mathcal{N}_i / \mathcal{N}_i^c} \nabla_{e_i} \psi_{\text{conn}}(\|e_{ij}\|) + e^T (L \otimes I_2) v \\
& + \sum_{i=1}^N \bar{v}_i^T \left\{ - \sum_{j \in \mathcal{N}_i} (e_i - e_j) - \sum_{j \in \mathcal{N}_i} (v_i^h - v_j^h) \right. \\
& - \sum_{j \in \mathcal{N}_i^c} \nabla_{p_i^h} \psi_{\text{col}}(\|p_{ij}^h\|) - \sum_{j \in \mathcal{N}_i / \mathcal{N}_i^c} \nabla_{e_i} \psi_{\text{conn}}(\|e_{ij}\|) \\
& \left. - \bar{v}_i - \bar{e}_i \right\} + \sum_{i=1}^N \bar{v}_i^T \text{dist} u_i^h + \sum_{i=1}^N \bar{v}_i^T \rho_i^h \\
& = - \sum_{i=1}^N \bar{v}_i^T \bar{v}_i - \sum_{i=1}^N (v_i^h)^T \sum_{j \in \mathcal{N}_i} (e_i - e_j) \\
& - \sum_{i=1}^N \bar{v}_i^T \sum_{j \in \mathcal{N}_i} (v_i^h - v_j^h) \\
& + \sum_{i=1}^N ((v_i^h)^T - \bar{v}_i^T) \left\{ \sum_{j \in \mathcal{N}_i^c} \nabla_{p_i^h} \psi_{\text{col}}(\|p_{ij}^h\|) \right. \\
& + \sum_{j \in \mathcal{N}_i / \mathcal{N}_i^c} \nabla_{e_i} \psi_{\text{conn}}(\|e_{ij}\|) \left. \right\} + \sum_{i=1}^N (v^t)^T \sum_{j \in \mathcal{N}_i} (e_i - e_j) \\
& + e^T (L \otimes I_2) v + \sum_{i=1}^N \bar{v}_i^T \text{dist} u_i^h + \sum_{i=1}^N \bar{v}_i^T \rho_i^h \\
\dot{V} & = - \sum_{i=1}^N \bar{v}_i^T \bar{v}_i - \sum_{i=1}^N (v_i^h)^T \sum_{j \in \mathcal{N}_i} (e_i - e_j) - \sum_{i=1}^N \bar{v}_i^T \sum_{j \in \mathcal{N}_i} (\bar{v}_i - \bar{v}_j) \\
& + \sum_{i=1}^N (v^t)^T \left\{ \sum_{j \in \mathcal{N}_i^c} \nabla_{p_i^h} \psi_{\text{col}}(\|p_{ij}^h\|) \right. \\
& + \sum_{j \in \mathcal{N}_i / \mathcal{N}_i^c} \nabla_{e_i} \psi_{\text{conn}}(\|e_{ij}\|) + \sum_{j \in \mathcal{N}_i} (e_i - e_j) \left. \right\} \\
& + e^T (L \otimes I_2) v \\
& + \sum_{i=1}^N \bar{v}_i^T \text{dist} u_i^h + \sum_{i=1}^N \bar{v}_i^T \rho_i^h
\end{aligned}$$

$$\begin{aligned}
\dot{V} & = - \sum_{i=1}^N \bar{v}_i^T \bar{v}_i - \sum_{i=1}^N (v_i^h)^T \sum_{j \in \mathcal{N}_i} (e_i - e_j) \\
& - \sum_{i=1}^N \bar{v}_i^T \sum_{j \in \mathcal{N}_i} (\bar{v}_i - \bar{v}_j) \\
& + V_1 + e^T (L \otimes I_2) v + \sum_{i=1}^N \bar{v}_i^T \text{dist} u_i^h + \sum_{i=1}^N \bar{v}_i^T \rho_i^h.
\end{aligned}$$

where

$$\begin{aligned}
V_1 & = \sum_{i=1}^N (v^t)^T \left\{ \sum_{j \in \mathcal{N}_i^c} \nabla_{p_i^h} \psi_{\text{col}}(\|p_{ij}^h\|) \right. \\
& \left. + \sum_{j \in \mathcal{N}_i / \mathcal{N}_i^c} \nabla_{e_i} \psi_{\text{conn}}(\|e_{ij}\|) + \sum_{j \in \mathcal{N}_i} (e_i - e_j) \right\}.
\end{aligned}$$

For an undirected graph, the matrix  $L$  is symmetric. Control law depends on  $L$  such that the forces generated by each virtual mobile robots are equal and opposite in direction [10]. Hence,  $V_1 = 0$ . Let us use the property of Laplacian

$$\begin{aligned}
\sum_{i=1}^N (v_i^h)^T \sum_{j \in \mathcal{N}_i} (e_i - e_j) & = v^T (L \otimes I_2) e \\
v^T (L \otimes I_2) e & = e^T (L \otimes I_2) v. \\
\sum_{i=1}^N \bar{v}_i^T \sum_{j \in \mathcal{N}_i} (\bar{v}_i - \bar{v}_j) & = \bar{v}^T (L \otimes I_2) \bar{v}
\end{aligned}$$

$$\text{where, } \bar{v} = [\bar{v}_1^T \cdots \bar{v}_N^T]^T \in (\mathbb{R}^2)^N.$$

Hence, the expression for  $\dot{V}$  can be written as

$$\begin{aligned}
\dot{V} & = - \sum_{i=1}^N \bar{v}_i^T \bar{v}_i - v^T (L \otimes I_2) e - \bar{v}^T (L \otimes I_2) \bar{v} + v^T (L \otimes I_2) e \\
& + \sum_{i=1}^N \bar{v}_i^T \text{dist} u_i^h + \sum_{i=1}^N \bar{v}_i^T \rho_i^h \\
\dot{V} & = - \sum_{i=1}^N \bar{v}_i^T \bar{v}_i - \bar{v}^T (L \otimes I_2) \bar{v} \\
& + \sum_{i=1}^N \bar{v}_i^T \text{dist} u_i^h + \sum_{i=1}^N \bar{v}_i^T \rho_i^h. \tag{16}
\end{aligned}$$

Let us consider  $\psi(\bar{v}_i, \bar{v}) = - \sum_{i=1}^N \bar{v}_i^T \bar{v}_i - \bar{v}^T (L \otimes I_2) \bar{v}$ , and rewrite (16) as follows:

$$\begin{aligned}
\dot{V} & = \psi(\bar{v}_i, \bar{v}) + \sum_{i=1}^N \bar{v}_i^T \text{dist} u_i^h + \sum_{i=1}^N \bar{v}_i^T \rho_i^h \\
& = \psi(\bar{v}_i, \bar{v}) + \sum_{i=1}^N \langle \bar{v}_i, \text{dist} u_i^h \rangle + \sum_{i=1}^N \langle \bar{v}_i, \rho_i^h \rangle
\end{aligned}$$

$$\begin{aligned}
&= \psi(\bar{v}_i, \bar{v}) + \sum_{i=1}^N \langle \bar{v}_i, P^h K^h \rangle + \sum_{i=1}^N \langle \bar{v}_i, \rho_i^h \rangle \\
\dot{V} &\leq \psi(\bar{v}_i, \bar{v}) + \sum_{i=1}^N \|\bar{v}_i\| \|P^h K^h\| + \sum_{i=1}^N \|\bar{v}_i\| \|\rho_i^h\| \\
&\leq \psi(\bar{v}_i, \bar{v}) + \sum_{i=1}^N \|\bar{v}_i\| \|P^h\| \|K^h\| + \sum_{i=1}^N \|\bar{v}_i\| \|\rho_i^h\| \\
&\leq \psi(\bar{v}_i, \bar{v}) + \lambda_{\max}(P^h) \sum_{i=1}^N \|\bar{v}_i\| \|K^h\| + \alpha \sum_{i=1}^N \|\bar{v}_i\|.
\end{aligned}$$

Since  $\|K^h\| = 1$ , therefore  $\dot{V} \leq \psi(\bar{v}_i, \bar{v}) + (\lambda_{\max}(P^h) + \alpha) \sum_{i=1}^N \|\bar{v}_i\|$ .

Since  $P^h$  is real symmetric negative definite such that  $(\lambda_{\max}(P^h) + \alpha) < 0$ , we can write as follows:

$$\dot{V} \leq \psi(\bar{v}_i, \bar{v}) + (\lambda_{\max}(P^h) + \alpha) \sum_{i=1}^N \|\bar{v}_i\| \leq 0. \quad (17)$$

Using (17), we can write as follows:

$$V(t) \leq V(0) < V_{\text{up}}. \quad (18)$$

From (18) and (13), it is observed that the variables in (13) are bounded for the system (1). Let us consider  $(\lambda_{\max}(P^h) + \alpha) \leq -C\|\bar{v}_i\|$ , then (17) can be written as

$$\dot{V} \leq \psi(\bar{v}_i, \bar{v}) - C \sum_{i=1}^N \|\bar{v}_i\|^2 \leq 0.$$

Again we can write as follows:

$$\dot{V} \leq - \sum_{i=1}^N \bar{v}_i^T \bar{v}_i - \bar{v}^T (L \otimes I_2) \bar{v} - C \sum_{i=1}^N \|\bar{v}_i\|^2 \leq 0 \quad (19)$$

$\dot{V}$  exists, and it is bounded as the variable  $\bar{v}_i$  and  $u_i^h$  are bounded. Hence from Barbarat's Lemma [27], we can write,  $\dot{V} \rightarrow 0$ , as  $t \rightarrow \infty$ . Employing this criteria in (19), and excluding the contradiction in inequality, we can write as follows: at  $t \rightarrow \infty$ ,  $-\sum_{i=1}^N \bar{v}_i^T \bar{v}_i - \bar{v}^T (L \otimes I_2) \bar{v} - C \sum_{i=1}^N \|\bar{v}_i\|^2 \rightarrow 0$  the above is possible iff  $\bar{v}_i \rightarrow 0$ , or  $v_i^h \rightarrow v^t \forall i$ . Hence, using (1) and (12), we can write as follows: as  $t \rightarrow \infty$

$$\begin{aligned}
&\dot{v}^t \leftarrow - \sum_{j \in \mathcal{N}_i} (e_i - e_j) - \sum_{j \in \mathcal{N}_i} (v_i^h - v_j^h) - \sum_{j \in \mathcal{N}_i^c} \nabla_{p_i^h} \psi_{\text{col}}(\|p_{ij}^h\|) \\
&\quad + \dot{v}^t - \sum_{j \in \mathcal{N}_i / \mathcal{N}_i^c} \nabla_{e_i} \psi_{\text{conn}}(\|e_{ij}\|) - (v_i^h - v^t) - (e_i - p^t) \\
&\quad + {}^{\text{dist}} u_i^h + \rho_i^h \\
0 &\leftarrow - \sum_{j \in \mathcal{N}_i} (e_i - e_j) - \sum_{j \in \mathcal{N}_i} (v_i^h - v_j^h) - \sum_{j \in \mathcal{N}_i^c} \nabla_{p_i^h} \psi_{\text{col}}(\|p_{ij}^h\|) \\
&\quad - \sum_{j \in \mathcal{N}_i / \mathcal{N}_i^c} \nabla_{e_i} \psi_{\text{conn}}(\|e_{ij}\|) - (v_i^h - v^t) - (e_i - p^t) \\
&\quad + {}^{\text{dist}} u_i^h + \rho_i^h.
\end{aligned}$$

$v_i^h \rightarrow v^t, \forall i$ , at  $t \rightarrow \infty$ . Hence  $v_i^h \rightarrow v_j^h, \forall i, j$ , confirms the velocity consensus. To satisfy the above equation, it is required  $e_i \rightarrow p^t, e_i \rightarrow e_j, {}^{\text{dist}} u_i^h + \rho_i^h \rightarrow 0, \forall i, j$  as  $t \rightarrow \infty$ . ■

**2) LLC design:** The control law for the nonholonomic model (3) is designed as

$$u_i^{nh} = Q_i^{-1}(-g\delta_i + v_i^h + {}^{\text{dist}} u_i^{nh}) \quad (20)$$

where  $v_i^h$  refers to the velocity response of the holonomic model (1) with the formation control law (12).  ${}^{\text{dist}} u_i^{nh} = P^{nh} K^{nh}$  is the disturbance compensation term for the  $i$ th nonholonomic mobile robot.  $P^{nh} \in \mathbb{R}^{2 \times 2}$  is symmetric matrix and  $K^{nh} \in \mathbb{R}^2$ . The control input given in (20) is a classical feedback linearization of a unicycle-like mobile robot.

**Theorem 2:** The control law given by (20) makes the system (3) stable in the sense of Lyapunov, if the following conditions are satisfied:

- 1)  $P^{nh}$  is real symmetric negative definite matrix.
- 2)  $g > 0$ .
- 3)  $(\lambda_{\max}(P^{nh}) + M) < 0$ , where  $M$  is a bound on the disturbances.
- 4)  $\|K^{nh}\| = 1$ .

*Proof:* To investigate the convergence, we consider the following Lyapunov function:

$$V = \frac{1}{2} \sum_{i=1}^N \delta_i^T \delta_i. \quad (21)$$

Let us evaluate  $\dot{V}$

$$\begin{aligned}
\dot{V} &= \sum_{i=1}^N \delta_i^T \dot{\delta}_i = \sum_{i=1}^N \delta_i^T (\dot{p}_i^{nh} - \dot{p}_i^h) \\
&= \sum_{i=1}^N \delta_i^T (Q_i u_i^{nh} + f_i - v_i^h).
\end{aligned}$$

Using (20), we can write the above equation as

$$\begin{aligned}
\dot{V} &= \sum_{i=1}^N \delta_i^T (Q_i Q_i^{-1}(-g\delta_i + v_i^h + {}^{\text{dist}} u_i^{nh}) + f_i - v_i^h) \\
&= -g \sum_{i=1}^N \delta_i^T \delta_i + \sum_{i=1}^N \delta_i^T f_i + \sum_{i=1}^N \delta_i^T ({}^{\text{dist}} u_i^{nh}) \\
&= -g \sum_{i=1}^N \delta_i^T \delta_i + \sum_{i=1}^N \delta_i^T f_i + \sum_{i=1}^N \delta_i^T P^{nh} K^{nh} \\
&= -g \sum_{i=1}^N \delta_i^T \delta_i + \sum_{i=1}^N \langle \delta_i, f_i \rangle + \sum_{i=1}^N \langle \delta_i, P^{nh} K^{nh} \rangle \\
&\leq -g \sum_{i=1}^N \|\delta_i\| \|\delta_i\| + \sum_{i=1}^N \|\delta_i\| \|f_i\| + \sum_{i=1}^N \|\delta_i\| \|P^{nh} K^{nh}\| \\
&\leq -g \sum_{i=1}^N \|\delta_i\| \|\delta_i\| + \sum_{i=1}^N \|\delta_i\| \|f_i\| + \sum_{i=1}^N \|\delta_i\| \|P^{nh}\| \|K^{nh}\|
\end{aligned}$$

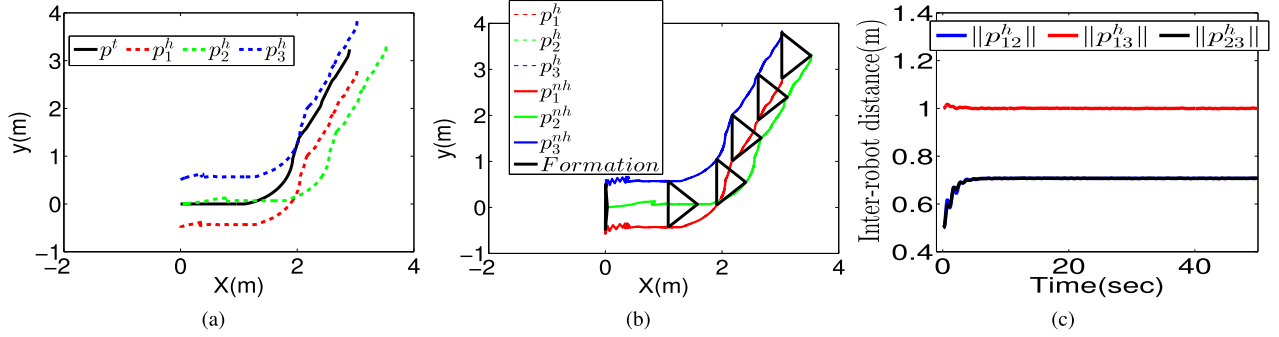


Fig. 5. Simulation: (a) Demonstrated path and reference trajectories. (b) Trajectory tracking by a group of mobile robots while obtaining the predefined formation without collision. (c) Distance among the robots over the time.

$$\begin{aligned} &\leq -g \sum_{i=1}^N \|\delta_i\| \|\delta_i\| + \sum_{i=1}^N \|\delta_i\| \|f_i\| \\ &+ \sum_{i=1}^N \|\delta_i\| \lambda_{\max}(P^{nh}) \|K^{nh}\| \\ &\leq -g \sum_{i=1}^N \|\delta_i\| \|\delta_i\| + \sum_{i=1}^N \|\delta_i\| \|f_i\| \\ &+ \lambda_{\max}(P^{nh}) \sum_{i=1}^N \|\delta_i\| \|K^{nh}\|. \end{aligned}$$

Using the disturbance bound, and putting  $\|K^{nh}\| = 1$

$$\begin{aligned} \dot{V} &\leq -g \sum_{i=1}^N \|\delta_i\| \|\delta_i\| + \sum_{i=1}^N \|\delta_i\| M + \lambda_{\max}(P^{nh}) \sum_{i=1}^N \|\delta_i\| \\ \dot{V} &\leq -g \sum_{i=1}^N \|\delta_i\| \|\delta_i\| + (\lambda_{\max}(P^{nh}) + M) \sum_{i=1}^N \|\delta_i\|. \end{aligned}$$

To make the system stable,  $g > 0$  and the matrix  $P^{nh}$  should be real symmetric negative definite, such that  $(\lambda_{\max}(P^{nh}) + M) < 0$ . Hence, based on this criteria, right-hand side of the above inequality will always be negative, and zero when  $\delta_i = 0$ . Thus, we can write as follows:

$$\dot{V} \leq -g \sum_{i=1}^N \|\delta_i\| \|\delta_i\| + (\lambda_{\max}(P^{nh}) + M) \sum_{i=1}^N \|\delta_i\| < 0.$$

Since,  $\dot{V} < 0$ , therefore, error dynamics is asymptotically stable. Hence,  $\delta_i$  converges asymptotically to zero. ■

## V. RESULTS AND DISCUSSIONS

### A. Simulation

The proposed scheme is validated through simulation and experiments as well. The three-robot system is considered to achieve a triangular formation. The design parameters are taken as  $R = 15$  m,  $r_{in} = 0.4$  m,  $r_{out} = 0.65$  m,  $g = 19.2$ ,  $P^h = \text{diag}\{-C\|\bar{v}_i\| - 0.6, -C\|\bar{v}_i\| - 0.6\}$ ,  $K^h = K^{nh} = [-0.866, -0.5]^T$ ,  $P^{nh} = \text{diag}\{-0.09, -0.09\}$ , and  $C = 0.32$ . Let  $\mathbf{N}(\mu, \sigma^2)$  denotes the normal distribution with its mean ( $\mu$ ) and variance ( $\sigma^2$ ). Normal distribution with

zero mean and unit variance has been considered to generate the random disturbances, i.e.,  $\mathbf{N}(0, 1)$ . Initial positions of nonholonomic and virtual robots are set at  $p_1^{nh} = [0.0, -0.6]^T$  m,  $p_2^{nh} = [0.0, 0.0]^T$  m,  $p_3^{nh} = [0.0, 0.6]^T$  m,  $p_1^h = [0.0, -0.5]^T$  m,  $p_2^h = [0.0, 0.0]^T$  m, and  $p_3^h = [0.0, 0.5]^T$  m. Desired formation shape is chosen as  $Z^* = [[0.0, -0.5]^T, [0.5, 0.0]^T, [0.0, 0.5]^T]^T$  m. The initially connected graph is described by the adjacency matrix:  $a_{12} = a_{21} = a_{23} = a_{32} = a_{13} = a_{31} = 1$ ;  $a_{11} = a_{22} = a_{33} = 0$ . In Fig. 5(a), black color indicates the demonstrated trajectory. Reference trajectories for Robot-A, Robot-B, and Robot-C are represented by red, green, and blue color, respectively. Fig. 5(b) suggests that the three robots maintain a triangular formation while tracking the reference trajectories.

In Fig. 5(c), the interrobot distances ( $\|p_{ij}^h\| = \|p_i^h - p_j^h\|$ ) are shown. It is observed that interrobot distances are always greater than 0.4 m. Simultaneously the interrobot distances never go beyond 15 m, implying that connection is always maintained. Hence, the collision avoidance and connectivity assurance are confirmed. The position errors  $e_i = (p_i^h - z_i^*)$ ,  $\forall i$  are shown in Fig. 6(a). This figure shows consensus on position error  $e_i$ ,  $\forall i$ . Tracking errors ( $\delta_i$ ,  $\forall i$ ) over the time are shown in Fig. 6(b). It can be seen that errors in both  $x$  and  $y$  components approach to zero. It also means that nonholonomic mobile robots track the reference trajectories in the presence of disturbances. Linear and angular velocities for nonholonomic mobile robots are shown in Fig. 6(c).

Three different levels of noise ( $L_1$ ,  $L_2$ , and  $L_3$ ) are considered to analyze the performance of the proposed scheme. These levels are defined as  $L_1 \sim \mathbf{N}(0, 1)$ ;  $L_2 \sim \mathbf{N}(0, 2)$ ; and  $L_3 \sim \mathbf{N}(0, 3)$ .  $L_1$ ,  $L_2$ , and  $L_3$  are used to generate the random disturbances. Ten separate trials have been taken for each one of these levels. The obtained root-mean square (RMS) tracking errors are reported in Table I. A total of 95% confidence intervals are calculated using  $t$ -distribution. The performance of the proposed scheme in terms of tracking error with respect to various levels of noise can be seen in Fig. 7. Table I and Fig. 7 suggest that the proposed method works well in the presence of various levels of noise. It has been observed that the lower value of variance gives better accuracy in terms of the tracking error.

Further, we have considered a 4-robot system to check the effectiveness and scalability of the proposed method.

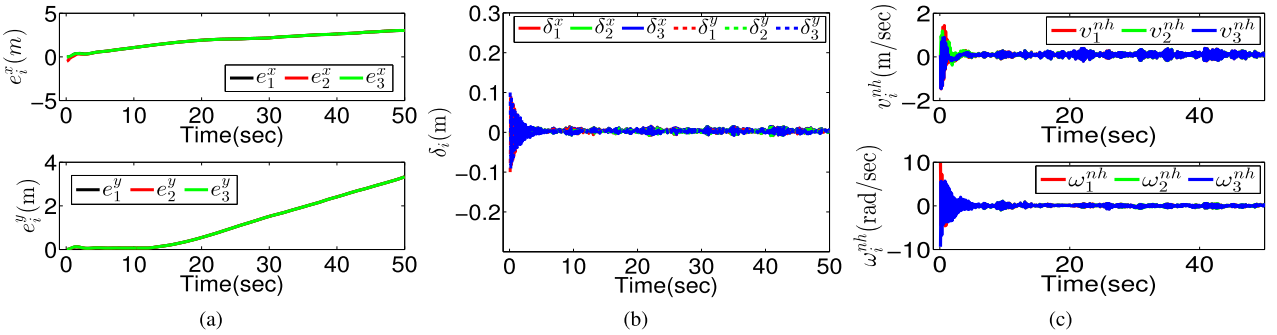


Fig. 6. Simulation: (a) Consensus in position error,  $e_i \forall i$ . (b) Tracking error. (c) Linear and angular velocities for nonholonomic mobile robots.

TABLE I  
RMS TRACKING ERROR (M)

Trial Number	Noise Level		
	L <sub>1</sub>	L <sub>2</sub>	L <sub>3</sub>
1	0.00148	0.00505	0.03079
2	0.00161	0.00130	0.00849
3	0.00376	0.01259	0.01590
4	0.00883	0.01745	0.00188
5	0.00709	0.01112	0.02008
6	0.00345	0.00203	0.00212
7	0.00200	0.01797	0.01206
8	0.00245	0.01927	0.01702
9	0.00643	0.01920	0.00422
10	0.00338	0.01570	0.01310

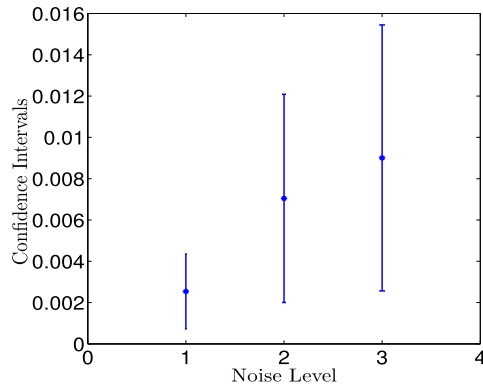


Fig. 7. Performance of the proposed scheme with respect to the different level of noise.

The design parameters are chosen as  $R = 8$  m,  $r_{\text{in}} = 0.4$  m, and  $r_{\text{out}} = 0.9$  m. Initial positions of nonholonomic and virtual robots are set at  $p_1^h = p_1^{\text{nh}} = [0.0, -0.5]^T$  m,  $p_2^h = p_2^{\text{nh}} = [0.0, 0.5]^T$  m,  $p_3^h = p_3^{\text{nh}} = [1.0, 0.5]^T$  m, and  $p_4^h = p_4^{\text{nh}} = [1.0, -0.5]^T$  m. Desire formation is chosen as  $Z^* = [[0.0, -0.5]^T, [0.0, 0.5]^T, [1.0, 0.5]^T, [1.0, -0.5]^T]^T$  m. The obtained results are incorporated in Fig. 8. It can be noticed that all four mobile robots navigate along the demonstrated path in a rectangular formation (desired formation in this case) while tracking the reference trajectories, as shown in Fig. 8(b). Fig. 8(c) suggests that the proposed approach not only avoids the collision but also ensures the connectivity, throughout the process.

### B. Hardware Description and Experimental Results

Three pioneer P3-DX mobile robots are used to perform the experiment, as shown in Fig. 9. Each robot is equipped with an onboard computer (OBC). One Desktop computer is also used to execute different robot operating system (ROS) node, remotely. All systems are running on Linux environment with ROS. These systems are connected through a ROS network. A dedicated wifi router (Netgear) is used to maintain a sufficient network strength throughout the experiment. RosAria is used to perform all required two-way communication between the OBC and mobile robot. We run a ROS master on a Desktop computer. This ROS master is then exported on each OBC. After that three different launch files are executed to connect all the systems to a common ROS environment. In the ROS environment, each robot can send its odometry data on the specific rostopic. Each robot can also receive the required data (parameters of the desired path and data related to its neighbors) from the respective rostopic. Odometry feedbacks are utilized to obtain the positions of nonholonomic mobile robots. Odometry data are available at the rate of 10 Hz. Hence, we use 0.1 s as a sampling interval.

One of the P3-DX mobile robots is used for the demonstration. We follow the steps of Fig. 3 to obtain position, velocity, and acceleration of a demonstrated trajectory, i.e.,  $p^t, v^t, u^t$ . These parameters are used while performing the experiment. The initially connected graph is described using the adjacency matrix such that  $a_{ij} = 1 \forall i \neq j$ ; and  $a_{ii} = 0 \forall i = j$ . Each nonholonomic mobile robot is perturbed by a pair of wires. One pair is shown in Fig. 2(d). These wires are used over the wheels of nonholonomic mobile robots. Numerical value of parameters are chosen as  $r_{\text{in}} = 0.7$  m,  $r_{\text{out}} = 0.9$  m,  $R = 15$  m,  $g = 80$ , and  $l = 0.2$  m. Initial positions of nonholonomic and virtual mobile robots are set at  $p_1^h \approx [0.0, -0.7]^T$  m,  $p_2^h \approx [0.0, 0.0]^T$  m,  $p_3^h \approx [0.0, 0.7]^T$  m,  $p_4^h = [0.0, -0.5]^T$  m,  $p_1^{\text{nh}} = [0.0, 0.0]^T$  m, and  $p_3^{\text{nh}} = [0.0, 0.5]^T$  m. Desire formation shape is chosen as  $Z^* = [[0.0, 0.5]^T, [0.5, 0.0]^T, [0.0, -0.5]^T]^T$  m.

Generated reference trajectories along with the demonstrated trajectory are shown in Fig. 10(a). Fig. 10(b) shows that the all three robots maintain a triangular formation while tracking the desired trajectory. The interrobot distances are always greater than 0.7 m as shown in Fig. 10(c). It means that there is no collision among the robots. It can also be seen that the interrobot

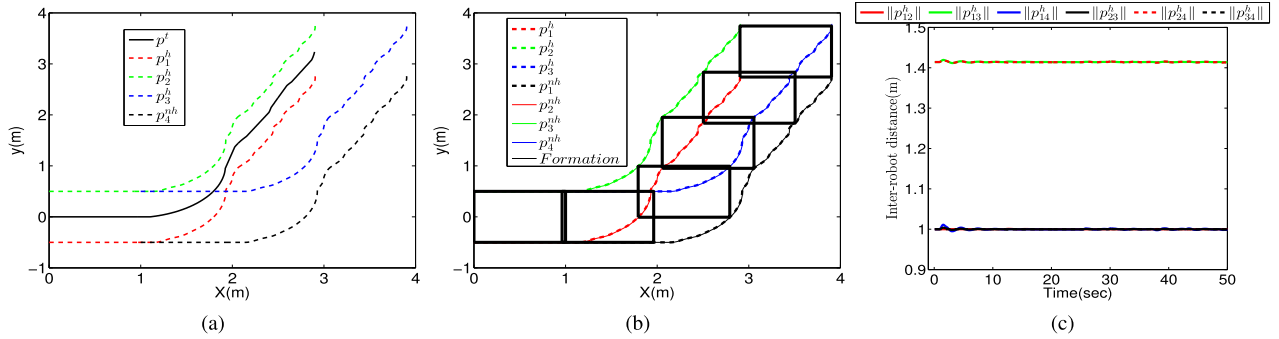


**Fig. 8.** Simulation [4-robot system]. (a) Demonstrated path and reference trajectories. (b) Trajectory tracking by a group of mobile robots while obtaining the predefined formation without collision. (c) Distance among the robots over the time.



**Fig. 9.** Experimental setup.

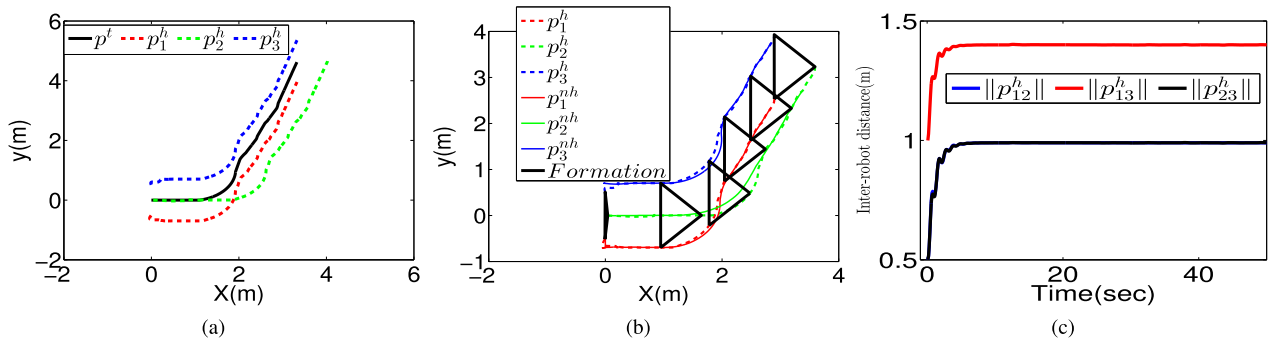


**Fig. 10.** Experiment: (a) Demonstrated path and reference trajectories. (b) Trajectory tracking by a group of mobile robots while obtaining the predefined formation without collision. (c) Distance among the robots over the time.

distances never go beyond 15 m. It suggests that the constraint of connectivity is ensured during the experiment. Position consensus among the mobile robots is shown in Fig. 11(a) while Fig. 11(b) shows the tracking error ( $\delta_i, \forall i$ ) over the time. Control inputs for nonholonomic mobile robots can be seen in Fig. 11(c).

Taped video images of the experiment are shown in the Fig. 12. Fig. 12(a) indicates the initial positions of nonholonomic mobile robots. It can be noted that all three nonholonomic mobile robots achieve a desired formation (triangular formation) from an initial formation pattern. A sequence of taped video images [see Fig. 12(a)–(f)] show that there is no collision among the

robots during the experiment. The video of the experiment is available at <https://youtu.be/EX2Hw-Bb7Gw>.

*Application:* To solve PTP, a demonstration is given to one of the nonholonomic mobile robots to obtain the parameters of the path of interest. We set a desired formation as  $Z^* = [[0.0, -0.7]^T, [0.0, 0.0]^T, [0.0, 0.7]^T]^T$  m. Initial positions of actual and virtual mobile robots are set at  $p_1^{nh} \approx [0.0, -0.7]^T$  m,  $p_2^{nh} \approx [0.0, 0.0]^T$  m,  $p_3^{nh} \approx [0.0, 0.7]^T$  m,  $p_1^h = [0.0, -0.7]^T$  m,  $p_2^h = [0.0, 0.0]^T$  m, and  $p_3^h = [0.0, 0.7]^T$  m. Obtained results are shown in Fig. 13. Taped video images of the experiment for this application are incorporated in Fig. 14. A group of three nonholonomic mobile robots is started from a point  $p_a$  in the

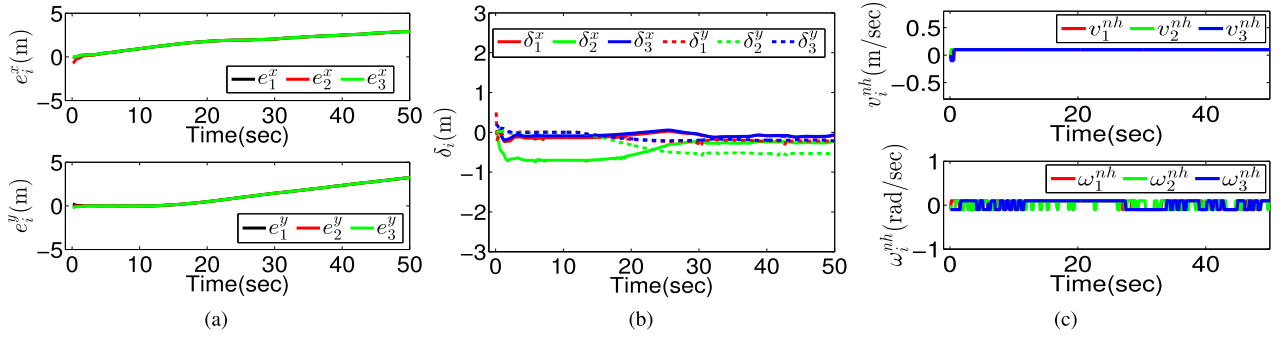


Fig. 11. Experiment: (a) Consensus in position error,  $e_i \forall i$ . (b) Tracking error. (c) Linear and angular velocities for nonholonomic mobile robots.



Fig. 12. Experiment: Trajectory tracking by a group of nonholonomic mobile robots while obtaining a desired formation.

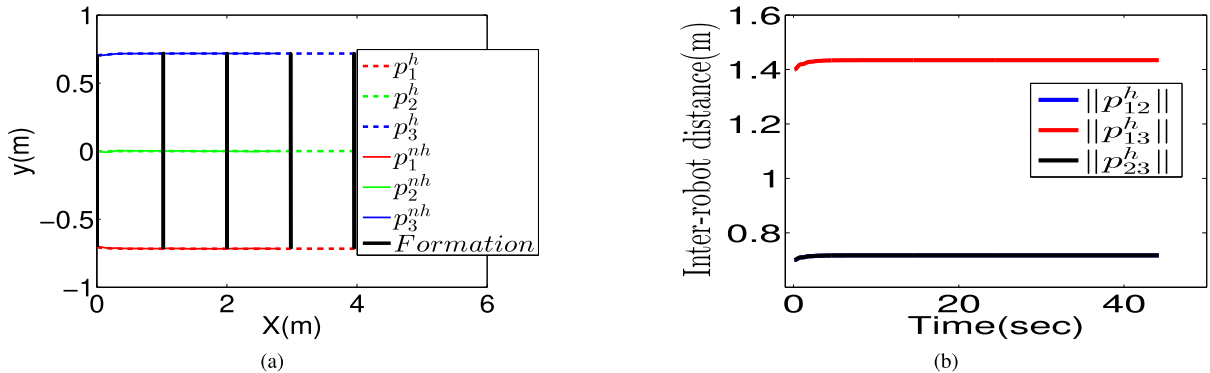


Fig. 13. Experiment [demonstration of an application]: (a) Trajectory tracking in formation. (b) Interrobot distances.



Fig. 14. Experiment [demonstration of an application]: Payload transport by a group of nonholonomic mobile robots from point  $p_a$  to the point  $p_b$  in the lab environment.

desired formation, as shown in Fig. 14(a). The obtained results and taped video images suggest that all three mobile robots move along the path of interest till the point  $p_b$  in the desired formation without collision. The YouTube link for the videos recorded during the experiments is: <https://youtu.be/EX2Hw-Bb7Gw>.

**Comparison:** In [24], two protocols are used to achieve multiobjective tasks. First protocol achieves translationally

invariant formations along with the synchronization of attitudes and heading velocities to the desired values. Second protocol helps the robots to move in formation while tracking a trajectory. However, practical issues like collision avoidance and connectivity assurance are not considered in [24]. In contrast to the work in [24], the proposed approach not only enables the robots to track the reference trajectories while maintaining the

desired formation pattern but also ensures collision avoidance and connectivity preservation.

In [22], mobile robots move in formation while tracking the trajectory of a virtual leader. This is shown in simulation only. In contrast to [22], in this article, the challenge of collision avoidance and connectivity assurance along with formation-tracking task has been solved and implemented on real hardware.

Work in [10] only deals with holonomic agents whereas the proposed approach also deals with nonholonomic mobile robots. Only simulation results are reported in [10], while the proposed scheme is validated from both simulation and experimental point of view. In contrast to [10] and [24], in this article, input disturbances are considered in both holonomic and nonholonomic models.

## VI. CONCLUSION

In this article, an integrated two-step design approach to formation control was presented while considering external input disturbances. The HR of the virtual mobile robots was used to generate reference trajectories for the actual mobile robots operating in the nonholonomic framework to follow. The mathematical analysis for the stability of the holonomic consensus formation in the presence of the disturbances was done. The stability of actual mobile robots in the nonholonomic framework was shown. These analyses took into account collision avoidance and connectivity assurance. The proposed framework was applied to three-robot system in real time; and was scalable to any arbitrary  $n$ -robot system as well. During the simulation and experiment, it was shown that interrobot distances are always greater than  $r_{in}$  and much less than  $R$ —the proposed approach takes care of collision avoidance and the later takes care of the connectivity. The proposed scheme was implemented in real time using three pioneer P3-DX nonholonomic mobile robots. Both simulation and experimental results were provided to show the effectiveness of the proposed scheme.

## REFERENCES

- [1] K.-K. Oh, M.-C. Park, and H.-S. Ahn, "A survey of multi-agent formation control," *Automatica*, vol. 53, pp. 424–440, 2015.
- [2] Y. Cao, W. Yu, W. Ren, and G. Chen, "An overview of recent progress in the study of distributed multi-agent coordination," *IEEE Trans. Ind. Informat.*, vol. 9, no. 1, pp. 427–438, Feb. 2013.
- [3] W. Ren and E. Atkins, "Distributed multi-vehicle coordinated control via local information exchange," *Int. J. Robust Nonlinear Control*, vol. 17, no. 10/11, pp. 1002–1033, 2007.
- [4] K. Do and J. Pan, "Nonlinear formation control of unicycle-type mobile robots," *Robot. Auton. Syst.*, vol. 55, no. 3, pp. 191–204, 2007.
- [5] W. Dong and J. A. Farrell, "Cooperative control of multiple nonholonomic mobile agents," *IEEE Trans. Autom. Control*, vol. 53, no. 6, pp. 1434–1448, Jul. 2008.
- [6] F. Dorfler and B. Francis, "Geometric analysis of the formation problem for autonomous robots," *IEEE Trans. Autom. Control*, vol. 55, no. 10, pp. 2379–2384, Oct. 2010.
- [7] B. Fidan, V. Gazi, S. Zhai, N. Cen, and E. Karataş, "Single-view distance-estimation-based formation control of robotic swarms," *IEEE Trans. Ind. Electron.*, vol. 60, no. 12, pp. 5781–5791, Dec. 2013.
- [8] J. Cortés, "Global and robust formation-shape stabilization of relative sensing networks," *Automatica*, vol. 45, no. 12, pp. 2754–2762, 2009.
- [9] K.-K. Oh and H.-S. Ahn, "Formation control and network localization via orientation alignment," *IEEE Trans. Autom. Control*, vol. 59, no. 2, pp. 540–545, Feb. 2014.
- [10] A. Mondal, C. Bhowmick, L. Behera, and M. Jamshidi, "Trajectory tracking by multiple agents in formation with collision avoidance and connectivity assurance," *IEEE Syst. J.*, vol. 12, no. 3, pp. 2449–2460, Sep. 2018.
- [11] M.-C. Park and H.-S. Ahn, "Distance-based control of formations with orientation control," in *Proc. 54th IEEE Conf. Decis. Control*, 2015, pp. 2199–2204.
- [12] W. Ren, "Consensus based formation control strategies for multi-vehicle systems," in *Proc. 25th Amer. Control Conf.*, 2006, pp. 4237–4242.
- [13] R. Olfati-Saber and R. M. Murray, "Consensus problems in networks of agents with switching topology and time-delays," *IEEE Trans. Autom. Control*, vol. 49, no. 9, pp. 1520–1533, Sep. 2004.
- [14] H. Wang, "Consensus of networked mechanical systems with communication delays: A unified framework," *IEEE Trans. Autom. Control*, vol. 59, no. 6, pp. 1571–1576, Jun. 2014.
- [15] A. Abdessameud, I. G. Polushin, and A. Tayebi, "Synchronization of nonlinear systems with communication delays and intermittent information exchange," *Automatica*, vol. 59, pp. 1–8, 2015.
- [16] R. Dutta, L. Sun, M. Kothari, R. Sharma, and D. Pack, "A cooperative formation control strategy maintaining connectivity of a multi-agent system," in *Proc. IEEE/RSJ Int. Conf. Intell. Robots Syst.*, 2014, pp. 1189–1194, 2014.
- [17] O. Khatib, "Real-time obstacle avoidance for manipulators and mobile robots," *Int. J. Robot. Res.*, vol. 5, no. 1, pp. 90–98, 1986.
- [18] J. Ji, A. Khajepour, W. W. Melek, and Y. Huang, "Path planning and tracking for vehicle collision avoidance based on model predictive control with multiconstraints," *IEEE Trans. Veh. Technol.*, vol. 66, no. 2, pp. 952–964, Feb. 2017.
- [19] X. Li, D. Sun, and J. Yang, "A bounded controller for multirobot navigation while maintaining network connectivity in the presence of obstacles," *Automatica*, vol. 49, no. 1, pp. 285–292, 2013.
- [20] D. V. Dimarogonas and K. J. Kyriakopoulos, "A connection between formation infeasibility and velocity alignment in kinematic multi-agent systems," *Automatica*, vol. 44, no. 10, pp. 2648–2654, 2008.
- [21] E. Montijano, E. Cristofalo, M. Schwager, and C. Sagües, "Distributed formation control of non-holonomic robots without a global reference frame," in *Proc. IEEE Int. Conf. Robot. Autom.*, 2016, pp. 5248–5254.
- [22] M. Maghenem, A. Loría, and E. Panteley, "Formation-tracking control of autonomous vehicles under relaxed persistency of excitation conditions," *IEEE Trans. Control Syst. Technol.*, vol. 26, no. 5, pp. 1860–1865, Sep. 2018.
- [23] R. S. Sharma, S. Shukla, H. Karki, A. Shukla, L. Behera, and V. K. Subramanian, "DMP based trajectory tracking for a nonholonomic mobile robot with automatic goal adaptation and obstacle avoidance," in *Proc. IEEE Int. Conf. Robot. Autom.*, 2019, pp. 8613–8619.
- [24] A. Saradagi, V. Muralidharan, V. Krishnan, S. Menta, and A. D. Mahindrakar, "Formation control and trajectory tracking of nonholonomic mobile robots," *IEEE Trans. Control Syst. Technol.*, vol. 26, no. 6, pp. 2250–2258, Nov. 2018.
- [25] T. H. Cormen, C. E. Leiserson, R. L. Rivest, and C. Stein, *Introduction to Algorithms*. Cambridge, MA, USA: MIT Press, 2009.
- [26] R. Olfati-Saber, "Flocking for multi-agent dynamic systems: Algorithms and theory," *IEEE Trans. Autom. Control*, vol. 51, no. 3, pp. 401–420, Mar. 2006.
- [27] S. H. Zak, *Systems and Control*, vol. 198. London, U.K.: Oxford Univ. Press, 2003.



**Radhe Shyam Sharma** (Student Member, IEEE) received the master's degree in modeling and simulation from the Defence Institute of Advanced Technology Pune, Pune, India, in 2013, and is currently working toward the Ph.D. degree in control and automation with the Department of Electrical Engineering, Indian Institute of Technology Kanpur, Kanpur, India.

His primary research interests include robot learning, visual servoing, and multirobot formation control.



**Arindam Mondal** received the master's degree in instrumentation and electronics engineering from Jadavpur University, Kolkata, India, in 2012, and the Ph.D. degree in electrical engineering from Indian Institute of Technology Kanpur, Kanpur, India, in 2018.

His main research interests include robust linear control and multiagent cooperative control.



**Laxmidhar Behera** (Senior Member, IEEE) received the B.Sc. and the M.Sc. degrees from the National Institute of Technology Rourkela, Odisha, India, in 1988 and 1990, respectively, both in engineering, and received the Ph.D. degree in electrical engineering from the Indian Institute of Technology Delhi, New Delhi, India, in 1996.

He completed his postdoctoral studies in the German National Research Center for Information Technology, GMD, Sank Augustin, Germany, from 2000 to 2001. He is currently a Poonam and Prabhu Goel Chair Professor with the Indian Institute of Technology (IIT) Kanpur having research and teaching experience of more than 24 years. Previously, he was an Assistant Professor with the Birla Institute of Technology and Science Pilani from 1995 to 1999 and a Reader at Intelligent Systems Research Center, University of Ulster, U.K., from 2007 to 2009. He was a Visiting Researcher/Professor with FHG, Germany, and ETH, Zurich, Switzerland. His research work lies in the convergence of machine learning, control theory, robotic vision, and heterogeneous robotic platforms. He has received more than INR 170 million research grants to support his research activities. He has established industrial collaboration with TCS, Renault Nissan, BEL, Bangalore, and ADNOC, Abu Dhabi while making significant technological development in the areas, such as robotics based ware-house automation, vision and drone guided driver assistance system, and drone guided pipeline inspection systems. He has published more than 250 papers in journals and conference proceedings. He has supervised 17 Ph.D. thesis to completion. His current research interests include intelligent control, semantic signal/music processing, neural networks, and control of cyber-physical systems and cognitive modeling.

Dr. Behera is a Fellow of INAE. He is a Technical Committee member on IEEE SMC on Robotics and Intelligent Systems.

## **Contact Information of Referees**

**Dr. Laxmidhar Behera**

Professor

Department of Electrical Engineering

IIT Kanpur

Kanpur–208016

India

☎ +91-8318968101

✉ lbehera@iitk.ac.in

**Dr. Venkatesh K S**

Professor

Department of Electrical Engineering

IIT Kanpur

Kanpur–208016

India

☎ +91-9451284966

✉ venkats@iitk.ac.in

**Mrs. Gauri Gupta**

Assistant Professor

Department of Biomedical Engineering

SGSITS Indore

Indore–452003

India

☎ +91-9300744226

✉ ggupta@sgsits.ac.in